CONICAL SCAN IMPACT STUDY

Volume I: General Central Data Processing Facility

Donald H. Ebert
Thomas A. Eppes
Douglas J. Thomas

Bendix Aerospace Systems Division
Ann Arbor, Michigan 48107

September 1973

Final Technical Report for Period
April through August 1973

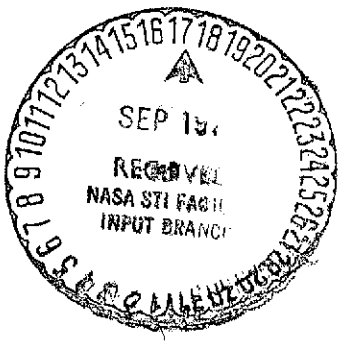

Prepared for:

GODDARD SPACE FLIGHT CENTER
Greenbelt, Maryland 20771

1. Report No. BSR 4150	2. Government Accession No.	3. Recipient's Catalog No.
4. Title and Subtitle CONICAL SCAN IMPACT STUDY Volume I: General Central Data Processing Facility		5. Report Date September 1973 6. Performing Organization Code
7. Author(s) Donald H. Ebert, Thomas A. Eppes, Douglas J. Thomas		8. Performing Organization Report No. BSR 4150
9. Performing Organization Name and Address Bendix Aerospace Systems Division Ann Arbor, Michigan 48107		10. Work Unit No. 11. Contract or Grant No. NAS 5-21903
12. Sponsoring Agency Name and Address National Aeronautics and Space Administration Goddard Space Flight Center Greenbelt, Maryland 20771		13. Type of Report and Period Covered Final Technical Report April through August 1973 14. Sponsoring Agency Code
15. Supplementary Notes		

16. Abstract

Studies were performed to determine the impact of a conical scan versus a linear scan multispectral scanner (MSS) instrument in terms of: (1) design modifications required in framing and continuous image recording devices and (2) changes in configuration of an all-digital precision image processor. A baseline system was defined to provide the framework for comparison. The baseline system included pertinent spacecraft parameters, a conical MSS, a linear MSS, an image recording system, and an all-digital precision processor. Lateral offset pointing of the sensors over a range of $\pm 20^{\circ}$ was considered. The study addressed the conical scan impact on geometric, radiometric, and aperture correction of MSS data in terms of hardware and software considerations, system complexity, quality of corrections, throughput, and cost of implementation. It was concluded that: (1) if the MSS data are to be only film recorded, then there is only a nominal conical scan impact on the ground data processing system and (2) if digital data are to be provided to users on computer-compatible tapes in rectilinear format, then there is a significant conical scan impact on the ground data processing system.

17. Key Words	18. Distribution Statement
Earth Resources Data Processing, Earth Observatory Satellite, Multispectral Scanners, Conical Scan Sensors, Image Recording, All-Digital Precision Processing	

19. Security Classif. (of this report)	20. Security Classif. (of this page)	21. No. of Pages	22. Price
Unclassified	Unclassified	108	

PREFACE

OBJECTIVES

The main objectives of this study were the determination of the impact of a conical multispectral scanner versus a linear multispectral scanner on ground data processing operations of image recording and all-digital precision processing. Secondary objectives were to evaluate the impact on both conical and linear scan processing of lateral offset pointing the scanners and to qualitatively evaluate data processing for three specific linear scanner configurations.

SCOPE

The study defined a baseline system consisting of pertinent spacecraft parameters, conical and linear multispectral scanners, image recording systems, and an all-digital precision processor. These baseline systems were evaluated in terms of hardware and software considerations, system complexity, quality of corrections, throughput, and cost of implementation. Problems associated with radiometric, aperture, and geometric corrections were investigated.

CONCLUSIONS AND RECOMMENDATIONS

The impact of the conical scan MSS on image recording is nominal if a flexible format image recorder such as an Electron Beam Recorder (EBR) is used. If a linear format image recorder is used, however, or if digital data in the form of rectilinear scan data tapes are required as an output product, then there is a significant impact on the ground data system. The impact in the latter case is in the requirement for a large computer memory for conversion of scan lines from conical to linear format. This memory can be most economically implemented in a combination of mass disc memory and semiconductor random-access memory. Lateral offset pointing does not seriously impact ground data processing operations if the pointing is implemented so that the offset scan line does not rotate relative to the zero-offset scan.

CONTENTS

ILLUSTRATIONS

ILLUSTRATIONS

ILLUSTRATIONS (CONT.)

TABLES

SECTION 1

INTRODUCTION AND SUMMARY

1.1 BACKGROUND AND GENERAL COMMENTS

This report describes the results of a study carried out by Bendix Aerospace Systems Division, Ann Arbor, Michigan, from April through August 1973, under NASA GSFC Contract NAS 5-21903. The study investigated the impact on ground data processing functions, system design, and performance of conical scan multispectral scanner (MSS) data relative to linear scan MSS data. Ground data processing in two forms of systems was investigated and is reported separately in the two volumes of this report. This volume, Volume I, is titled "Conical Scan Impact Study: General Central Data Processing Facility." Volume II is titled "Conical Scan Impact Study: Small Local User Data Processing Facility."

The general central data processing considered in the study was of the order of the ERTS NDPF system. The system was specified to consist of an image recording system and an all-digital precision image processing system. The problems associated with radiometric, geometric, and aperture correction of the scanner data were studied relative to both the image recording and all-digital precision processing systems. Full consideration was given in the study to lateral offset pointing of the scanners over a range of $\pm 20°$ from local vertical in $5°$ steps. The final results of the study are described in terms of the impact of conical scan geometry on the system hardware and software complexity and cost of implementation and data throughput and quality.

To eliminate the effects of the elements of scanner design which have no bearing on geometric, radiometric, or aperture correction, the specified conical scanner is compared to a contrived linear scanner. This is necessary if meaningful, quantitative comparisons are desired. Other specified linear scanners were briefly studied to determine their qualitative impact on ground data processing operations.

The approach used in this study was: (1) define a baseline system including a spacecraft, conical and linear scanners, and ground data processing systems, (2) define the image correction functions for geometric, radiometric, and aperture corrections, (3) determine the image processing requirements in terms of the magnitudes and significant types of geometric, radiometric, and aperture corrections, (4) configure image recording and

all-digital precision processors for linear scan data, and (5) evaluate the impact of conical scan data on the processor configurations. As a spin-off of this study process, several recommendations were developed relative to scanner and satellite configuration and operation which, with little impact on the spaceborne system, provide significant gains in the ground data processing system.

1.2 SUMMARY OF FOLLOWING SECTIONS

Section 2 of the report describes the baseline systems used in the study to permit valid and meaningful comparisons of the conical and linear scan data processing.

Section 3 describes the geometric, radiometric, and aperture correction functions considered in the study. The correction functions are described as though they are independent effects and do not interact. This is done to better understand each individual effect. The effects are described largely in nonquantitative terms.

In Section 4 the image correction functions are quantified and described in terms of image processing requirements. All of the interactions are included.

Section 5 develops the functional description of an all-digital precision processor and studies the impact of the conical scanner on this system. The findings of this section are equally applicable to an image recording system that uses an inherently linear image recorder such as a simple linear scan Laser Beam Recorder (LBR).

Section 6 develops the functional description of image recorder systems using a continuous motion and a framing image recorder. The impact of conical scan data is studied and described for each type of recorder system.

Section 7 summarizes the data processing impact of the three "other" specified linear scanners.

The study conclusions and recommendations are described in Section 8.

In describing the geometric performance of any specific scanner, difficulty was encountered in determining whether or not the instantaneous field of view (IFOV) rotated during the scan period. Since this has a significant

impact on the geometric and aperture correction processes, a model and procedure was developed for determining this factor of scanner performance. This model is described in Appendix A.

SECTION 2

BASELINE SYSTEM

In investigating conical and linear scanners to evaluate their comparative impact on ground data processing and recording operation, it is useful to define a baseline system. Indeed, it is essential to establish baseline scanners if meaningful cost comparisons are to be made. The baseline system described in this section includes the spacecraft, conical and linear scanners, and ground data processing subsystems.

The spacecraft baseline parameters used in this study are given in Table 2-1. The orbital characteristics listed are convenient values within the range of values found in the EOS Definition Phase Report and scanner sensor study reports. Selection of different orbital characteristics over this range would not seriously impact the ground data processing and has negligible effect on comparative studies of conical and linear scanner data processing. The tracking and attitude control characteristics represent data received from the EOS Program midway in this study. The conical versus linear scan impact has some sensitivity to attitude control and/or measurement; however, relaxing these values to be equivalent to the ERTS system would not alter the significant comparative results of this study.

Table 2-1

Spacecraft Baseline

Orbit:	735 kilometers at Equator Sun Synchronous 98.35° Inclination
Attitude Control:	
Pointing Accuracy	$< \pm 0.01°$
Pointing Stability (geocentric)	
Average Rate Deviation	$< \pm 10^{-6}$ degrees/second
Attitude Deviation	
1. Up to 30 Second Period	$< \pm 0.0003°$
2. Up to 20 Minute Period	$< \pm 0.0006°$
Tracking Accuracy:	
Position Along Track	30 meters
Position Cross Track	50 meters

The baseline conical scanner is derived from the January 1973 Design Study Report on the Honeywell Seven-Band Scanning Radiometer. The essential parameters used are tabulated in Table 2-2. The baseline specifies a cone axis which produces a conical scan line passing through the spacecraft nadir and concave forward as shown in Figure 2-1, line a.

Table 2-2

Conical Scan Baseline

Orbit: 735 kilometers (km) at Equator Sun Synchronous, 98.35° Inclination
Swath width: 185 km
Cone semi-angle: 17.08°
Cone axis: 17.08° forward from local vertical
Bands 1-6: 8 scan lines per sweep 43 μrad x 43 μrad IFOV 5,722 pixels per scan line
Band 7: Two scan lines per sweep 172 μrad x 172 μrad IFOV 1,430 pixels per scan line
Offset pointing: ±20° lateral from local vertical in 5° steps
Quantization levels: 6 bits per pixel
Duty Cycle: 80%

The concave forward conical scan geometry is chosen because it requires only about 46% of the memory required by the equivalent convex forward scan geometry when converting the conical scan lines to linear form in a computer. The comparative geometry of concave and convex forward scan is shown in Figure 2-2. This result is independent of whether or not the scan cone axis passes through the spacecraft nadir. Scanning through the spacecraft nadir was chosen because it produces the minimum geometric distortions from terrain effects. Other than these exceptions, the effects of scanning as shown in Figure 2-1, lines a, b, or c, are equivalent in terms of impact on ground data processing.

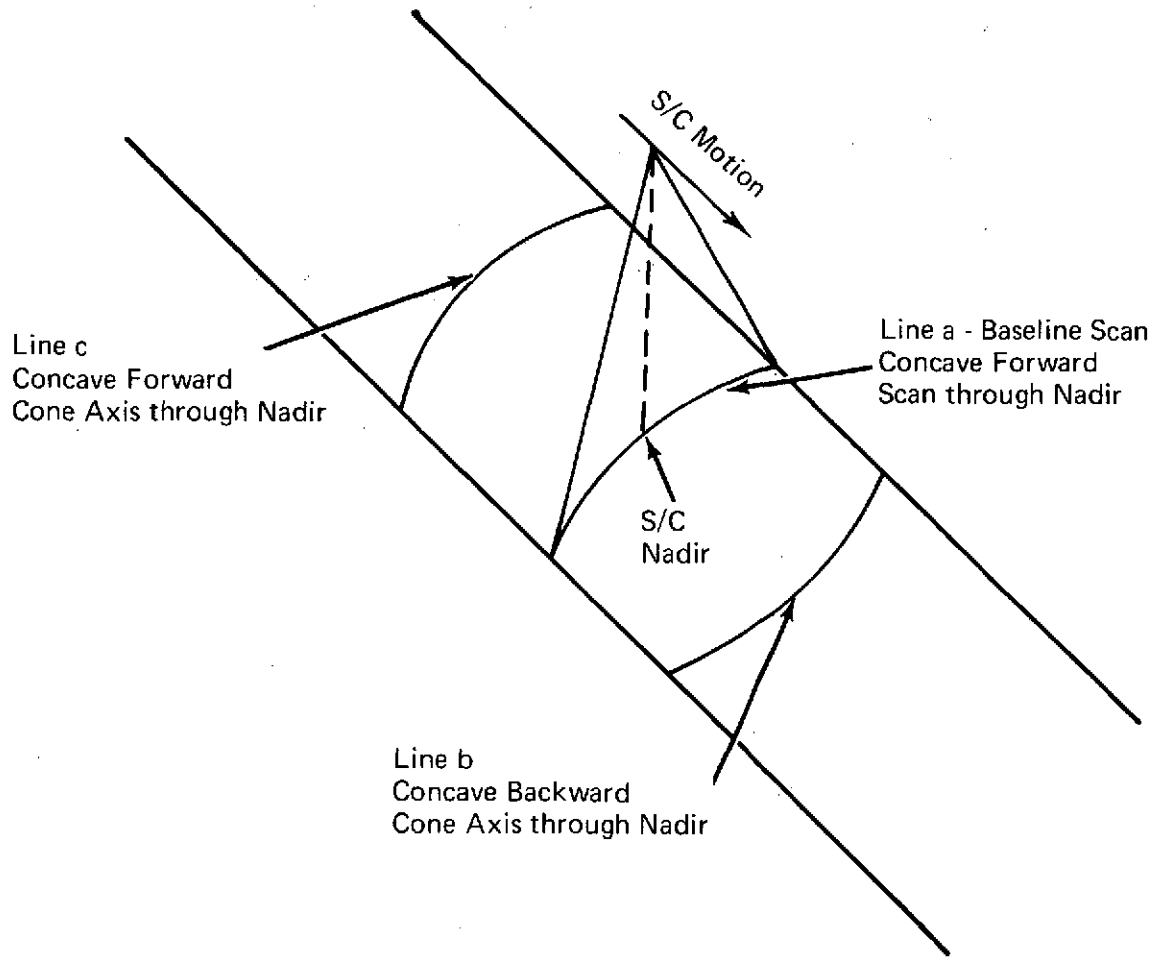

Figure 2-1 Baseline Conical Scan Geometry

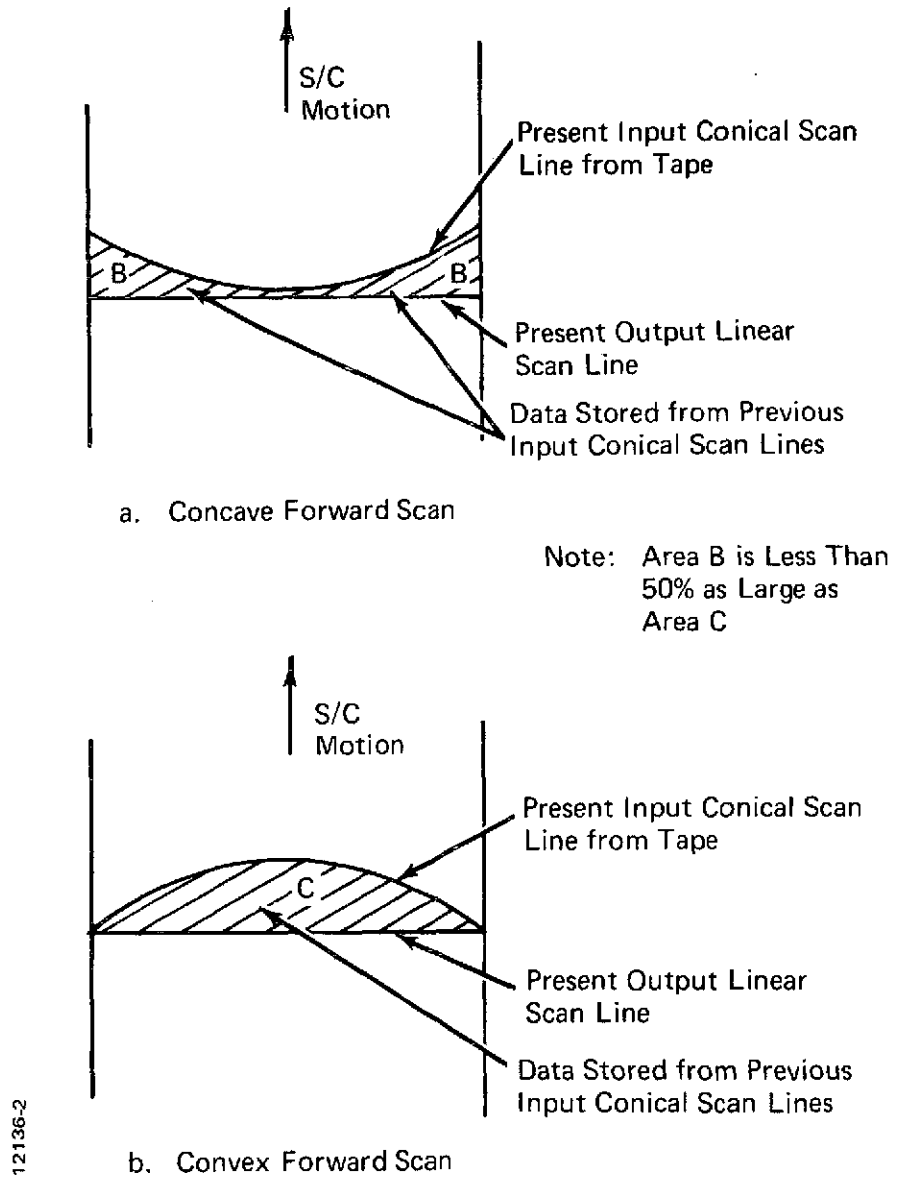

Figure 2-2 Data Storage Requirements for Conical Scan Linearization

The baseline linear scanner, described in Table 2-3, is a contrived set of characteristics to permit comparison of the baseline conical scanner with a linear scanner similar in details important to the comparison of data recording and precision data processing. In this way, the elements of scanner design that have no bearing on geometric, radiometric, or aperture effects are removed from consideration.

Table 2-3

Linear Scan Baseline

Orbit: 735 kilometers at Equator Sun Synchronous, 98.35° Inclination
Swath width: 185 km
Half-Scan Angle: 7.22°
Offset pointing: ±20° lateral from local vertical in 5° steps
Duty Cycle: 80%
Quantization levels: 6 bits per pixel
Bands 1-6: 8 scan lines per sweep 43 x 43 μrad IFOV 5,861 pixels per scan line
Band 7: Two scan lines per sweep 172 x 172 μrad IFOV 1,465 pixels per scan line

For comparative purposes, the baseline ground data processing subsystem is divided into an image recording processor and an all-digital precision processor. The essential differences are in data output formats and in the transformation of data to UTM projection coordinates by the digital precision processor. Table 2-4 summarizes the data inputs, outputs, and other pertinent factors of the baseline data processor subsystems.

Table 2-4

Baseline Data Processor Subsystems

A. Image Recording Subsystem

Data Input: Conical or linear scanner (MSS)
(see Tables 2-2 and 2-3)
Digital Data – high density digital tape
Format – to be determined

Data Processing: Geometric, radiometric, and aperture corrections
Film annotation

Data Output: 70-mm film recording, black and white, all bands, 200 scenes/day

B. All Digital Precision Processor Subsystem

Data Input: Same as A above, plus minimum ground control points (GCPs) and predicted orbit data.

Data Processing: Same as B above plus transformation to Universal Transverse Mercator coordinates (UTM)

Data Output: 9.5-inch film recording, black and white, all bands, 40 scenes/day

CCTs - 20 scenes/day, 800 bpi, 1,600 bpi linear scan format

The Conical Scan Impact Study is particularly sensitive to one element of data output product requirement; that of rectilinear format computer-compatible tapes (CCTs). If the data were to be film recorded only, or if a conical scan CCT format were acceptable to the user community, then the complexity and cost of a conical scan all-digital precision processor approach those of the linear scan all-digital precision processor. Since rectilinear format CCTs are specified as output products of the all-digital precision processor, this point is not further addressed in this study.

SECTION 3

IMAGE CORRECTION FUNCTIONS

For purposes of evaluating the impact of conical scan geometry versus linear scan geometry on a general central data processing system (on the order of the ERTS NDPF), the system is divided into an image recording subsystem and an all-digital precision image processing subsystem. Both subsystems include geometric, radiometric, and aperture correction capabilities; they differ primarily in data output formats and in that the precision processor has the additional capability of data conversion to a standard reference grid, such as a UTM map projection. This section describes the geometric, radiometric, and aperture correction functions which are considered in the study. From evaluation of these corrections, relative to the baseline sensors and satellite system, the image processing requirements described in Section 4 are derived.

3.1 GEOMETRIC CORRECTION CONSIDERATIONS

Geometric errors introduced into satellite-borne line scan sensor imagery arise from earth orbit geometric considerations, scanner geometry considerations, ephemeris attitude perturbations, other scanner instrument design considerations, and scanner instrument electromechanical perturbations. The error sources listed in Table 3-1 are described in following paragraphs.

3.1.1 Sensor Platform State Vector Effects

The platform state vector $\underline{V}$ is defined as:

$$\underline{V} = \begin{cases} \text{Pitch angle} \\ \text{Roll angle} \\ \text{Yaw angle} \\ \text{Velocity error} \\ \text{Altitude error} \end{cases}$$

in the coordinate system defined in Figure 3-1. The figure also shows the effects of state vector variations on the image geometry for both line scan and shuttered imagery. The effects upon the shuttered image depend only on $\underline{V}$ at the instant of exposure, while the continuous line scanned image includes all state vector effects as a function of time.

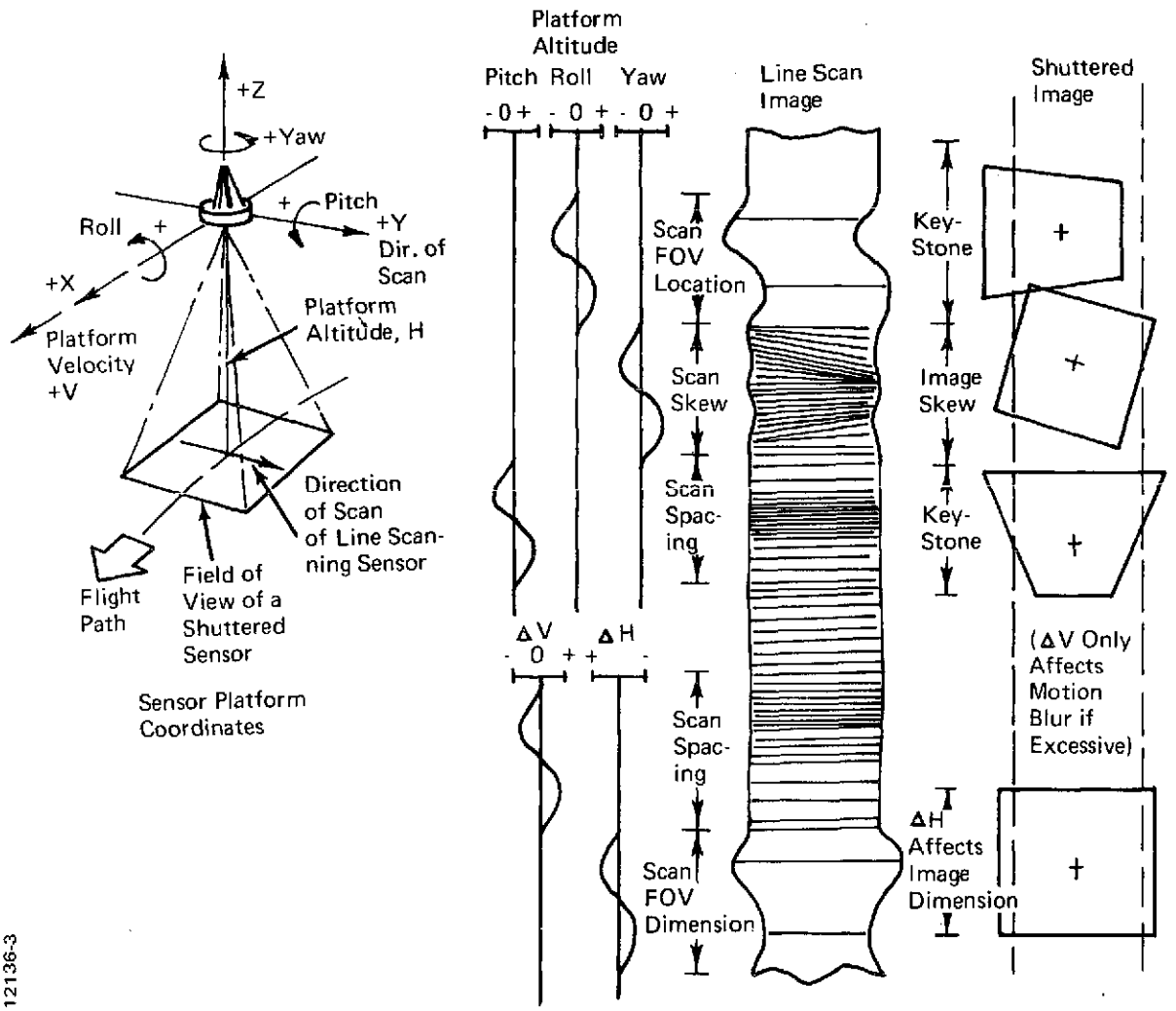

Figure 3-1 Platform State Vector Effects on Image Geometrics

Table 3-1

Geometric Correction Considerations

1. Sensor platform state vector
2. Ephemeris
3. Earth rotation
4. Variable slant range
5. Terrain
6. Ellipsoidal earth
7. Finite scan time
8. Earth curvature
9. Finite array sample rate
10. Variable ground sampling rate
11. Nonuniform sample rate
12. IFOV rotation
13. Scan line rotation
14. Internal sensor errors

3.1.2 Ephemeris Effects

The S-band ranging system to be employed on EOS will have a position determination error in both the along-track and cross-track positions. These errors in determining the orbital position of the spacecraft will result in corresponding errors in image positional accuracy.

3.1.3 Earth Rotation Effects

As the spacecraft travels along its orbital path, the earth is rotating below. The local earth velocity vector can be resolved into along- and across-track components, which will vary as functions of the orbital parameters and spacecraft latitude. Since the scanner image is built up of successive scan lines (or groups of scan lines), the across-track earth motion produces an image skew or shear as shown in Figure 3-2(a). The along-track earth motion variations produce underlap or overlap of successive swaths, depending upon the latitude for which the system is optimized, but in

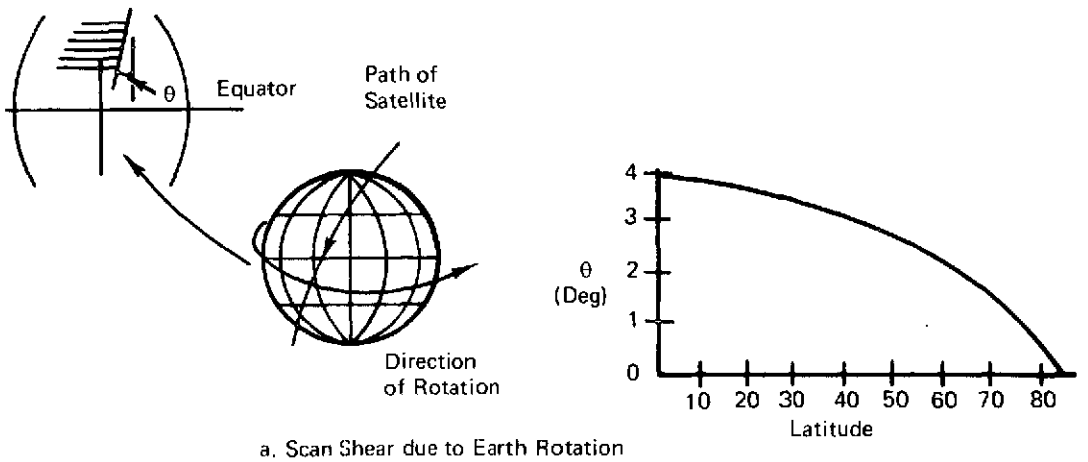

a. Scan Shear due to Earth Rotation

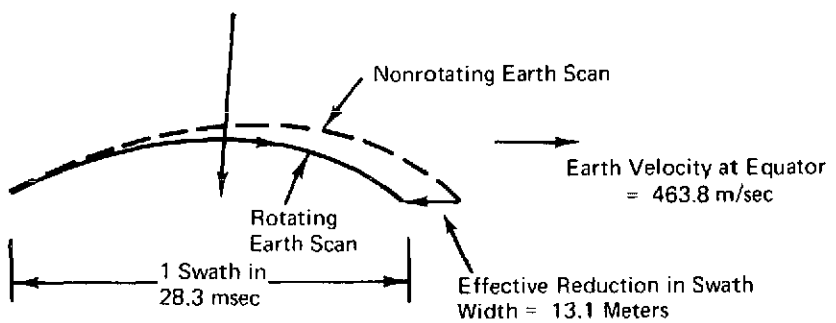

b. Swath Reduction due to Earth Rotation

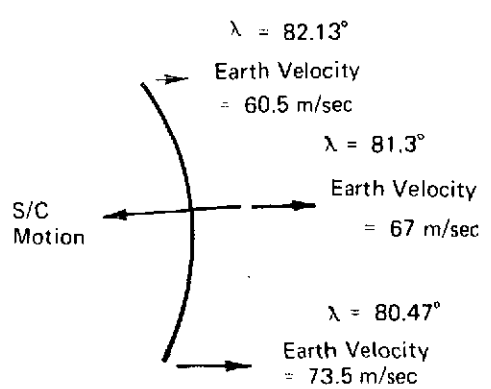

12136-4

c. Scan Twist due to Earth Rotation

Figure 3-2 Earth Rotation Effects on Continuous Line Scan Sensor

practice these effects are very small. For a spherical earth and a circular orbit, the along-track earth motion component would be constant; for an ellipsoidal earth, the variation amounts to only 0.003% of the total along-track velocity, or approximately 1 cm overlap/underlap between successive swaths.

In addition to the skew and overlap/underlap effects, there are two effects of earth rotation which can slightly alter the shape and twist of the scan, but not to a significant extent.

Near the equator the scan is nearly east-west and the earth rotation effectively reduces the cross-track scanning velocity by 463.8 m/second. The active scan period is 28.3 milliseconds and hence the nominal scan width is reduced by 13.1 m, equivalent to a scale change of 0.007%, which is negligible.

The scan-twist effect occurs when different parts of the scan are at different latitudes and hence experiencing different earth rotational velocities. The worst case occurs at the maximum latitude, when the satellite is traveling east-west (see Figure 3.2(c)) and amounts to a difference of 13 m/second between the two ends of the scan. At 28.3 m/sec per scan, the additional movement of the lower-latitude end of the scan is 0.4 m, which again is negligible.

3.1.4 Variable Slant Range Effects

Scanners, in which the angle θ between local vertical and a line drawn to each sequential field of view varies as a function of time, exhibit the property of variable slant range effects. Figure 3-3 shows these effects for a linear scanner. As θ increases, both the length and width of the instantaneous field of view (IFOV) change, producing a change in IFOV aspect ratio, resolution, and overlap between scans as shown.

3.1.5 Terrain Effects

The geometric image displacement error resulting from terrain effects is shown in Figure 3-4. The line scan instrument at point S measures the radiometric intensity of the terrain at the actual position, which is determined by sensor altitude h, scan angle θ, orientation and location of the sensor S, and terrain elevation of the actual position A. In general, each of these factors is well known with the exception of terrain elevation. When recording an image on film, a smooth earth is assumed. As a result, the radiometric value sensed at A is recorded at the virtual position A', introducing a positional error Δx. A terrain elevation of h meters introduces a Δx of:

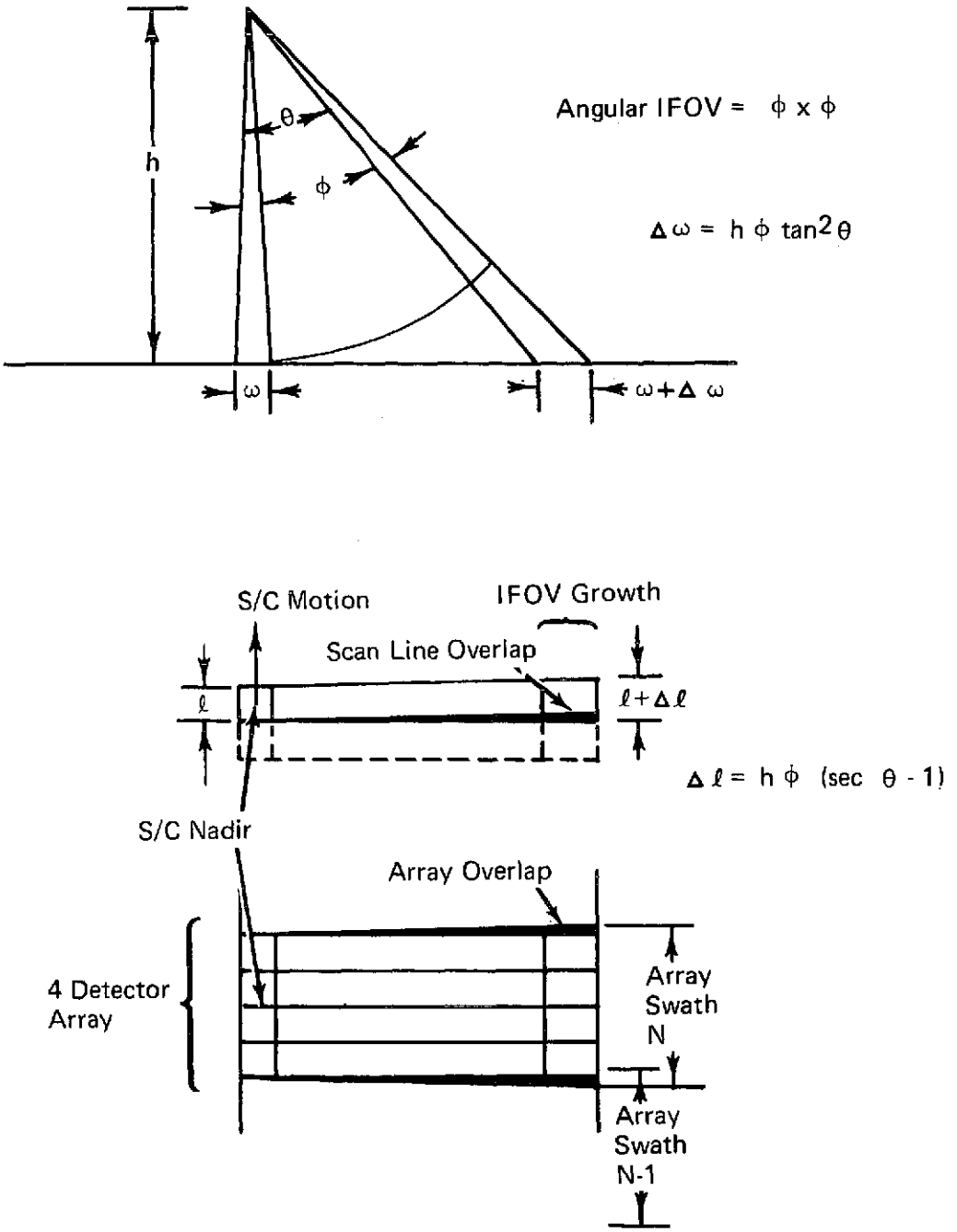

Figure 3-3 Variable Slant Range Effect

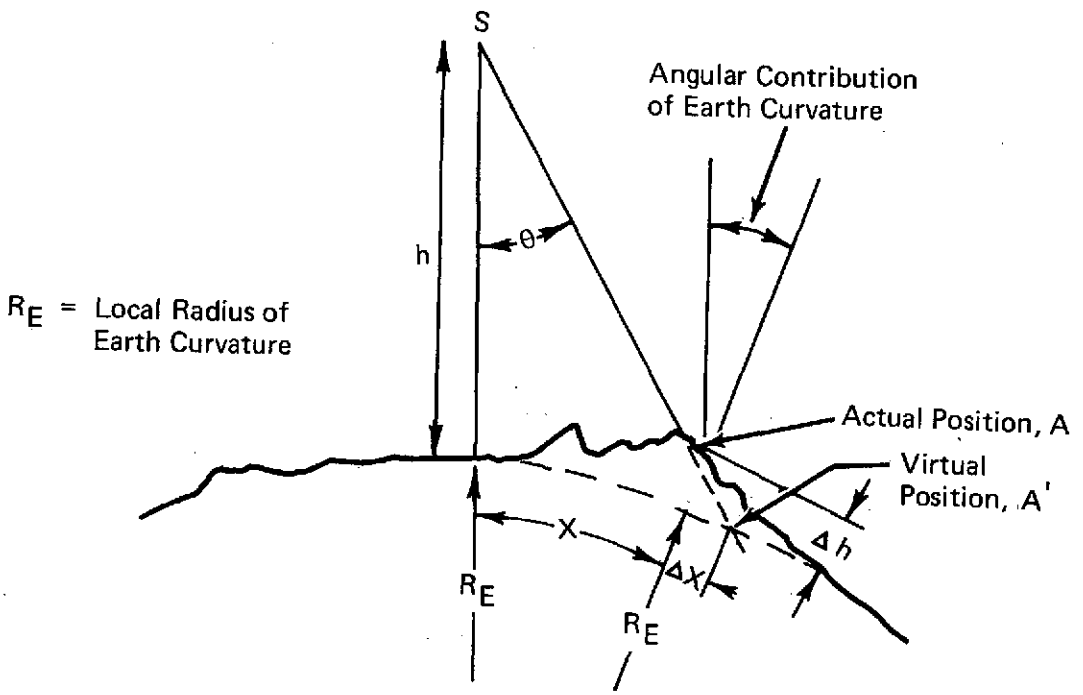

Figure 3-4 Image Displacement from Terrain Effect

$$\Delta x = \Delta h \left[\tan \theta + \left(\frac{x}{R_e}\right) \sec^2 \theta\right]$$

where the second term on the right-hand side is the effect of earth curvature upon terrain height correction.

3.1.6 Ellipsoidal Earth Effects

Although the satellite is nominally in a constant velocity, circular orbit about the earth, the ellipsoidal shape of the earth introduces altitude, attitude, ground velocity, and scan shape variations as a function of orbital position. (See Figure 3-5.)

Altitude — The equatorial radius of the earth (i.e., distance from the center) is 6,378.2 km and the polar radius is 6,356.8 km; since the orbit is only a few degrees from a polar orbit, there is an altitude variation of very nearly the full 21.4-km difference. For the 735-km orbit considered in this study, this altitude difference produces an imagery scale change of 2.9% over the orbit, with a similar change in the size of the swath and in the size of each pixel. The variation of scale is a significant but predictable function of the orbit parameters and the orbital position, and can be compensated in the film recording processes. The change in swath dimensions will cause up to 7-m underlap or overlap between successive swaths, which is also significant. The variation of pixel size affects the resolution and the optimum aperture correction functions, but it is questionable in this case whether it will prove to be worthwhile providing special compensation for such a small variation.

Attitude — At the equator and at the poles, the geodetic and geocentric latitudes are the same, but at any other latitudes the local vertical and the line to the center of the earth are not coincident (see Figure 3-5(a)). The maximum difference is approximately 0.2° and occurs at latitude 45°. The plane of the difference is always north-south but, since the azimuth of the orbit varies with latitude, the relative magnitudes of the along- and across-track components also vary with latitude. Figure 3-5(b) shows that the locus of the base of the local vertical relative to the point of intersection of the earth-center line with the surface of the earth is a squashed figure-of-eight, with a maximum radial displacement of approximately 2.5 km. If the satellite is stabilized to point at the center of the earth, then this displacement must be treated as a cyclic attitude error.

Ground Velocity — For a scanner which is stabilized to the instantaneous local vertical, the velocity of the base of the local vertical over the ground is given to sufficient accuracy by:

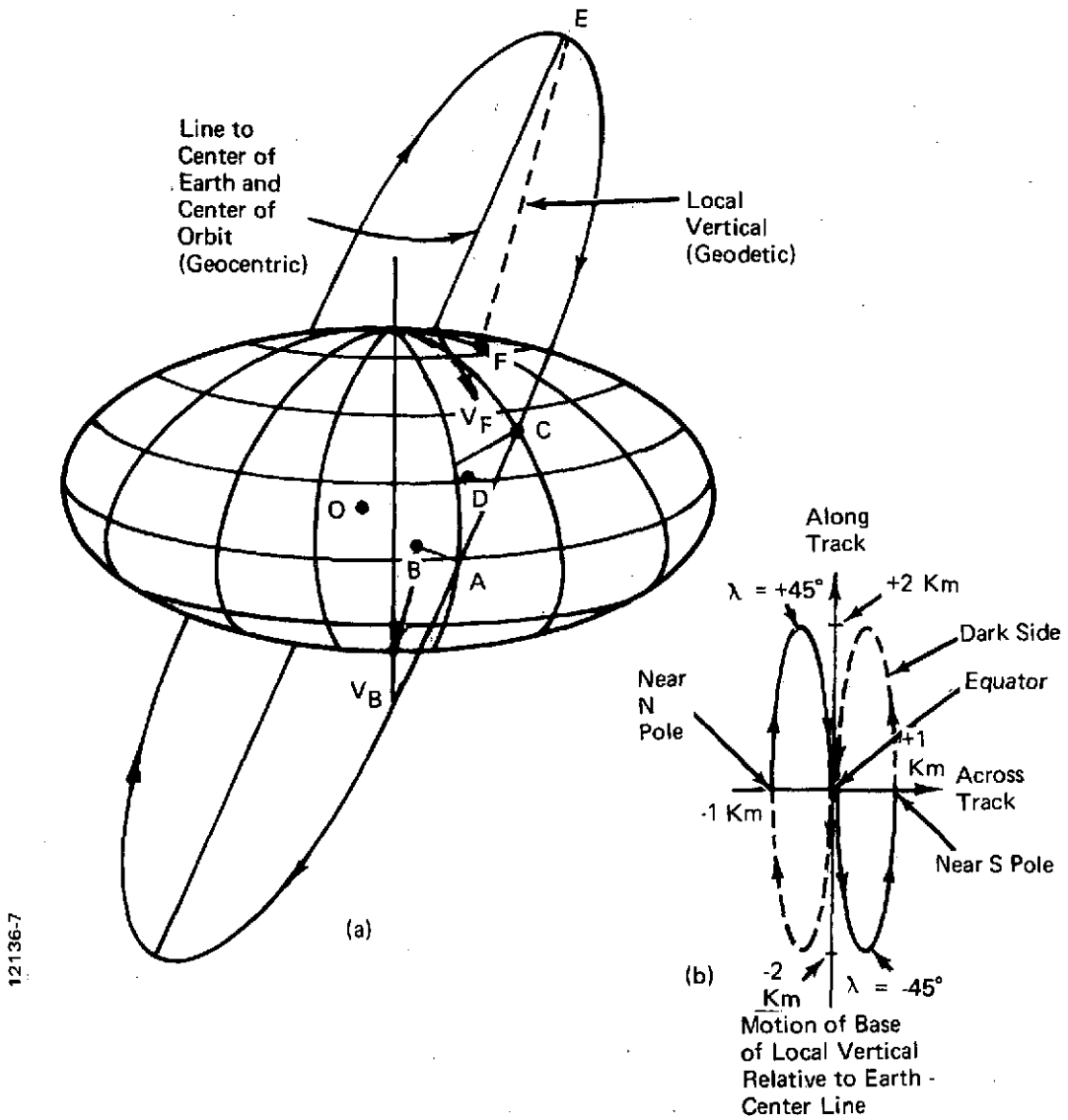

Figure 3-5 Ellipsoidal Earth Effect

$$\frac{\text{(Satellite Orbital Velocity)} \times \text{(Along-Track Radius of Curvature of Earth)}}{\text{(Along-Track Radius of Curvature of Earth)} + \text{(Altitude Above Surface)}}$$

At the equator the relevant radius of curvature is approximately 6, 336 km and the altitude is 735. 2 km. Near the poles the radius of curvature increases to approximately 6, 400 km and the altitude to 756. 4 km. The increase in radius of curvature toward the poles is too small to compensate for the change in altitude, the net result being a ± 0. 1% ground velocity variation or ± 6. 5 meters/second about the mean of 6, 701 m/second. With a time between corresponding points on successive swaths of 35 milliseconds, the maximum overlap or underlap between swaths which this velocity variation can cause is only 0. 5 m.

Scan Shape — On a spherical earth the basic scan shape, ignoring earth rotation effects, is constant for any point in the orbit. On an ellipsoidal earth the basic scan shape varies slightly with latitude. The effect upon each scan shape component is illustrated in Section 4.

3. 1. 7 Finite Scan Time and Varying Scan Velocity Effects

As a result of the forward velocity of the spacecraft and the finite time required to scan a single scan line (or a single sweep of a detection array to produce multiple scan lines), the scan line is skewed slightly relative to the normal to the spacecraft velocity vector and, depending upon the cross-track scanning velocity profile, may also be subject to a slight "s" shaped distortion (not to be confused with the "s" contribution from earth curvature, discussed in Section 3. 1. 8).

Figure 3. 6(a) shows a flat-earth, straight-line scan with skew, and Figure 3. 6(b) shows how the "s" distortion arises even on a flat earth, due to the varying cross-track velocity associated with a constant angular velocity scan. With conical scanning, the cross-track scanning velocity component is smaller at the ends of the scan than at the center, leading to an "s" distortion which is curved in the opposite manner, i. e., greatest skew at the ends and least skew at the center.

3. 1. 8 Earth Curvature Effects

Earth curvature produces several geometrical effects. Figures 3. 6(c) and 3. 6(d) illustrate the way in which additional "s" distortion is produced. The ground track of the spacecraft is a great circle while the ground tracks of the ends of the scan are small circles. Since the angular velocity about the center of the earth is constant, the along-track ground velocity

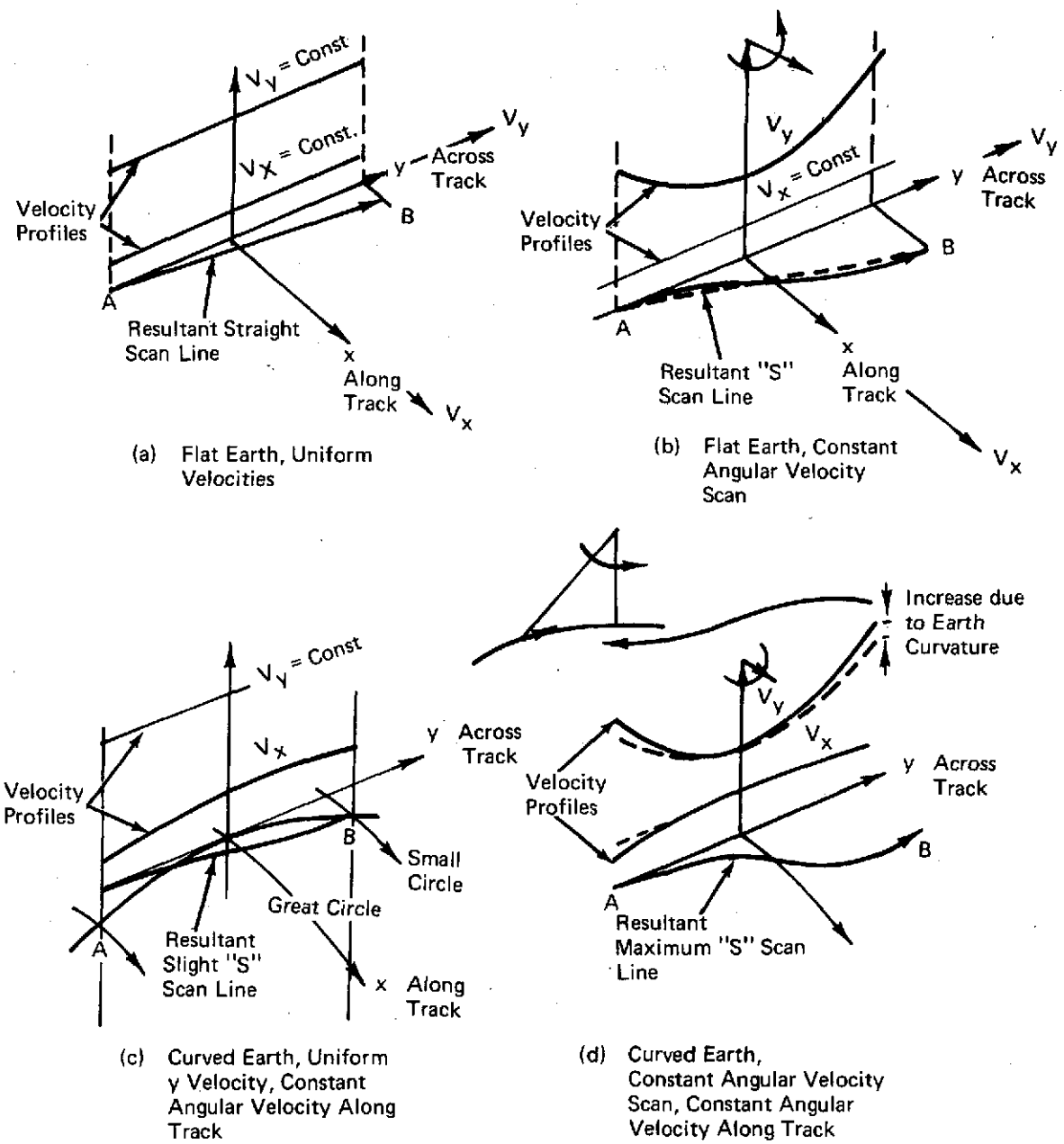

Figure 3-6 Finite Scan Time and Velocity, and Earth Curvature Effects - The S Component

must be greatest at the center of the scan, leading to maximum skew at that point. In addition to the reduction in along-track velocity at the ends of the scan, the cross-track velocity at the ends of the scan line is increased. The increase in slant range and reduction in angle of observation due to the fall-off of the earth's surface cause the scanning point to move more rapidly than it would on a flat surface.

The "s" contribution due to earth curvature is always of the type shown in Figures 3-6(c) and 3-6(d), with the maximum skew at the center of the scan. The "s" contribution that was discussed in Section 3.1.7 may curve in either direction, depending upon the scanning velocity profile, and it is therefore possible that in some cases the two contributions may be of opposite signs and will tend to cancel.

The variation in along-track velocity due to the center scan following a great circle while the ends follow small circles leads to scan overlap at the edges (see Figure 3-7). As the spacecraft moves a distance L along the great circle, a distance L (1 - $\Delta H/R$) is moved along the small circles. Assuming that the scan lines are contiguous along the spacecraft ground track, they must overlap at the swath edges.

The fall-off of the earth's surface ΔH is given by the approximation:

$$\Delta H = 1/2 \quad \frac{d^2}{R}$$

For a 185-km swath width with no offset, ΔH is about 670 m and the compression of the picture edges relative to the center is approximately 0.01%, i.e., 18.5 m per complete frame, or 2.4 cm overlap of successive swaths. With a 20° offset the distance d rises to a maximum of 360 km and ΔH is approximately 10 km. The compression at the edges is now 0.16%, i.e., 300 m per complete frame or 37.5 cm overlap of successive swaths.

In trying to produce a two-dimensional representation of the earth's three-dimensional curved surface, the usual problems of map projections arise. This subject is discussed separately in Section 3.1.16.

3.1.9 Finite Array Sample Rate Effect

Figure 3-8(a) shows the ground footprint of a detector array in which all elements of the array are sampled simultaneously. The effect of sequential sampling of the same array is shown in Figure 3-8(b). The offset between the leading edge of IFOV number 1 and the leading edge of IFOV

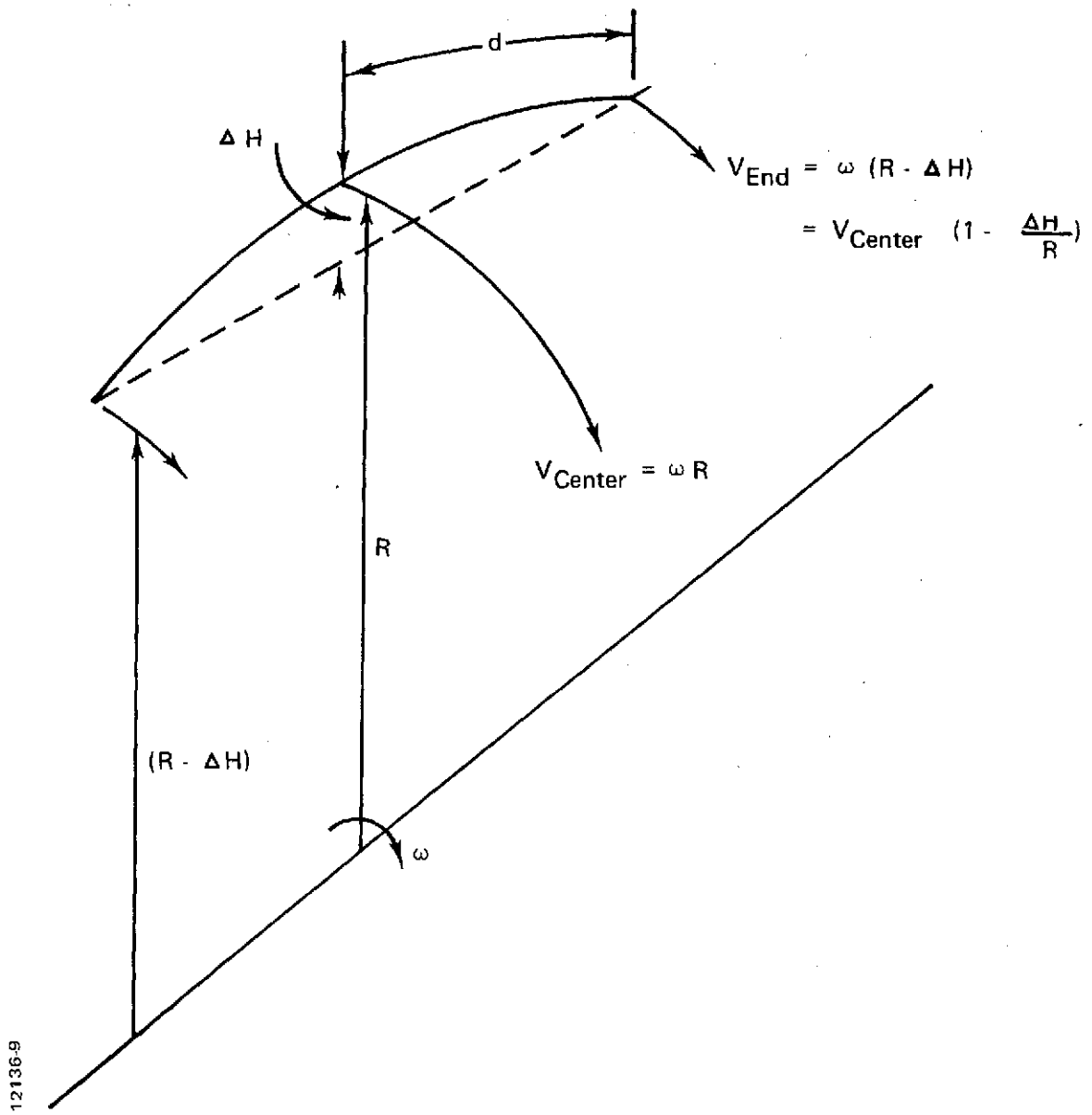

Figure 3-7 Scan Edge Overlap due to Earth Curvature

number 5 is equal to the reciprocal of the number of samples per IFOV; or for the scanner configurations considered in this study where 1.5 samples per IFOV are taken, the offset is 2/3 of an IFOV.

3.1.10 Variable Ground Sampling Rate

Under certain scanning and sampling conditions, an effect is present which is described as variable ground sampling rate effect. Figure 3-9 shows this effect for a conical scanner under the conditions of constant angular velocity scan, equi-angle samples, and nonrotating IFOV. The overlap shown is the result of this effect.

3.1.11 Nonuniform Sample Rate

A nonuniform sampling rate results in misalignment of samples from line-to-line, uncertainty of pixel location along a line, and line expansion or contraction as shown in Figure 3-10.

3.1.12 IFOV Rotation

For any given scanner, the orientation of the IFOV is a geometric relation between the scan circle, the target plane, and the field stop direction as described in Appendix A. The geometric effect of IFOV rotation on data collected is shown for a typical case in Figure 3-11. In general, each detector in the array produces a scan line of a different width, the swath length in direction of spacecraft motion is foreshortened, and adjacent sample overlap may increase or decrease.

3.1.13 Scan Line Rotation in Offset Pointing

In a scanner, which uses a separate mirror for lateral offset pointing of the scan swath, the scan line can be offset with or without rotation as shown in Figure 3-12. The specific line rotation is a function of the scanner and mirror geometry; lines c and d are only two representative cases.

3.1.14 Scale Change in Offset Pointing

As a result of the slant range effect (Section 3.1.4), the scan line is longer when offset than when scanned directly below the spacecraft and each IFOV is longer in the direction of scan. Furthermore, the scan line is asymmetric when offset pointed.

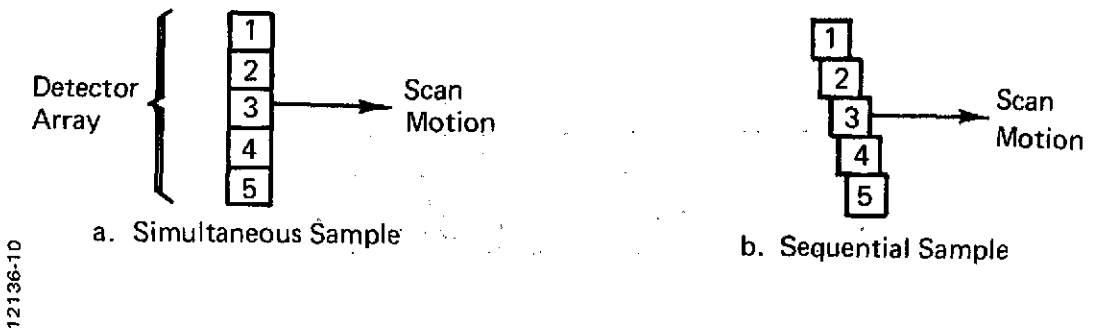

Figure 3-8 Finite Array Sample Effect

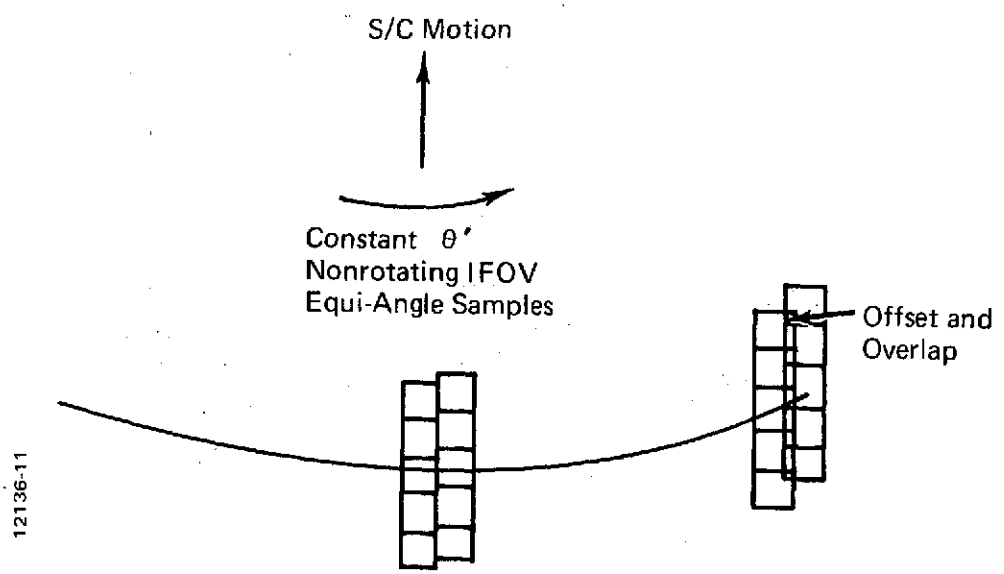

Figure 3-9 Effect of Variable Ground Sample Rate Shown without All Other Effects.

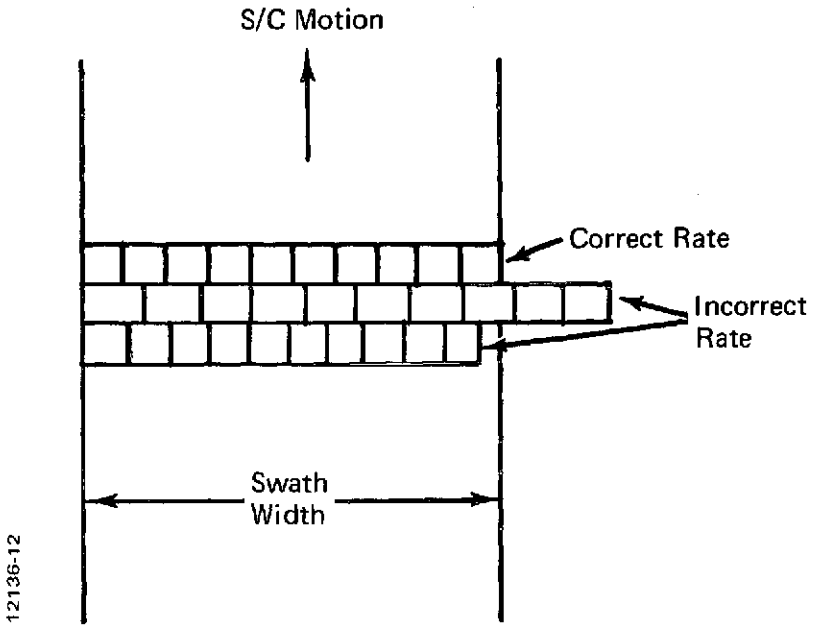

Figure 3-10 Nonuniform Sample Rate Effect

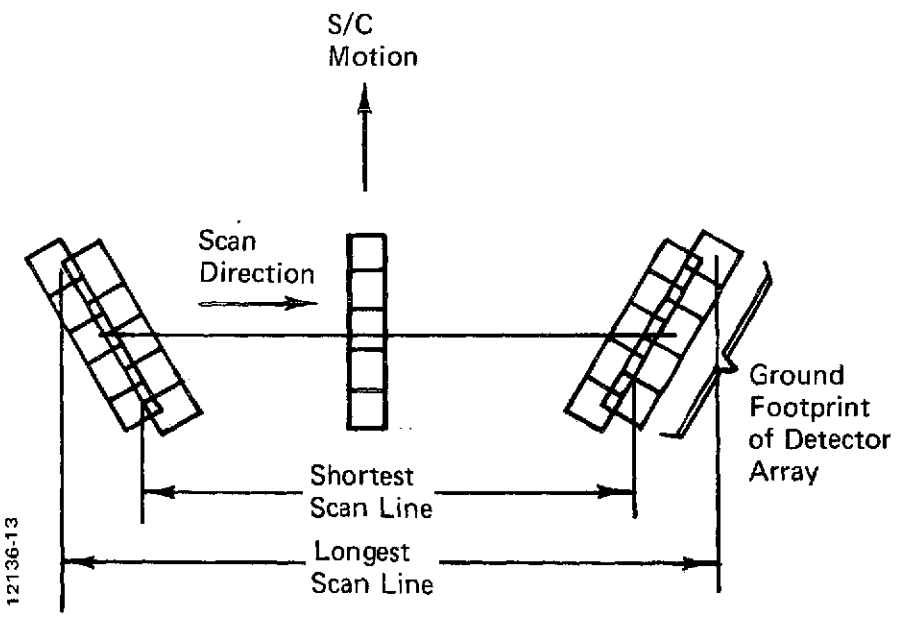

Figure 3-11 Geometric Effect of IFOV Relation

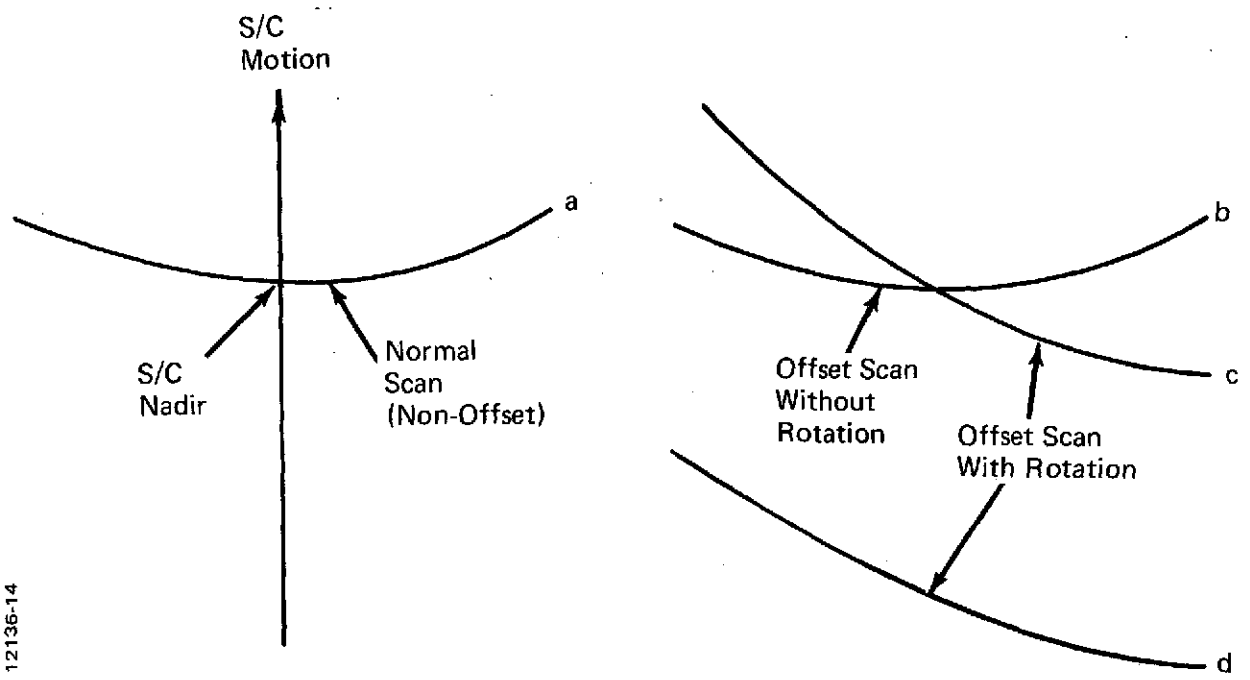

Figure 3-12 Scan Line Rotation in Offset Pointing

3.1.15 Internal Sensor Error

Each scanner configuration and implementation will have internal errors that will introduce geometric errors in the data produced. Some examples of these errors are boresight errors, alignment errors, and scan shaft bearing errors.

3.1.16 Mapping Corrections

The required map projection for the precision processor output is the Universal Transverse Mercator (UTM) projection. The UTM system requires that points be plotted on a rectangular grid of northings and eastings, which are curved distance measurements and not angular measurements. The northing is measured along one of a number of standard meridians and then the easting is measured along the parallel of latitude through the point. The effect of UTM mapping upon scan shapes is that they develop an approximately parabolic curved component, which increases with distance from the equator and which is always concave towards the equator. Figure 3-13 illustrates the effect for the simple case of a linear scanner traveling due north-south

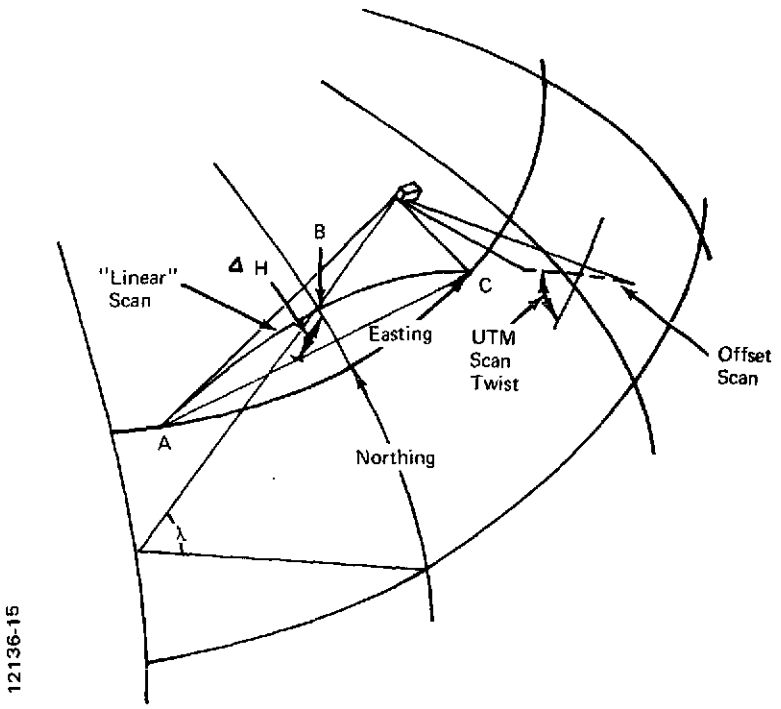

Figure 3-13 UTM Mapping Effect

along the reference meridian. The curvature of the earth causes points A and C at the ends of the scan to be at a lower latitude (northing) than point B at the center of the scan. In this simple case the "UTM droop" for a 185-km east-west nadir scan at latitude 45° would be approximately 670 m. When the scan is offset, the effect becomes much more marked, up to 10 km for a 20° offset, and an overall scan twist appears.

In practice, the spacecraft azimuth varies and it is never traveling north-south, the scan may be conical or follow some other nonlinear profile, and the UTM mapping corrections will be required along-film and across-film components. Various numerical examples are given in Section 4.

3.2 RADIOMETRIC CORRECTION CONSIDERATIONS

Ideally, each data sample point, or pixel, recorded by a passive line scan instrument would be a measure of the reflectance of the terrain at this point (in reflectance bands) or the radiance of the point (in thermal bands). Such ideal data would maximize the ability to categorize terrain pixels into classes corresponding to unique spectral reflectances and would also maximize the ability to temporally and spatially compare and correlate these classifications. Departure from this ideal are caused by sensor and environment-induced errors described in this section.

The radiance sensed by the spacecraft sensors associated with a given target depends not only upon the reflectance of the target, but also upon the characteristics of the incident sunlight (irradiance H) on the target and upon the spectral absorption and scattering of the atmosphere between the target and the spacecraft. This atmosphere both attenuates the radiance reflected from the target (transmission in path from target to spacecraft = τ) and adds to the foreground radiance by backscatter of sunlight from the atmosphere L_{ATM}. The composite radiance signal recorded by the spacecraft, $\bar{L}$, is therefore modified by the sensor responsivity K and the intervening solar and atmospheric parameters H, τ, L_{ATM} in the manner:

$$\bar{L} = K \ (\bar{\rho} \ H \ \tau + L_{ATM})$$

These parameters more precisely defined are:

K = The band responsivity that is determined from ground calibration. This parameter transforms the radiance L viewed by the detector to the signal output that is recorded, $\bar{L}$. Factors defining K include aperture field of view (resolution), diameter of collecting optics, optical efficiency, detector responsivity, electronic gain, etc.

$\bar{\rho}$ = The desired characteristics of the target considered as a reflectance distribution function; for most cases it is assumed that the target reflects diffusely and $\bar{\rho} = \rho/\eta$.

H = The total irradiance (global irradiance) on a horizontal target illuminated by the sun at an angle θ_s, which is measured from the zenith. The global irradiance is a result of contributions from the sky (H_{sky}, scattered skylight) and from the direct-beam solar $H_{ds} = H_{sun}$ (m) cos θ_s.

τ = The beam transmittance of the path of sight between the target and the sensor.

L_{ATM} = The path radiance (path reflectance) between the target and sensor.

Sensor responsivity errors can be corrected from data obtained during ground calibration or periodically from onboard calibration sources. These errors change slowly if at all and are readily corrected in ground data processing. Figure 3-14 shows one type of radiometric error, that of different detector sensitivity for detectors in an array. Each letter in the data array shown represents the radiance of a single pixel of a homogeneous water scene. All pixels should have the same value; however, it is seen that every sixth scan line is different. This is a result of a six-detector array in which one detector's responsivity differs from that of the others.

Environment-induced errors result from the effects of, and variations in, atmospheric and sun irradiance characteristics. The ERTS data supplied to experimenters are presently not modified to compensate these effects: each experimenter must provide his own means of such data processing. There are, however, several ERTS experiments investigating techniques for collecting the necessary calibration data and for performing the calibration. Should it ever be deemed necessary to perform this processing on all data collected, this decision could have a serious impact on the ground data processing system because of the temporal and locale variations in these effects.

When the data processing operations include recording the data on film, radiometric correction for film gamma is required to achieve a linear relationship between film density and the sensor-measured radiance.

3.3 APERTURE CORRECTION CONSIDERATIONS

Aperture correction, as considered in this study, consists of the compensation of total system effects which degrade spatial frequency response. These effects are functions of system elements including sensor optics, detector size, detector integration time, and video amplifier response. If the data are output on film, an additional element of aperture correction is considered, that of compensating for the shape of the recording spot of the film recorder. These effects, and their compensation or correction, are described in Section 5.4.

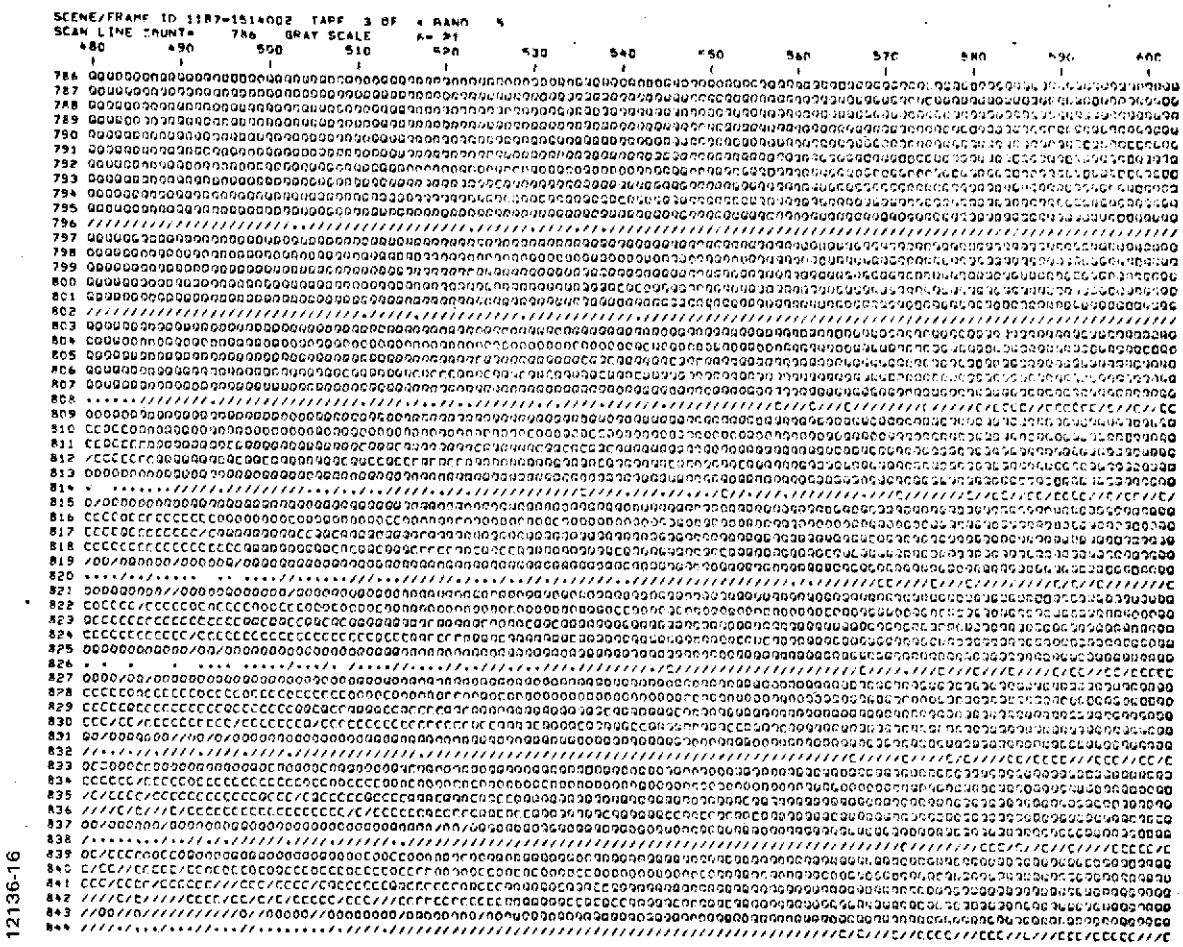

Figure 3-14 MSS Scene Showing Unequal Detector Response to Uniform Scale

SECTION 4

IMAGE PROCESSING REQUIREMENTS

In Section 3 the image correction functions were discussed mainly in qualitative terms to provide some insight to their origins. In this section the processing requirements with regard to the basic image and its correction functions are considered quantitatively.

Although several different contributions to the scan shape are discussed and quantified as if they existed independently, it will be realized that this is done simply for convenience in determining broad system requirements. A scan shape which was in reality computed by summing all the "contributions" would not be sufficiently accurate, due to the neglect of many second and higher order cross-product terms. In practice, the systematic scan shape variations would be stored after being calculated off-line, using an accurate computer model of the complete spacecraft-scanning ray-earth situation. Expressions such as "individual error contributions" and "error cross-product terms" then have no meaning since the actual scan shape can be computed directly, to whatever accuracy is required, or is permitted by knowledge of basic system parameters.

4.1 BASIC SCAN SHAPE

Figures 4-1 and 4-2 show the basic scan shapes for linear and conical scanning, for a nonrotating ellipsoidal earth, and for a stationary satellite. In Figure 4-1 the conical scan along-track deflection x is plotted against the across-track deflection y for zero and 20° offsets. (All cases for a linear scan are represented by the y-axis.) In Figure 4-1 the deviations of various conical scan shapes from the equatorial nadir scan shape are shown. The particular point to note is that a change in offset produces a far greater change in scan shape than does a change in latitude, although the latter can still amount to several hundred meters and can by no means be ignored. In Figures 4-3 and 4-4 the x and y components are plotted against time, which are related to the deflection current waveforms in a flexible format image recorder such as an EBR. The greatest across-track variation is caused by scan offset, while the differences between conical and linear scans amount to only a few tens of meters. In the case of the along-track, x, component, there is considerable difference between linear and conical scans, but the variations due to scan offset are somewhat smaller than in the across-track case.

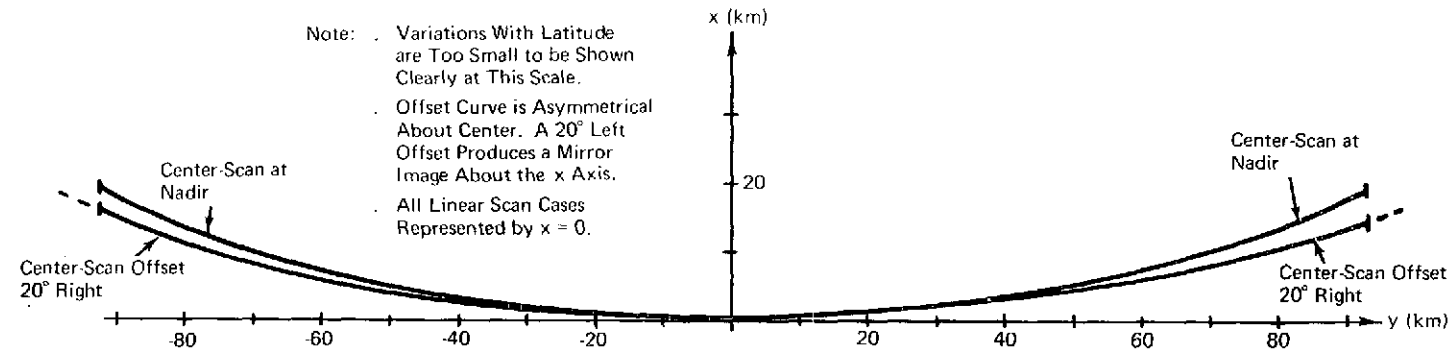

Figure 4-1 Basic Conical Scan Shapes

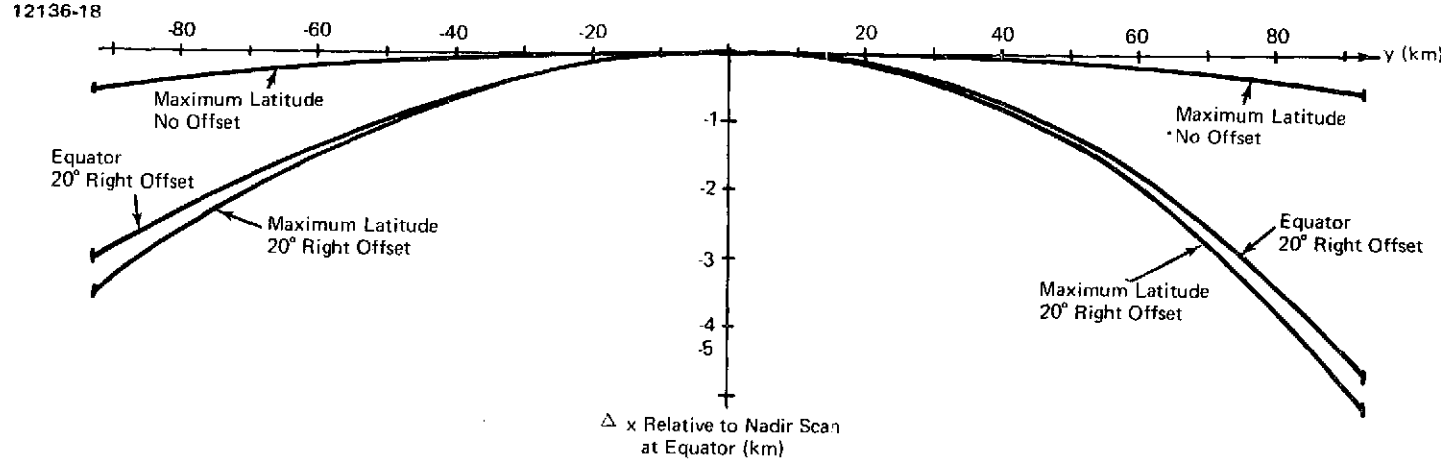

Figure 4-2 Basic Conical Scan Shape Variations Relative to Nadir Scan at Equator

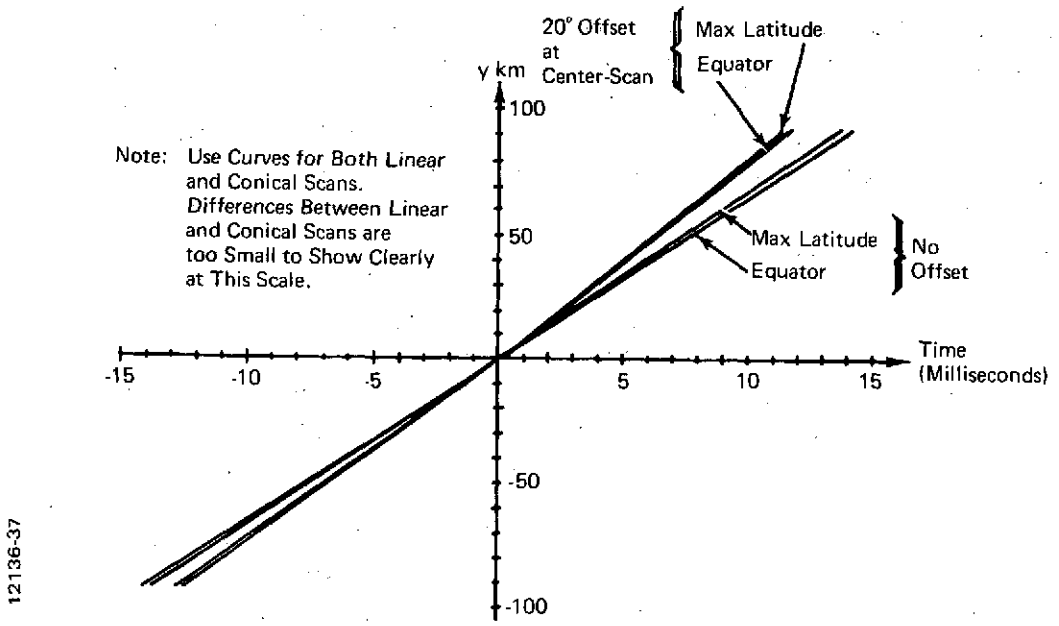

Figure 4-3 Across-Track Coordinates vs. Time
(Stationary Earth and Satellite)

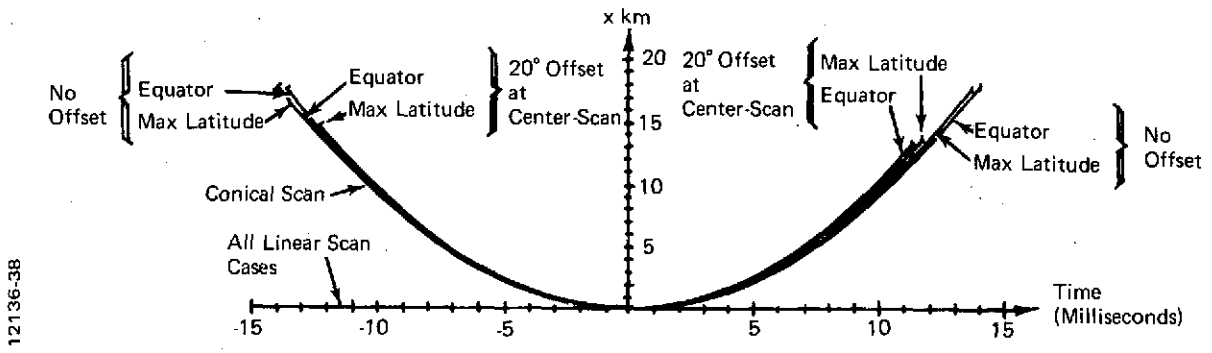

Figure 4-4 Along-Track Coordinates vs. Time
(Stationary Earth and Satellite)

4.2 CROSS-TRACK SCALE/RESOLUTION CHANGES

The combination of constant angular velocity scanning, variable slant range, the earth's ellipsoidal curvature, and equal-time-interval sample gives rise to variable across-track resolution and, in a simple system, variable picture scale. Figure 4-5 shows the magnitude of these effects at the equator, assuming that in each case the system is normalized to the conditions at the nadir. If the deflections discussed in Section 4.1 are faithfully reproduced in the image recorder, then the scale-change problem disappears, but the cross-track resolution change does not. Figure 4-5(a) shows that for a nonoffset scan the effect within a single swath is about 2% for a linear scan and 6% for a conical scan. Over the complete latitude range there is a 4.7% variation for a linear scan and a 9% variation for a conical scan. In the offset-scan case, Figure 4-5(b), the movement per sample differs from the equatorial nadir scan value by up to 30%, the linear scan now being slightly the worser of the two. The significance of these movement-per-sample variations is that in order to maintain the best possible resolution in the picture, the along-swath aperture correction function should be varied accordingly. In the case of the nonoffset scans, it might be reasonably argued that a constant aperture-correction function would be adequate, but in the 20° offset case the variation is too great to be ignored. The problem of aperture correction is discussed in detail in Section 5.

4.3 FINITE SCAN VELOCITY AND EARTH CURVATURE EFFECTS: SCAN SKEW AND THE "S" COMPONENT

Figure 4-6 shows the combined contributions to scan skew and "s" distortion due to finite scan velocities and earth curvature. It will be seen that the "s" component is so small that it may safely be ignored: in no case does it exceed 5 m for an offset scan or approximately 1 to 5 m for a nadir scan. As a matter of academic interest, only the nadir conical scan has a noticeable true "s" component. The linear nadir scan does not differ significantly from a straight line, and all the offset scans, being in reality at one end of a large "s", are concave rearwards.

Considering now the mean straight line, or skew component, it will be seen that the linear scan and conical scan curves do not differ by more than 1 or 2 m from each other, and that the only really significant variations are caused by the 20° offset. If one mean straight line was used to represent all cases, then the maximum error would never exceed 10 m or one-third of a pixel.

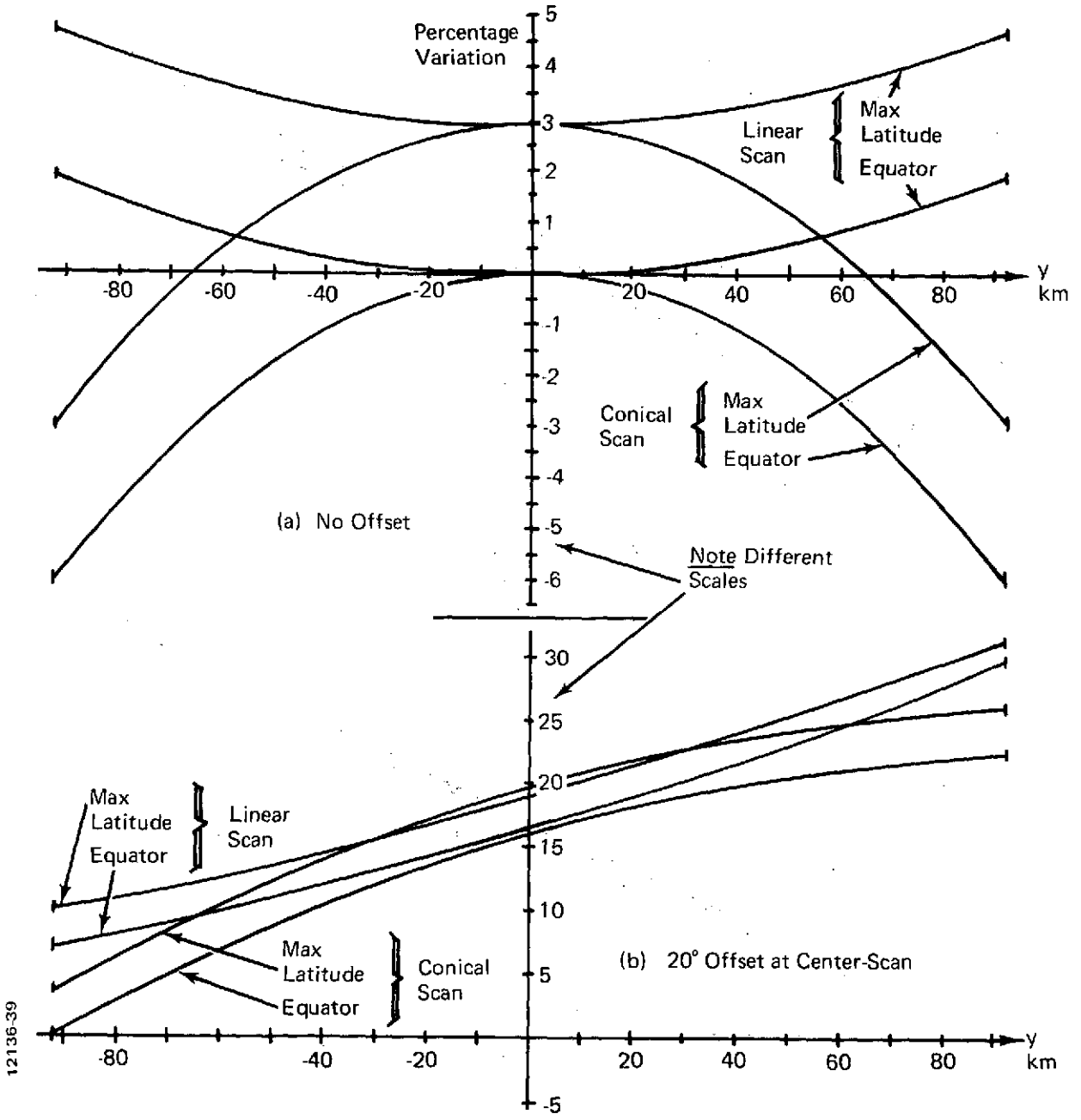

Figure 4-5 Variation in Cross-Track Ground Movement per Sample Relative to Nadir Ground Movement per Sample at Equator

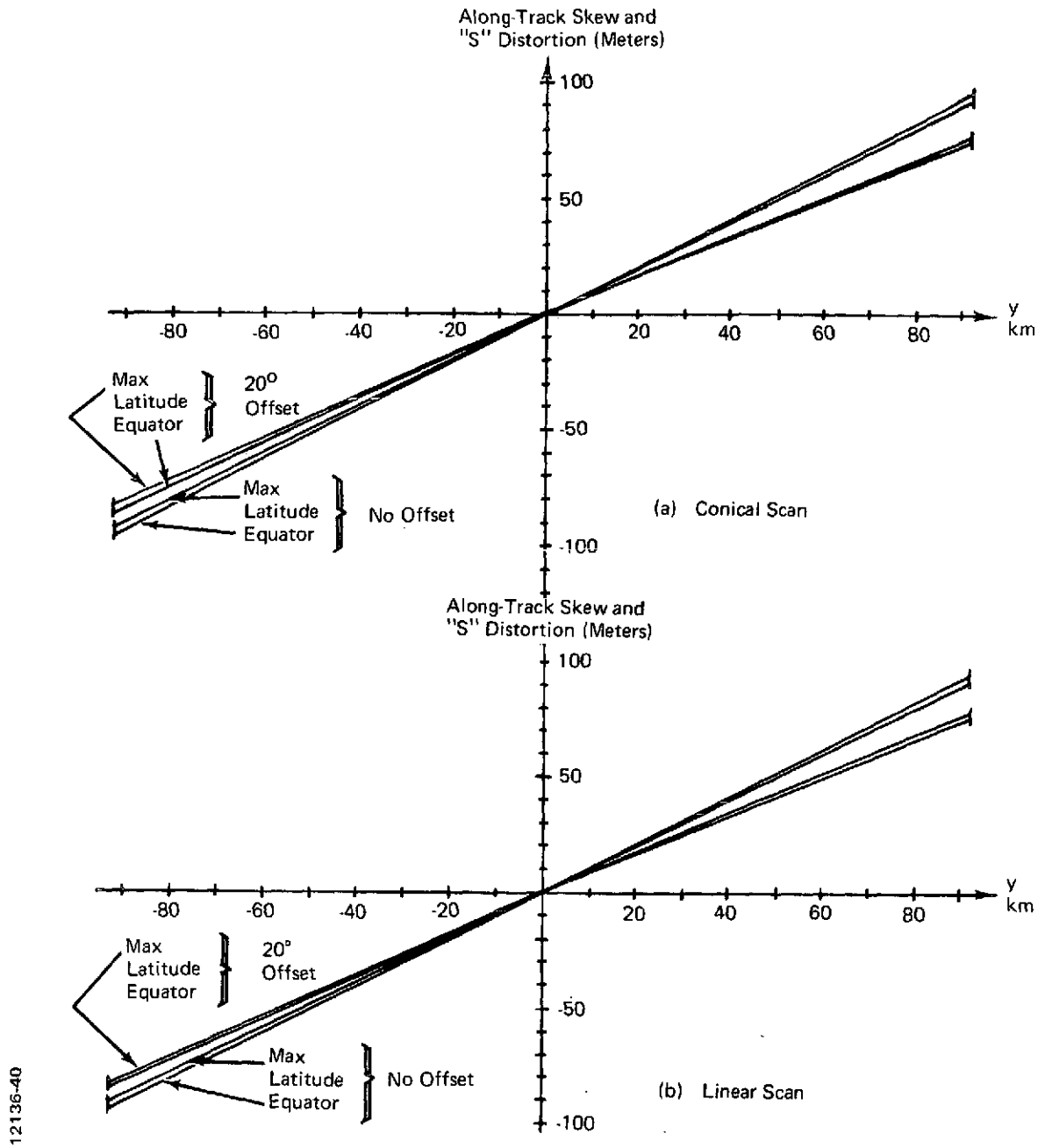

Figure 4-6 Along-Track Skew and "S" Distortion

4.4 UTM CORRECTIONS

The UTM along-track and across-track mapping projection corrections for ±45° latitude are shown in Figures 4-7 and 4-8, respectively. The major corrections are produced by offset scanning and high latitudes, the differences due to changing from linear to conical scanning being relatively small, particularly in the case of along-track corrections. Although the maximum along-track correction is about 10 km and the maximum across-track correction is about 2.5 km, the mean value of any correction may be taken out by simply shifting the frame reference latitude-longitude tick marks by the appropriate amounts. However, this still leaves along-track deviations of up to ±300 m about a mean straight line which is twisted by up to 2.3°. In the case of the across-track deviations, the overall effect after removal of the mean component by shifting the tick-marks is a nonlinear compression or expansion of the scale of the scan by up to 1%.

4.5 SUMMARY OF SYSTEMATIC SCAN SHAPE CORRECTIONS

The previous sections have shown that the only really significant difference between linear and conical scanning is in the basic scan shape (see Section 4.1). In all other cases the scanning mode produces only minor variations about a much larger common component.

4.6 PLATFORM STATE VECTOR EFFECTS

It has been assumed that the attitude accuracy of the baseline satellite will be ±0.01° about all axes. A pitch error of this magnitude produces a ±125-m along-track shift of the whole swath. A yaw error twists the scan, leading to a maximum along-track error of 60 m at the outer end of an offset scan, 30 m at the inner end of an offset scan, and 15 m at the end of a nadir scan. A roll error produces a nonlinear across-track error given approximately by $\Delta y = H \sec^2 \theta \Delta\theta$ where θ is the angle of the scanning ray measured upward from the vertical. At the nadir, a 750-km orbit gives a cross-track error of 125 m; at the outer end of a 20° offset scan, the cross-track error is 170 m.

Altitude errors produce, to a good first approximation, a general expansion or contraction of the scale of the image. With a nominal 750-km orbit, a 1-km variation in altitude would cause a nadir scan to vary by a total of 247 m in 185.2 km; in the case of a 20° offset scan, the center-scan point would shift by 360 m and the 185.2-km scan would vary by a total of 250 m.

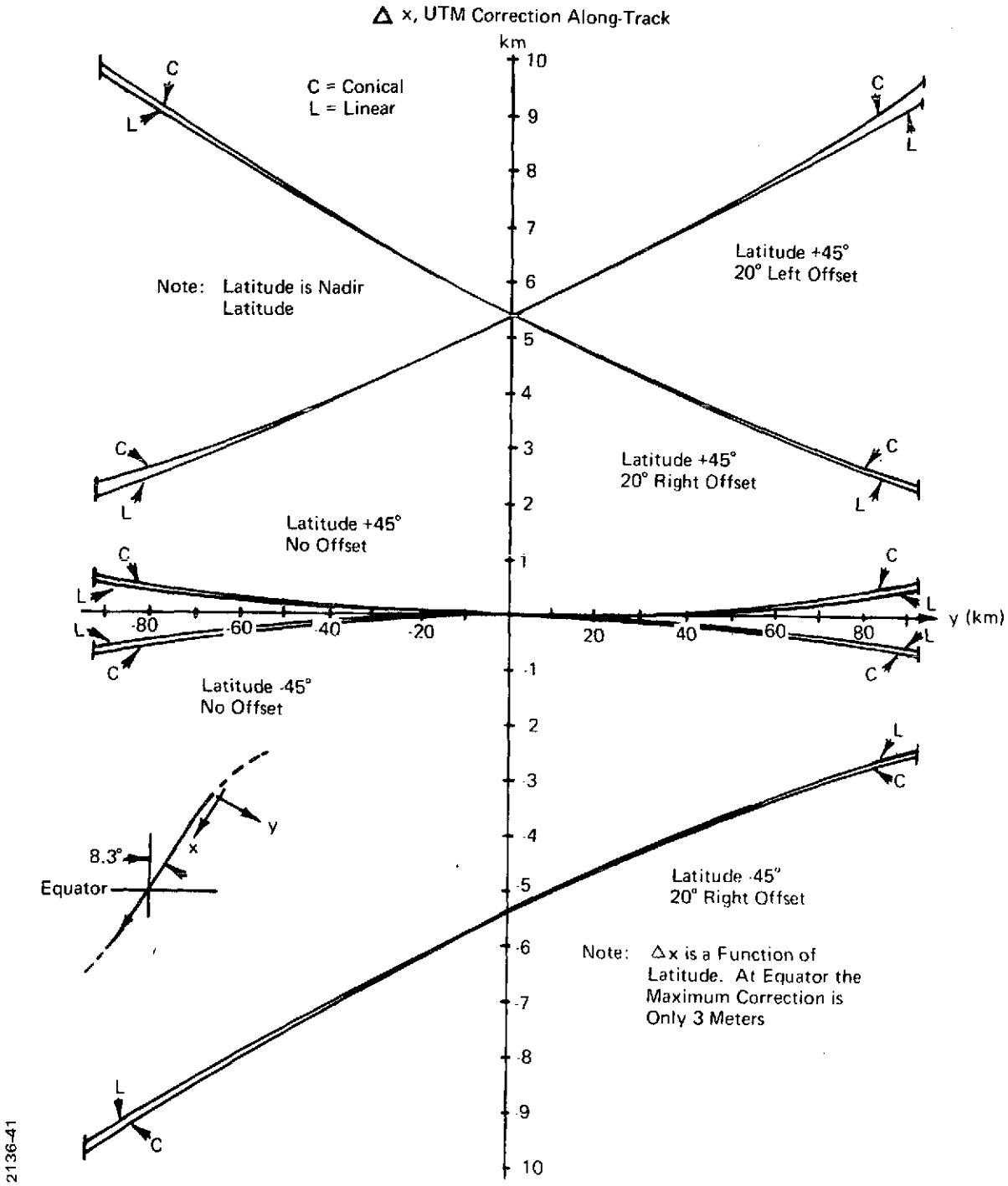

Figure 4-7 Along-Track UTM Corrections

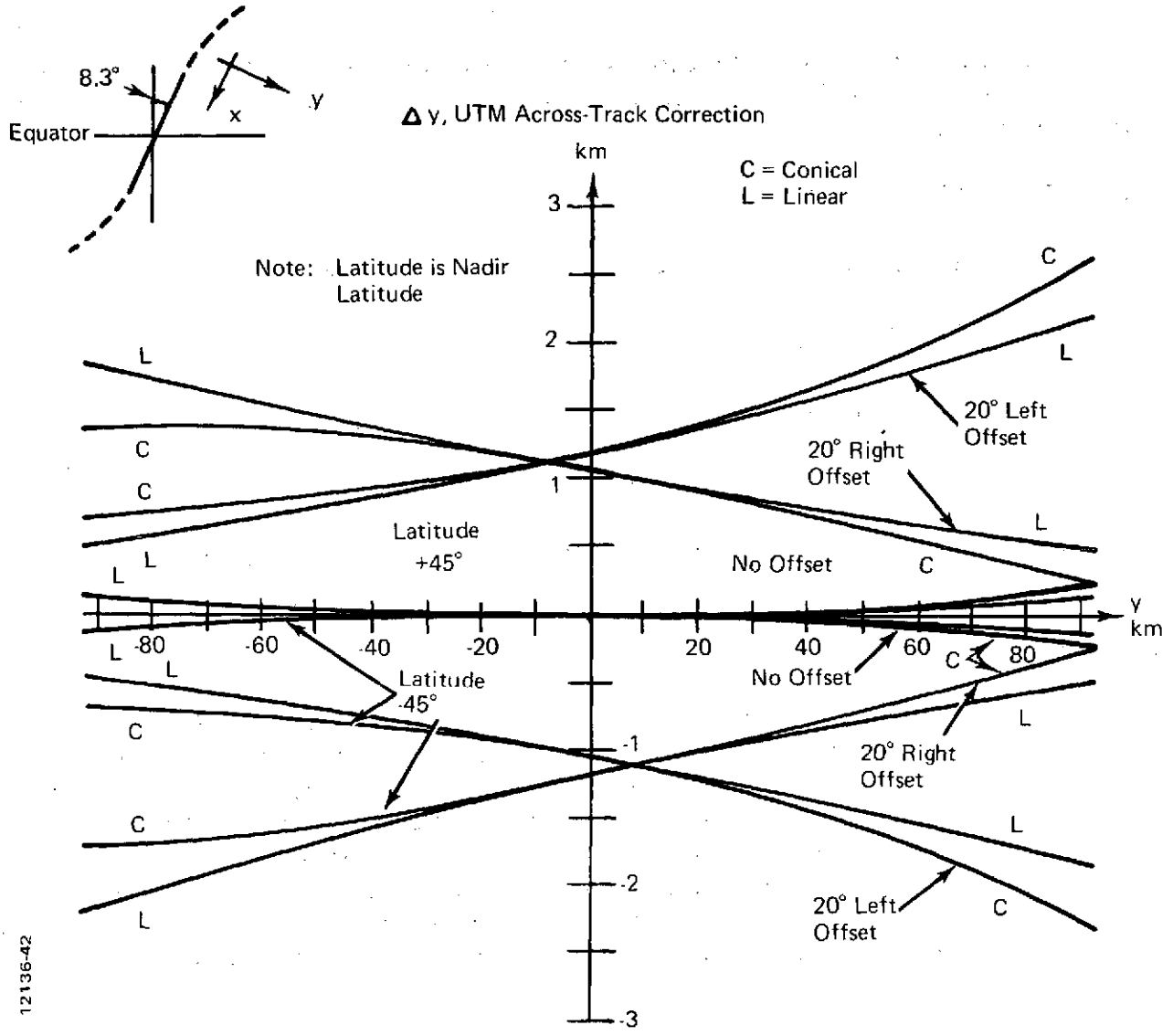

Figure 4-8 Across-Track UTM Corrections

Since in practice the altitude of the satellite will probably be known to better than 100 m, it is not likely that this error will be the major source of mapping errors.

The uncertainties in the along- and across-track positions of the satellite, assumed to be 50 and 30 m, respectively, appear directly as equivalent mapping position errors.

4.7 TERRAIN EFFECTS

In Section 3.1.5 the approximate terrain effect error was given as:

$$\Delta y = \Delta h \left[\tan \theta + \frac{y}{R_e} \sec^2 \theta\right]$$

At the end of a nadir scan, the angle θ is about 7.8° and

$$\Delta y = 0.15 \, \Delta h$$

For a 20° offset scan θ, is approximately 30° and y is approximately 360 km, giving

$$\Delta y = 0.65 \, \Delta h$$

Thus, a terrain height variation of 1 km gives a maximum of 150-m cross-track error for a nadir scan and 650-m error for an offset scan. This is clearly an important source of mapping error. If the terrain being scanned is elevated but basically flat (i.e., a plateau), then the terrain effect error is similar to a satellite altitude error and may be compensated accordingly; the scale may need adjustment, but the relative positions of features will be correct. If the terrain is mountainous, the error may be minimized by setting in a mean altitude error compensation, but the relative position errors will remain.

4.8 DETAILED EFFECTS UPON PICTURE ELEMENT (PIXEL) PATTERNS

As discussed in general terms in Section 3, the ideal rectangular contiguous picture element pattern can only be obtained at one latitude, which may be chosen arbitrarily. At all other points the pattern will expand, twist, overlap, or slide backward and forward relative to adjacent swaths. Figures 4-9 through 4-12 illustrate these effects for typical linear and conical, nadir, and offset scans.

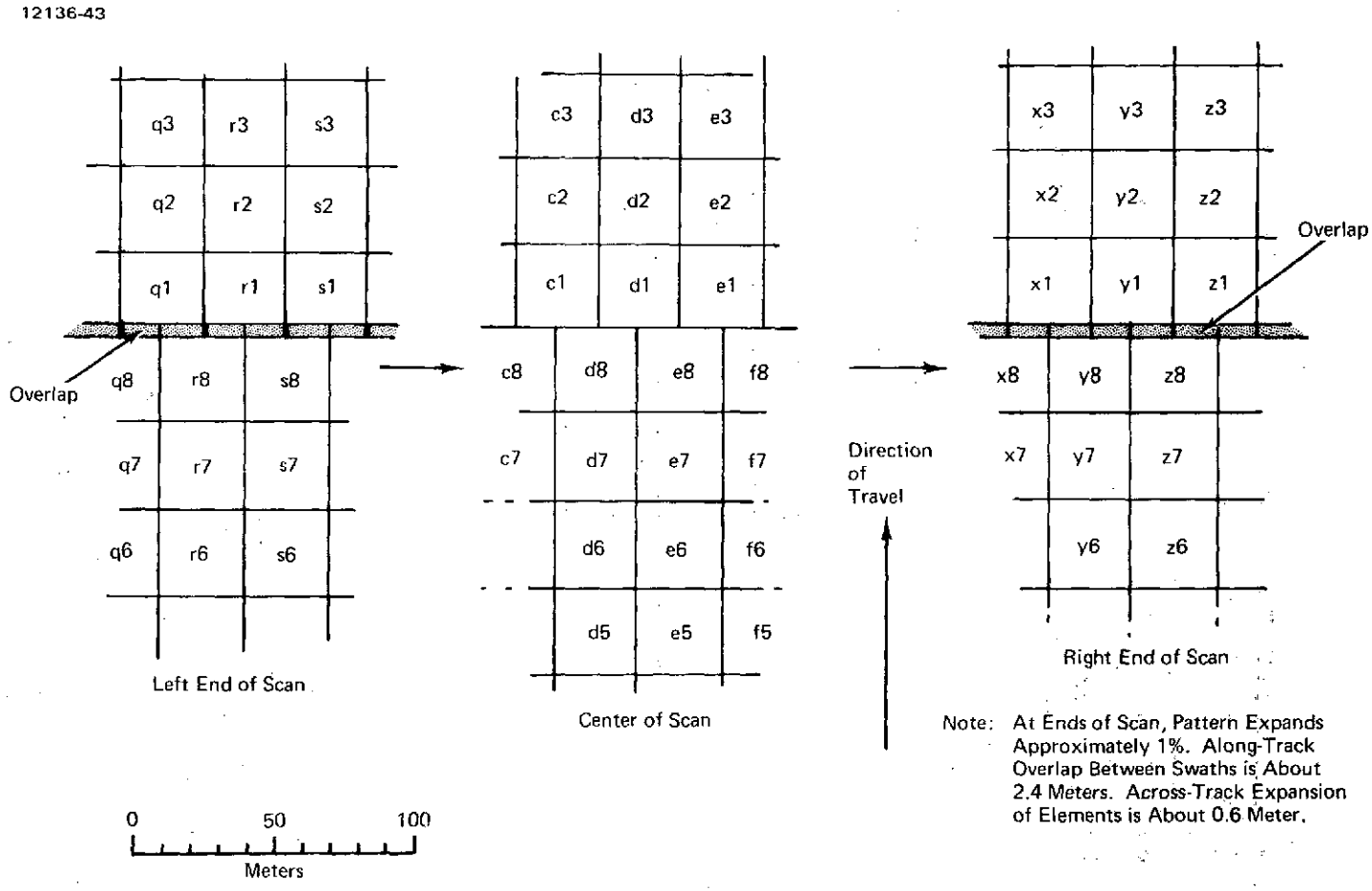

Figure 4-9 Typical Picture Element Patterns for Linear Nadir Scan, No Offset

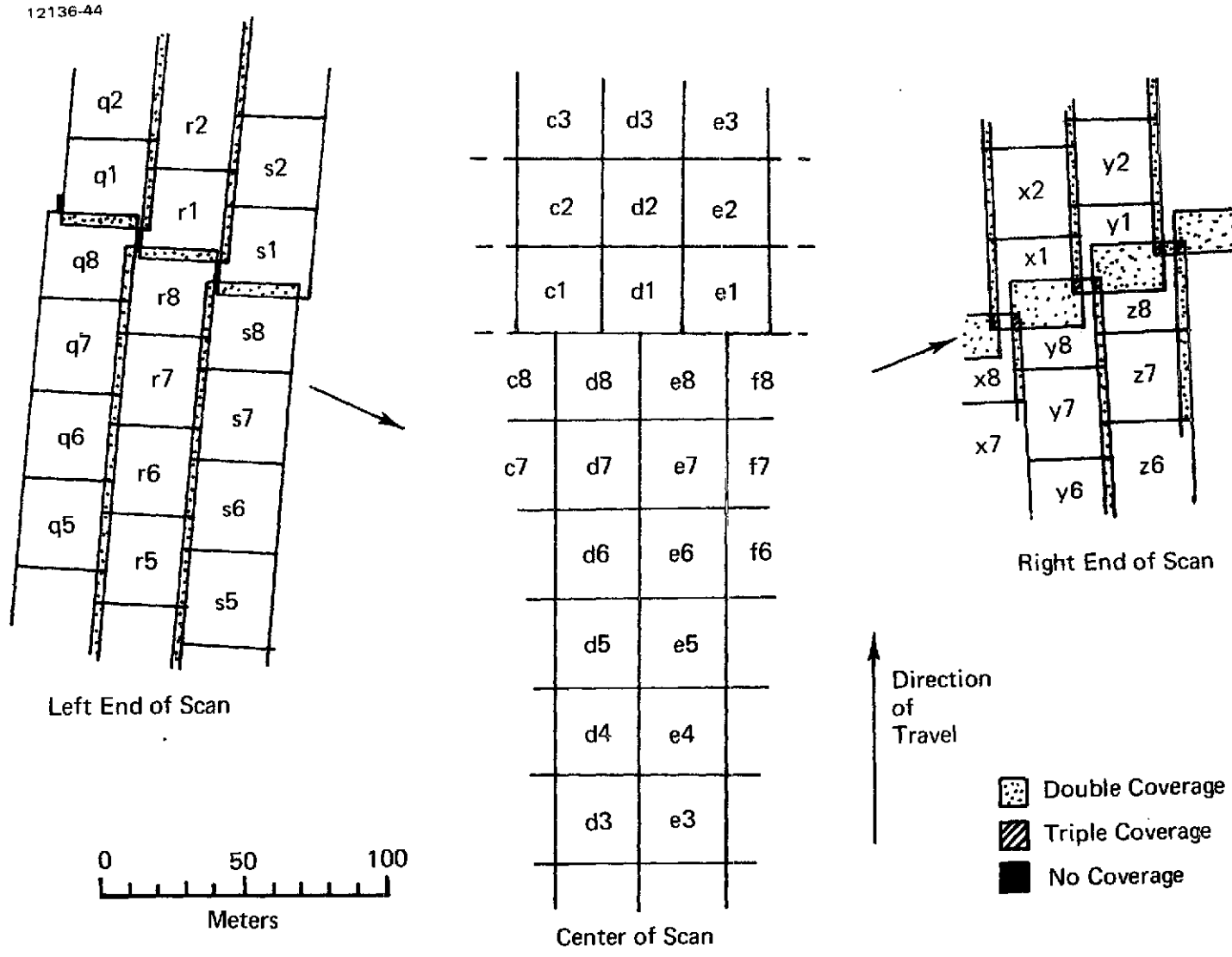

Figure 4-10 Typical Picture Element Patterns for Conical Nadir Scan, No Offset

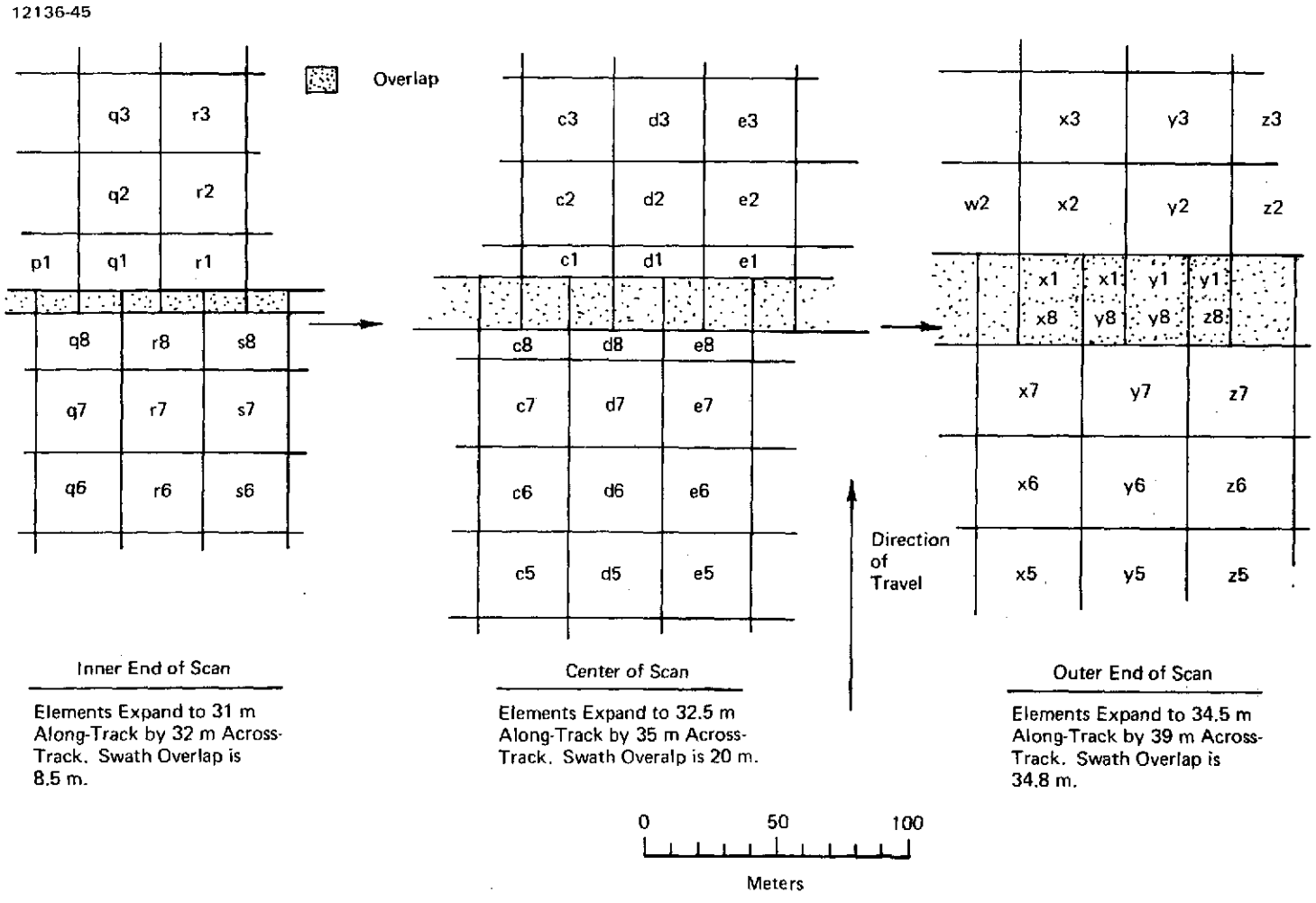

Figure 4-11 Typical Picture Element Patterns for 20° Offset Linear Scan, No Twist

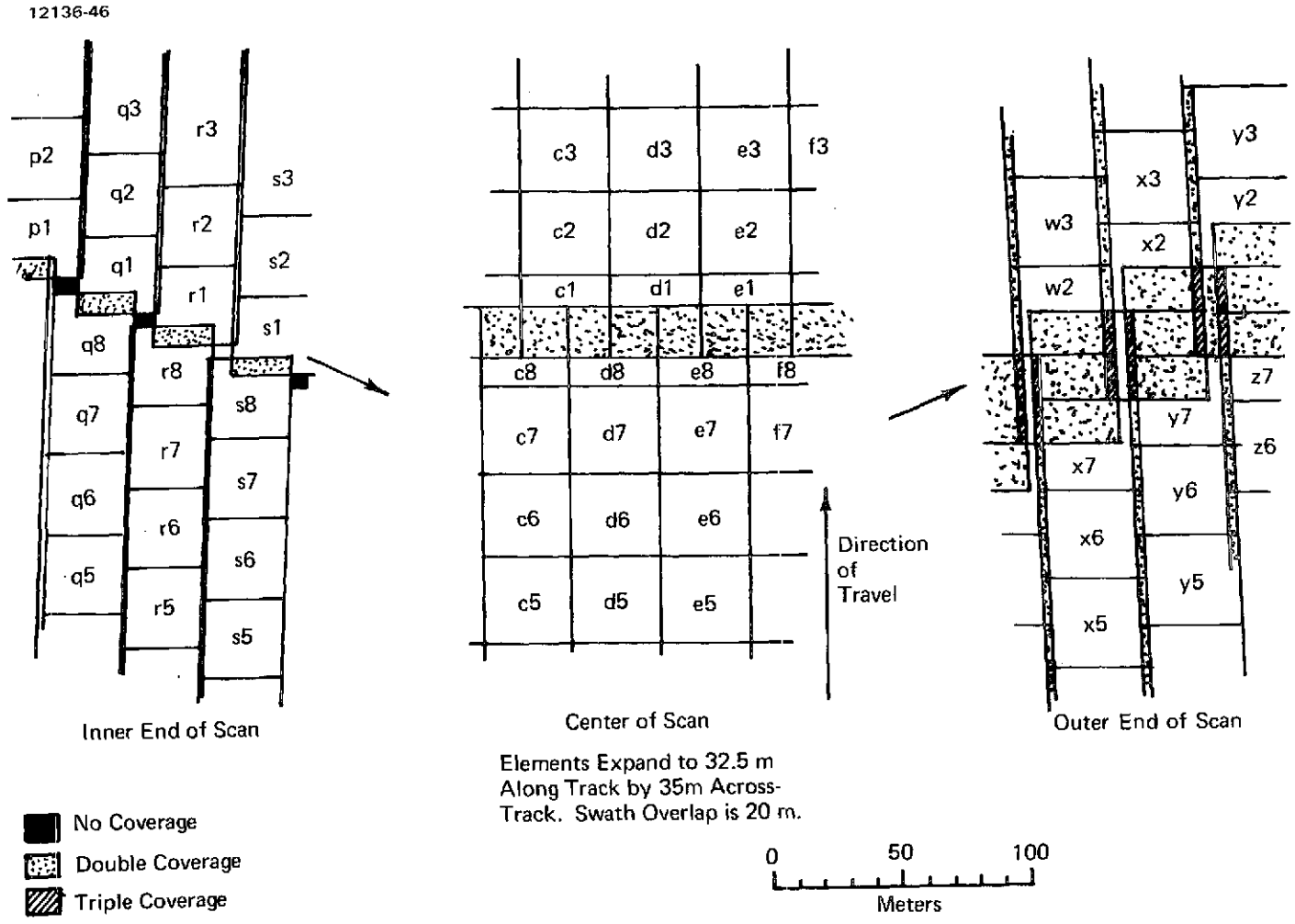

Figure 4-12 Typical Picture Element Patterns for 20° Offset Conical Scan, No Twist

The degree of pixel expansion is similar for linear and conical scans, but the conical scan produces more difficulties in other respects. The most obvious differences are that the element groups at the ends of the conical scans are twisted by approximately 2.3° and step in an echelon formation. These two effects together produce more complicated overlap and aperture correction problems than for the linear scan case, but even in the linear case the problems still exist. The echelon formation is due simply to the basic scan shape (see Section 4.1), the angle at the ends of the scan being 24°. The twist of the element groups is caused by tilting the scanning cone so that it will pass through the nadir. If the axis of the scanning cone were vertical, then the twist would not occur, but the increased slant range and angle from the vertical would have other undesirable effects, principally in terrain effect errors.

4.9 RATIONALE FOR ASSUMING NADIR SCANNING AND A NONROTATING OFFSET FOV

Throughout this section the errors and corrections have been evaluated on the following assumptions:

- A nonoffset scan, whether conical or linear, will always pass through the nadir.
- When the scan is offset, the center-scan point will move directly sideways, normal to the satellite heading, and the scan pattern will not twist.

Figures 4-13 and 4-14 show why it is most desirable to try to realize these two features. In Figure 4-13 the scan at A is a nonoffset, nadir scan, with the tilted cone axis, while the scan at L is the nonoffset conical scan with the cone axis vertical. The maximum ground distance to any point on the nadir scan is 92.6 km, while to any point on the axis-vertical scan it is approximately 228 km. The mapping error due to yaw is therefore at least 2.5 times greater than for the nadir scan and an average of five times greater. Pitch errors will be about 10% greater and roll errors will be approximately the same. The maximum angle from the vertical for the scan at A is about 7.8°, with an average of 3.9°, while for the scan at L it is constant at approximately 17.1°, with an additional 2° for earth curvature. The terrain effects for the scan at L are therefore at least 2.5 times worse than for the scan at A, and an average of five times worse. For the offset scans the same arguments can be made for the scan to be at E rather than Q, but the relative improvement is not so marked as in the nonoffset case.

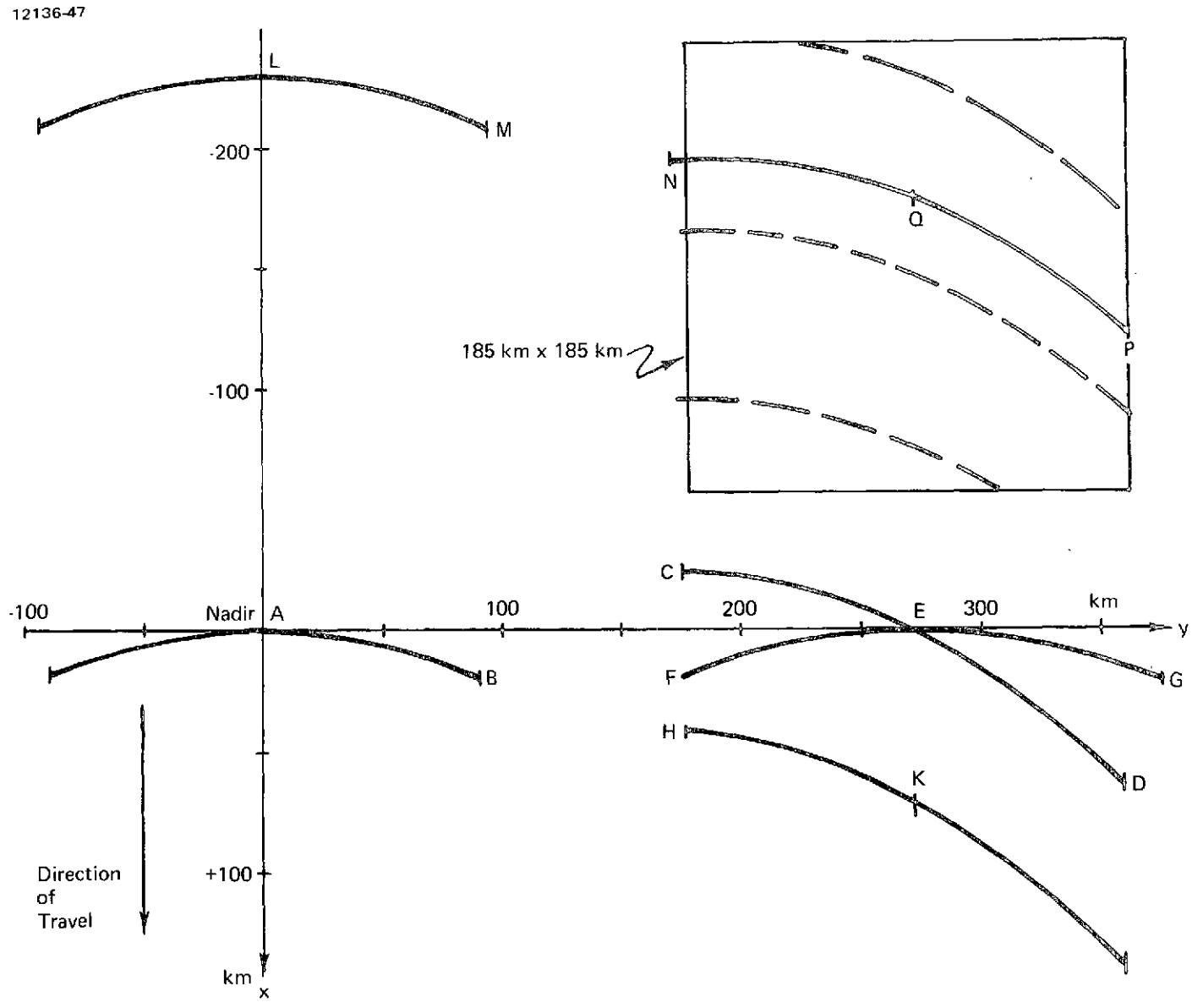

Figure 4-13 Conical Scan Positions and Twists

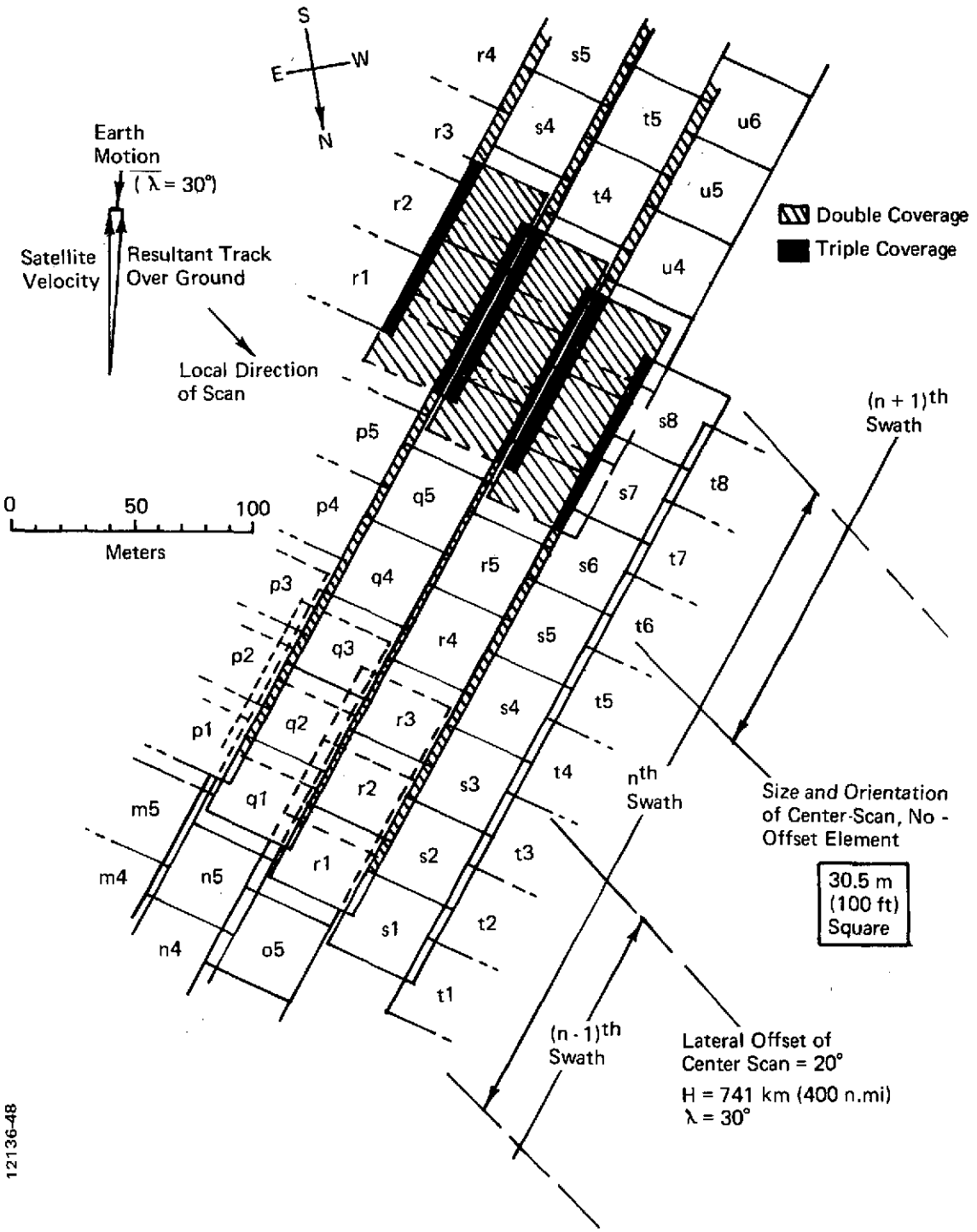

Figure 4-14 Picture Element Pattern for Conical Offset Nadir Scan (Point "D" in Figure 4-13)

The case for a nontwisting offset scan is clearly shown by the difference between the scans CED and FEG in Figure 4-13 and the element pattern shown in Figures 4-14 through 4-16. These patterns are typical of those which would be produced by one early EOS conical scanner proposal. The along-track distance from C to D in Figure 4-13 is approximately 90 km, which has a severe impact on both precision digital processing and direct image recording. Both these points will be discussed in the appropriate sections of this report.

The picture element patterns in Figures 4-14 through 4-16 require little additional comment to emphasize the potential mapping, cosmetic, and aperture correction problems. Figures 4-11 and 4-12 show that pixel expansion and increased side and fore-and-aft overlap are characteristic of any offset system. However, with the addition of twist of the whole scan, the overall problem becomes worse. The patterns shown are for a conical scan, but the common twist of the picture element groups is characteristic of either type of scanner. By coincidence, it is approximately 24°, which is the scan angle variation of the conical scan. Thus, at the outer end of the offset, twisted conical scan, Figure 4-14, the scanning direction is at an angle of 48° and actually has an along-track component that is slightly greater than the across-track component. At the inner end of the scan, the twist compensates the conical scan and the scan direction is almost directly cross-track. However, the overall 24° twist of the individual elements remains.

The length of each eight-element group is nominally 240 m. With an overall twist of 24°, the cross-track difference between the ends is approximately 100 m, or about three times the nominal picture resolution. It will be obvious that the resultant sawtooth distortion of linear features in a picture that is not corrected on a line-by-line basis would be very noticeable and quite unacceptable. In an overall untwisted scan, the maximum error of a similar type is the slight element twist at the end of a tilted conical scan — approximately 2.3° or a 10-m sawtooth. Even uncorrected it is doubtful whether this would be noticeable.

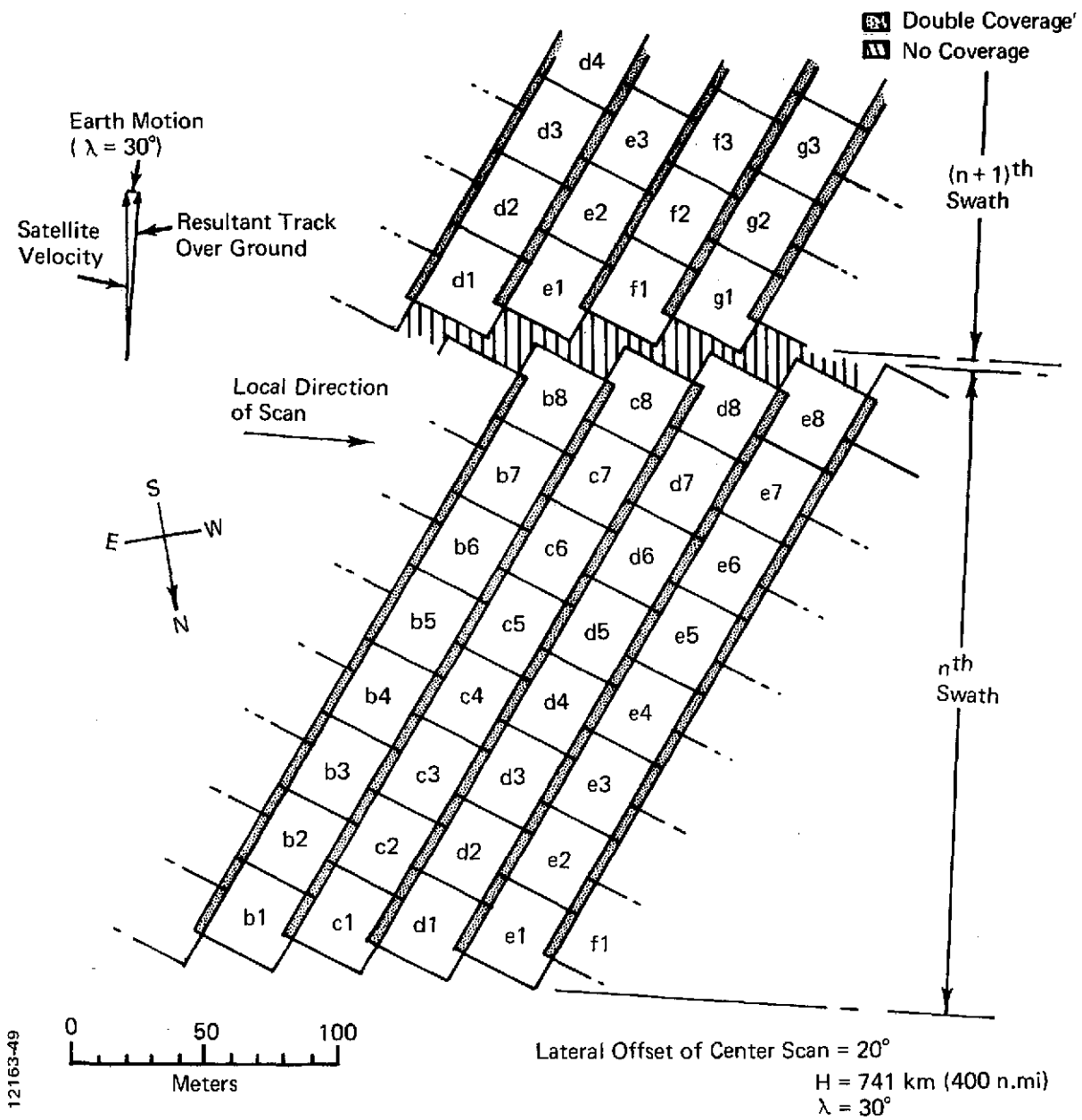

Figure 4-15 Picture Element Pattern for Conical Offset Nadir Scan (Point "C" in Figure 4-13)

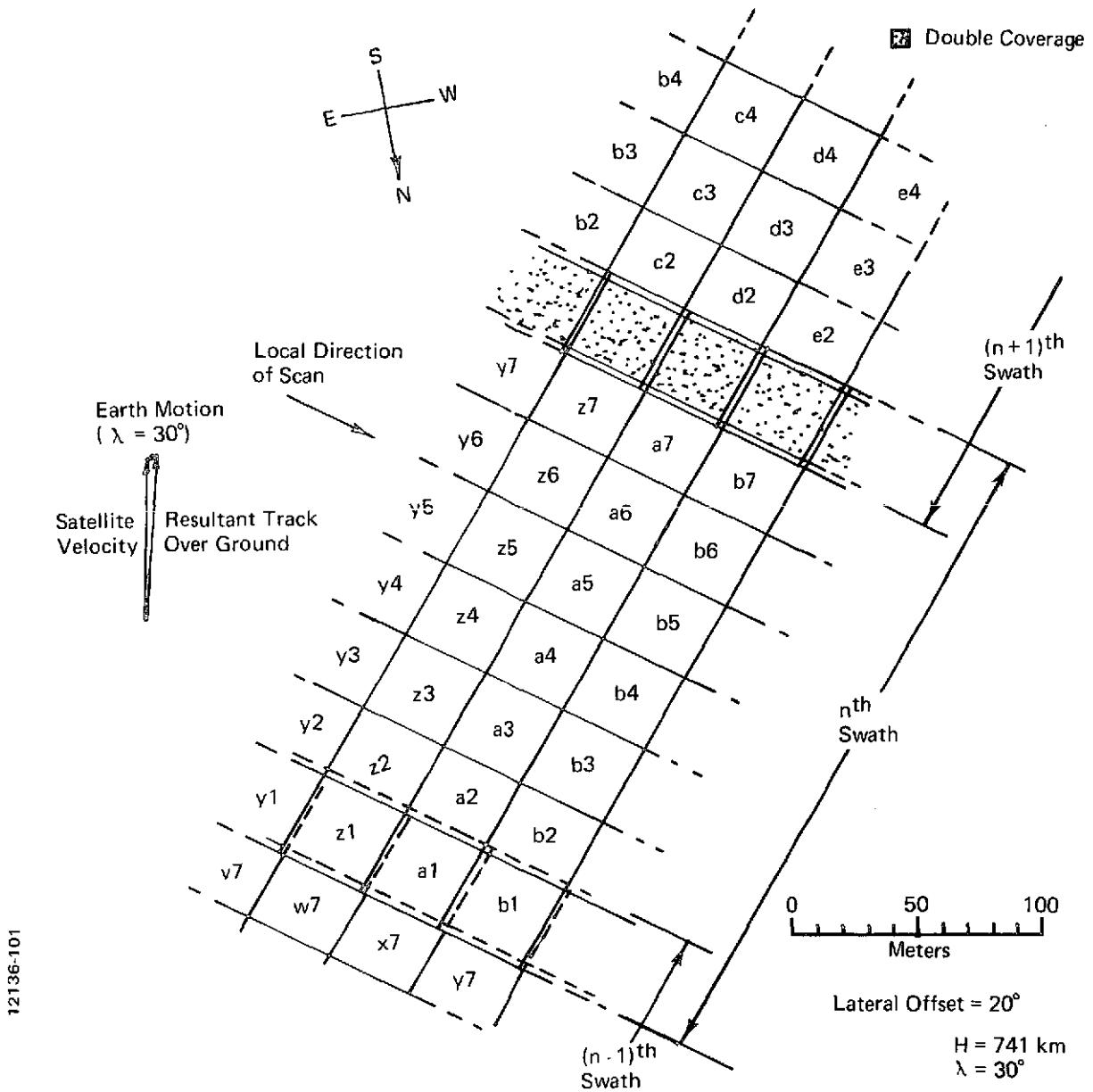

Figure 4-16 Picture Element Pattern for Conical Offset Nadir Scan (Point "E" in Figure 4-13)

SECTION 5

DIGITAL PROCESSOR IMPACT

5.1 INTRODUCTION

An analysis was performed to determine the impact of a conical scanner versus a linear scanner on an all-digital precision processor. The previously configured conical and linear scanners were used in this analysis. The results of the analysis were expressed in terms of cost, throughput, accuracy, and complexity. Recommendations were also made regarding sensor operation and ground processor products. These recommendations were chosen so as to minimize the impact of the conical scanner with virtually no impact on the sensor-spacecraft or utility of the data products.

All-digital processing is particularly appealing to image processing because of the flexibility of operations that may be performed on the data. In addition, physical realization of some processing operators may be extremely difficult if not impossible using analog systems. To cost-effectively take advantage of the all-digital processing concept, the configuration and implementation of such a processor are critical.

As a part of this analysis, an all-digital processor was configured as far as functional operators were concerned. Three requirements were apparent with respect to the processor configuration. The processor should be designed and dedicated to perform generalized image processing in order to maximize throughput. Also, the processor should be flexible enough to allow different processing operations to be performed. Finally, in view of the immense data sets, instruction execution times need to be minimized to meet image throughput requirements (40 scenes/day with two 8-hour operating shifts means 4.8 μ sec/pixel).

Based on the above requirements, the all-digital processor was assumed to consist of a medium-size general-purpose controller and special-purpose implementation hardware. The functions of the controller would be to provide computational support for performing corrections, to supervise the data flow, and to supply control to output devices such as magnetic tape recorders and image recorders. The special-purpose hardware would be used to perform the actual processing operations. Such a system could take advantage of state-of-the-art techniques while simultaneously processing adequate software and hardware flexibility to incorporate new advances and meet future processing requirements.

The actual processing operations are grouped into three areas (radiometric, aperture, and geometric correction) and the all-digital processor was configured into these three operational areas. The following section contains this definition of the digital processor along with justification for performing particular operations at given points during the correction process. The last three sections discuss the impact of the conical scanner versus a linear scanner on the radiometric, aperture, and geometric correction processes, respectively.

5.2 DEFINITION OF THE DIGITAL PROCESSOR SUBSYSTEM

The digital processor consists of all hardware and software necessary to perform required data corrections and to generate data products such as high density digital tape (HDDT), computer compatible tape (CCT), and film. It receives an HDDT supplied by the telemetry subsystem and performs radiometric, aperture, and geometric corrections. In addition, the necessary data products are generated.

In order that the conical scan impact problem be addressed, a digital processor was configured. Figure 5-1 is a diagram of that configuration.

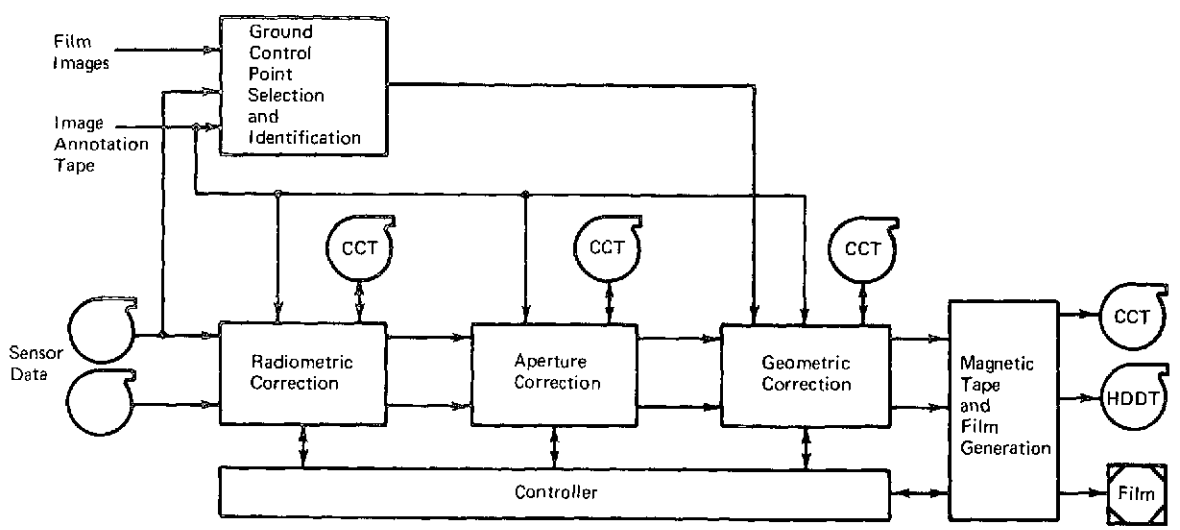

Figure 5-1 Data Processing System Concept

The first operation performed on the data is radiometric correction. This operation is best performed initially, because the order in which pixels are read from the input tape is a well-defined sequence of the detector array in each band and spatially. Once geometric or aperture correction processing is performed, this sequential order may not necessarily be true. Since the radiometric correction is one-dimensional, it could be accomplished using a table look-up incorporating a high-speed random access memory. The memory could be refreshed if necessary using the image annotation tape (IAT). Since there are 50 individual detectors in the baseline scanners, each with 64 (6-bit) addresses, the total storage required to implement the correction process would be 3.2 K pixels.

Another form of radiometric correction that will be performed later is film gamma compensation. This correction is done on all data being outputted on film. Assuming this correction is homogeneous across one frame, only 64 pixels of memory would be required.

Subsequent to radiometric correction is aperture correction. This may be optional depending on image content, signal-to-noise ratio, and user requests. The aperture correction operation must also be performed before geometric correction, since after that point, adjacent pixels may not necessarily have adjacent or near adjacent IFOVs on the ground. It should be performed after radiometric correction so that the memory required for geometric correction can be used during aperture correction, because it is a two-dimensional operation.

Aperture correction is performed by deconvolving all system effects that degrade spatial frequency response. Such items as the optics, detector size, detector integration time, and video amplifier are considered. The actual deconvolution is carried out by "combing" the data with a function derived from the inverse MTF curve of the system and the signal-noise spectra (Wiener filter).

An additional type of aperture correction might also be performed on all data that are to be outputted on film. The purpose is to compensate for the shape of the recording spot of the film recorder, i.e., an electron beam recorder (EBR) or a laser beam recorder (LBR). This operation would be done after geometric correction and before output to the film recorder.

Except for the film recorder aperture correction, the last operation that is performed is geometric correction. At this point the image is converted to the specified map projection, whether UTM, Polar Sterographic, or the recently proposed "Space Oblique Mercator Projection." Such effects as

earth rotation and curvature, attitude and ephemeris, and internal sensor geometry are compensated. The correction is implemented by taking an oversized rectangular image output area and filling it up by pulling pixels from appropriate locations in the input image. Geometric correction can also be done by using a film recorder that may be deflected in both dimensions dynamically; however, if digital tape is also a product, curved film scanning does nothing to correct these data.

In general, the desired pixels will lie along curved lines between available pixels in the input data array, in which case either nearest-neighbor selection or interpolation must be used. To minimize input-to-output computations, the output is usually divided into a rectangular grid chosen so that straight lines connecting the corners in the input space deviate from the true curved lines by only a fraction of a pixel. Figure 5-2 illustrates how the output grid is selected. In this way only a few pixels have to be mapped from output to input image. All other pixel locations may be inferred using bilinear interpolation, which is valid since the size of the print blocks was chosen accordingly.

The actual computation of the pixel address is done by the general-purpose computer and is implemented by special-purpose hardware. If the computing load is heavy, this task may have to be delegated to a special-purpose system.

As pixels are obtained from the input image (nearest neighbor or interpolation), each output image line is filled up until the entire image is complete. The important system property during this phase of the correction process is high-speed random access with bulk memory in order to fetch pixels at a rate which would contribute to high throughput. As each line is formed, it is loaded into a storage medium (disk, drum, or magnetic tape). If the output is to be HDDT or CCT, the image is transferred on a line-to-line basis to the associated tape.

A peripheral activity to geometric correction is ground control point (GCP) location. This operation identifies points on the ground with points in the image based on an image library as shown in Figure 5-1. The input to GCP operator is the sensor data, the IAT, and some form of uncorrected images. The images are used only to initially select and define the GCP. Once selected, the actual GCP detection and matching is performed digitally using the library for temporal registration. GCP identification will be used only for a few selected points in each pass primarily to develop position offset and rotation data which in effect update the accumulated biases in the attitude measurement system. The supplemented positioning data are used during the geometric correction phase.

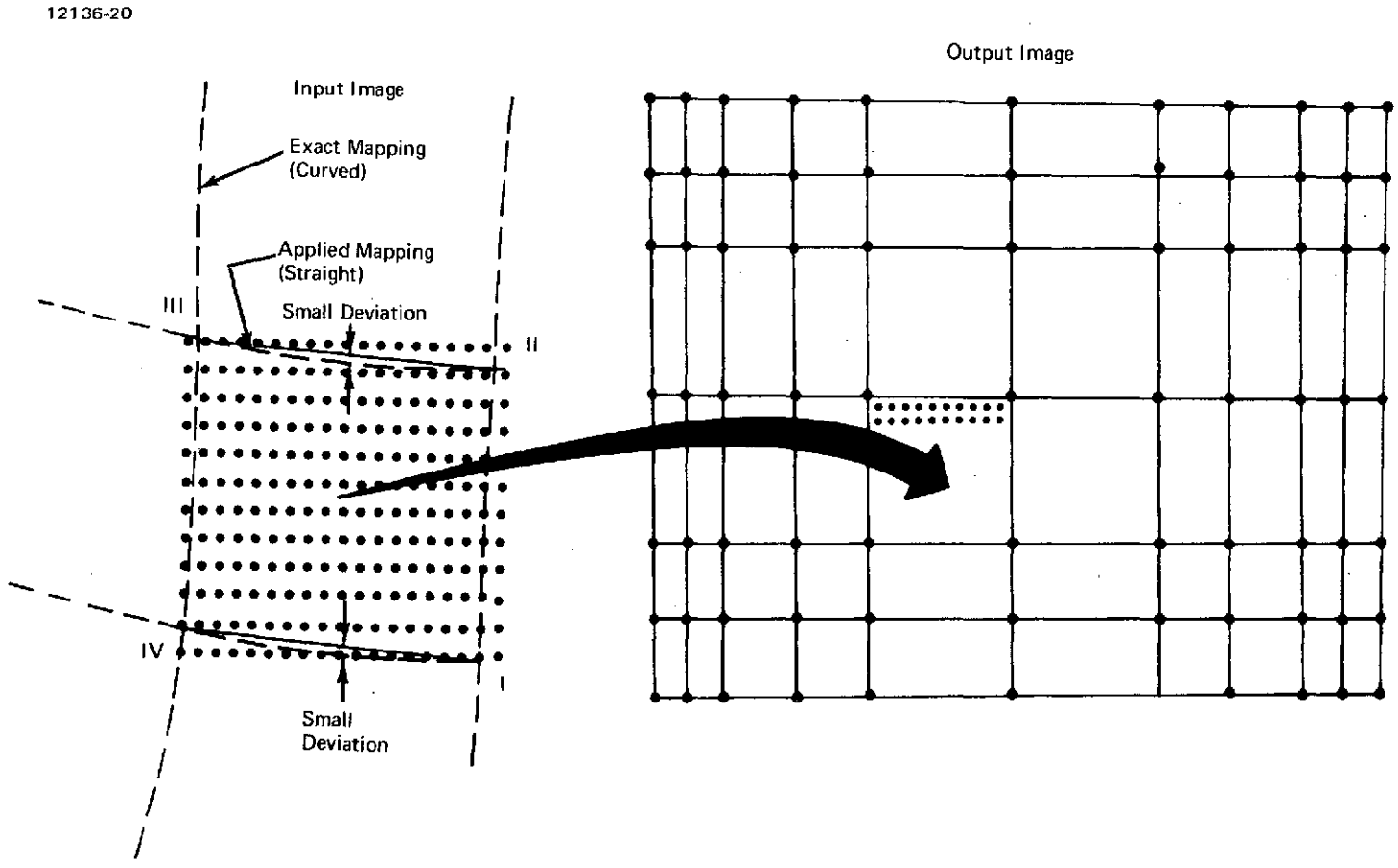

Figure 5-2 Print Block Selection

5.3 RADIOMETRIC IMPACT

Radiometric correction is used to make the sensed radiant levels more closely related to the input radiant power or the true ground-reflected radiant power. The difference between these powers is defined as radiometric error and is usually due to a multiplicity of causes. Some of the resulting effects may be calibrated out while others are complex functions of sun angle and look-direction.

All radiometric errors may be classified in one of two categories, internal and external. Examples of external errors are variation in atmospheric absorption, reflection, emission, and scattering. Examples of internal errors are shading due to the optics, detector bias, drift, and nonlinearity, and variation in amplifier gain. The easiest to correct are the internal errors. In fact, many of them may be performed onboard the spacecraft. External errors tend to be more complex and are known with less confidence than internal ones. To date, little of the knowledge of external errors has been incorporated into the correction process.

For the purpose of this analysis, all radiometric correction was assumed to be performed on the ground on only internal errors. It is assumed that the sensor will include an internal calibration system that periodically obtains the response of each detector to a known range of radiance. Using the calibration data, a set of correction coefficients for each detector in each spectral band is computed. These coefficients are used to compute the corrected radiometric value given the uncorrected one. The actual correction process is carried out by using a data point's radiometric value as the address of a memory where corrected values are stored. If the location addressed contains the corresponding corrected value, the data read out will be the radiometrically corrected version of the original data point. The above table look-up approach is the most efficient when throughput is premium and the errors themselves are stable. The memory is used in the "read" mode with the "write" mode used to refresh the correction process when necessary.

If this approach is used, two specifications are necessary: (1) storage required and (2) memory refresh rate. The impact of a conical scanner versus a linear scanner hinges on these specifications. Since both sensors have the same number of detectors (50), the memory required for each is 3.2 K pixels. Because of the radiometric stability of solid-state detectors, the refresh rate in both cases will be low. No evidence is apparent that indicates either of the scanners introduces excessive radiometric drift. The conclusion is that no impact is incurred during this phase of the correction process. In retrospect, this conclusion applies to all radiometric correction schemes including onboard processing.

5.4 APERTURE CORRECTION IMPACT

In multispectral scanners, aperture correction is the compensation for system effects which degrade spatial frequency response. Once aperture correction is performed, the MTF should be near unity for all spatial frequencies present in the image. The degree to which unity MTF can be obtained is a function of the MTF and the signal and noise spectra. Aperture correction is implemented by "combing" the data with a function derived from the inverse MTF curve of the system. A noise compensation or Wiener filter is also included.

The impact of the conical scanner versus a linear scanner involves the computation and implementation of this inverse MTF function. In discussing this impact, the method of derivation of the inverse MTF function (applicable to both the linear and conical scanners) will be presented. The operations performed in this derivation will be the same for both scanners; however, the specific functions involved will vary. The derivation will be discussed in detail because the impact of the conical scanner is not superficially apparent.

Although the method of derivation of the inverse MTF is discussed in detail, the example derivation is not rigorous as a result of simplifying assumptions. The actual rigorous derivation would be a one-time calculation for the specific scanner(s) finally used in the system. The less-than-rigorous example which follows is, however, adequate to illustrate the impact of the conical scanner versus the linear scanner.

Regardless of the scanner geometry, the first necessary information is the MTF of the system. This curve contains the spatial frequency degradation due to the optics, the finite size of the IFOV, the integration time of the IFOV, and the video amplifiers. It is important that the MTF be known in the coordinate system where the data will be "combed." Since aperture correction will be performed before geometric correction, the relevant coordinate system is one of swath or line number and lateral element number.

To simplify the calculations, the telescope will be assumed as perfect (unity MTF). In addition, the detector integration time will be assumed to be zero. The bandwidth of the video amplifiers will be specified later. Based on these assumptions, the primary MTF degradation is due to the finite size of the IFOV. The MTF curve may be computed from the shape of the IFOV in the image coordinates, the line number, and the lateral element number.

For the linear scanner, it is a square with a width of 2 T. The two-dimensional MTF of the system is given by the Fourier transform of the IFOV, namely:

$$MTF = \frac{4 \sin \omega_x T \sin \omega_y T}{\omega_x \omega_y} \qquad (5\text{-}1)$$

where

MTF	=	value of MTF curve at (ω_x, ω_y)
ω_x, ω_y	=	radian spatial frequency in x and y, respectively
T	=	one-half the width of the IFOV.

Before the IFOV in the relevant coordinate of the conical scanner may be found, some discussion is necessary regarding this coordinate system. Since data are obtained in equal polar angle increments, an x-coordinate defined as the distance along the scanning arc will be linear in the polar angle. The y-coordinate will be measured from the origin to where the arc crosses the y-axis. Figure 5-3 shows the scanning arc, the coordinate system, and the shape of the square IFOV in this system. The MTF in this system is obviously a function of location within the swath. For the linear scanner, the MTF is spatially invariant; however, this is not true for the conical scanner.

In general, the MTF for the conical scanner will be:

$$MTF = \frac{4 \sin \omega_y T \sin [\omega_x - \tan \eta \omega_y] T}{\omega_y [\omega_x - \tan \eta \omega_y]} \qquad (5\text{-}2)$$

where

MTF	=	value of MTF curve at (ω_x, ω_y)
ω_x, ω_y	=	radian spatial frequency
T	=	one-half width of normal square IFOV
η	=	polar angle ($\pm 24°$) of conical scanner.

For simplicity, the Wiener filter will be assumed constant for all (ω_x, ω_y). In practice, it will not be true; however, this assumption will not affect the impact study. Hence, the incoming optical radiation has been subjected to an MTF curve of the form of Equations 5-1 or 5-2, depending on which scanner was used.

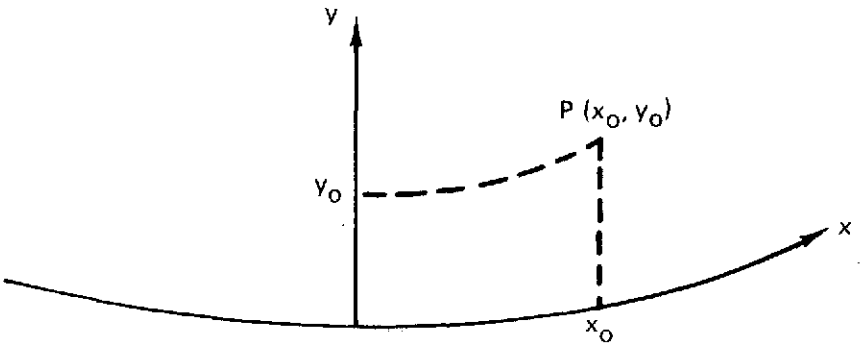

Angular Cartesian System

IFOV in Above Coordinate System

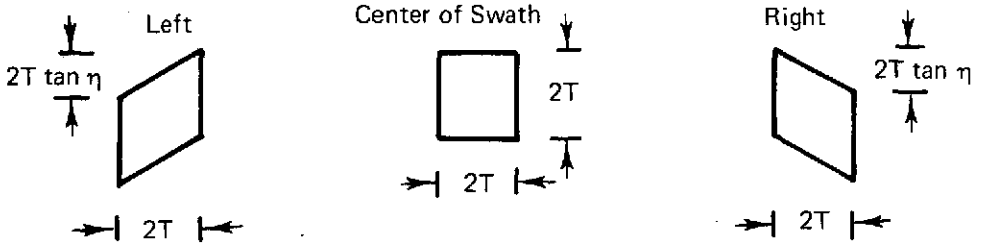

12136-21

Figure 5-3 Conical Scan Coordinate System

The final piece of information is the sample rate of the detector as it traverses the region of interest. The sample rate will determine in part the limiting resolution of the system. Since spatial frequencies exist beyond one-half the sample frequency, aliasing will occur, but measures may be taken to prevent it. Figure 5-4 illustrates this problem for the linear scanner assuming one-third IFOV overlap between samples in the across-track direction and adjacency in the along-track dimension.

At this point the bandwidth of the video amplifier may be picked so that it is unity out to some cut-off frequency and zero thereafter. This could be done by inserting a Butterworth filter into the video system and would eliminate aliasing for all spatial frequencies lying directly on the x-axis. All other spatial frequencies will be aliased to a degree depending on the relative magnitudes of its x and y components. Aliasing could be solved in the y-axis using delay lines; however, since it must be done onboard the spacecraft, it may not be feasible.

Once the detector is sampled, regardless of the spatial frequency content, the maximum apparent frequency will be one-half the sample rate. Hence, the MTF curve that is to be compensated may be assumed to be periodic outside this frequency interval of interest. Since no information lies outside the fundamental period centered about the origin, no change has been effected.

The function used to deconvolve the data will be the arithmetic inverse of the MTF curves given by Equations 5-1 or 5-2. The resultant periodic inverse MTF curve will be expanded into a Fourier series. The result will be a set of coefficients of "sines" and "cosines" terms as a function of increasing harmonics of the fundamental period. As is the case in this derivation, the inverse MTF function is not closed form integrable. For this reason, the MTF function for the linear scanner is assumed to be of the form:

$$\text{MTF} \frac{K}{(\omega_x^2 + r^2)(\omega_y^2 + s^2)} \tag{5-3}$$

where

K, r, and s are constants.

The constants K, r, and s were chosen to match the true curve given by Equation 5-1 at the origin and at the end points in each axis. Since the inverse of Equation 5-3 is a second-order polynomial in ω_x and ω_y, it is integrable in closed form.

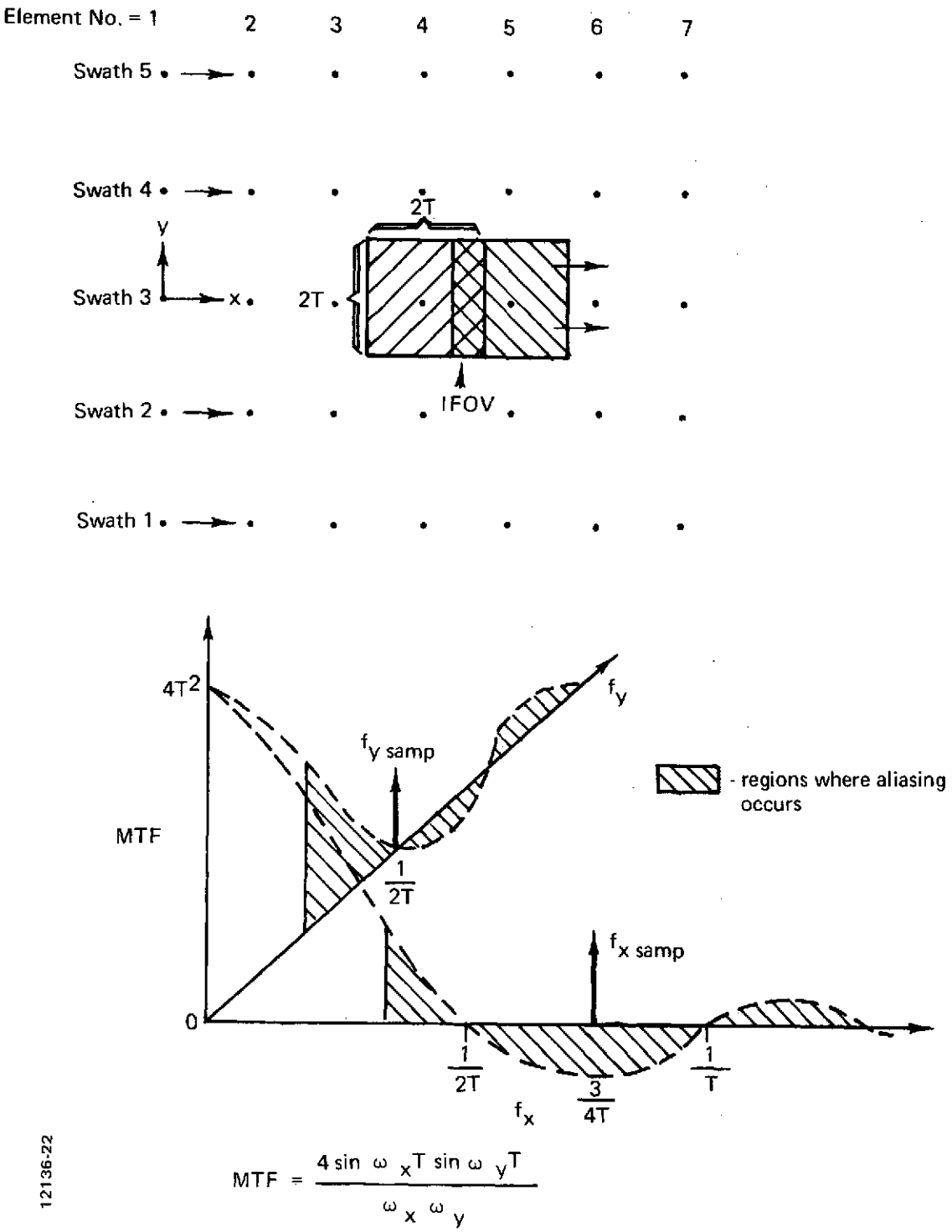

Figure 5-4 Aliasing in Sampling

The Fourier series will now be Fourier transformed to return to the spatial domain. The result will be a set of delta functions of varying weights equally spaced in some fashion. These locations should conform to the locations of available samples. In retrospect, the arguments of the "sine" and "cosine" term should have been chosen so that this occurs.

At this point, skew caused by finite array sampling and earth rotation must be discussed. This skew does not significantly affect the shape of the MTF curve; however, it does cause a shift when a detector output is sampled. This shift is important because, when the Fourier series is computed, it is necessary to ensure that the arguments of the "sines" and "cosines" correspond to points in the spatial domain where sample points exist. The shift causes the arguments of the Fourier series to not be merely a product of an ω_x series and an ω_y series. The amount of cross-producting necessary is, of course, a function of the skew. This problem is independent of which type of scanner is used and must be addressed for both. The problem is more severe analytically for the conical scanner, since the skew varies depending on swath location. This is caused by the unorthodox coordinate system necessary to maintain equally spaced samples. To simplify the derivation, skew effects will not be considered.

Once transformation is accomplished, the set of delta functions constitutes the deconvolving function. The center of the delta function array is placed on some sample point. The various weights are multiplied by the values of the data points and summed. This sum is the new value for that central data point. The entire delta function array is then stepped over one pixel, and the above arithmetic process is repeated. This procedure continues until all the data have been corrected. It should be noted that the swath ends will not be aperture corrected because part of the delta function array will extend into an area where data are not available. The number of coefficients that should be used is related to the quantization level. If 6 bits are used, the weighting of any point should be less than 1/2 bit or 1/128. Any weight less than this should be neglected.

The coefficients of the arrays were computed for the linear scanner neglecting skew and are shown in Figure 5-5. Note that the alternation of the sign tends to emphasize high frequencies and deemphasize low frequencies. Computation of the array for the conical scanner is not shown; however, the nature of the coefficients will not change to any great extent.

The impact of a conical scanner versus a linear scanner involves the computation and implementation of the deconvolving array. The computation is considerably more complex, but it involves only about one-half an additional

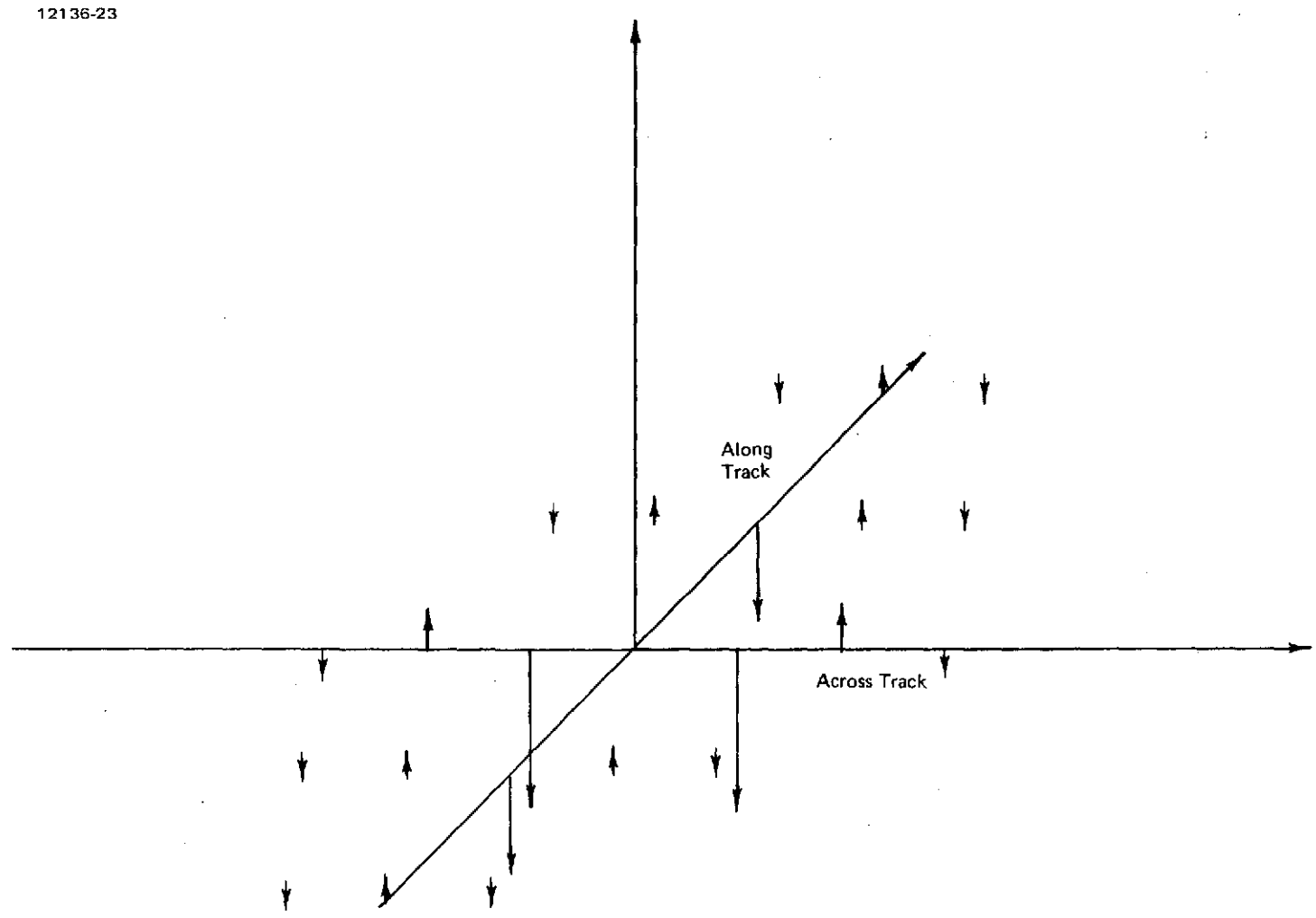

Figure 5-5 Aperture Correction Function for the Linear Scanner

man-month. Implementation impact may be significant since several sets of arrays must be stored, and the MTF and thus the deconvolving function vary depending on the location within a swath. To maintain a 1/2-bit correction, approximately 20 sets of arrays need to be stored. The impact is that these arrays must be stored and some decision logic is needed to designate when and which array is actually applied to the data. Although the impact of an aperture correction is peculiar, the impact on cost, throughput, and accuracy is small.

5.5 GEOMETRIC IMPACT

As might be expected, the greatest impact of the conical scanner occurs during the phase of geometric correction. Because the data are taken in curved swaths, rectilinearization of the data requires that rapid random pixel access be available over large quantities of data. Since one swath of conical scan data contains about 435 K pixels (all bands) and one line of output contains pixels derived from 75 different swaths, the scope of the problem is major.

At this point, something must be assumed regarding the orientation of the final product with conventional N-E-S-W placement. Since it is desirable that the output scan lines be parallel to the input scan lines, it will be assumed that the data products need not be rotated to yield conventional map orientation. Even if a linear scanner is used, storage requirements on the order of 100 million pixels would be required if the output scan lines were not near parallel to the input scan lines. Consequently, each output image will be specified by some arbitrary orientation angle which refers it to conventional north-south map orientation.

The impact of the conical scanner on geometric correction depends largely on the access times and transfer rates of the devices used in the correction process. Consequently, two approaches were considered as a means of performing the correction: (1) mass memory and (2) peripheral memory augmented by a small, rapid, random-access memory. Both of the above approaches were explored based on a cost-throughput tradeoff. To adequately introduce the details of the above two solutions, the correction requirements of the conical scanner will be discussed below.

Figure 5-6 shows the geometry of the scanner on the earth. The shaded area denotes the quantity of pixels that must be stored in some form since they have been read from the input HDDT and are not yet transferred to the output. Since the orientation of the output scan line as mentioned earlier is arbitrary even in the presence of spacecraft heading change, the storage requirement remains invariant. Using the conical scanner previously shown results in a storage per band of about 1.8 million pixels. Since the attitude stabilization of the platform is less than $\pm 0.01°$ per axis, storage required because of yaw is negligible.

12136-24

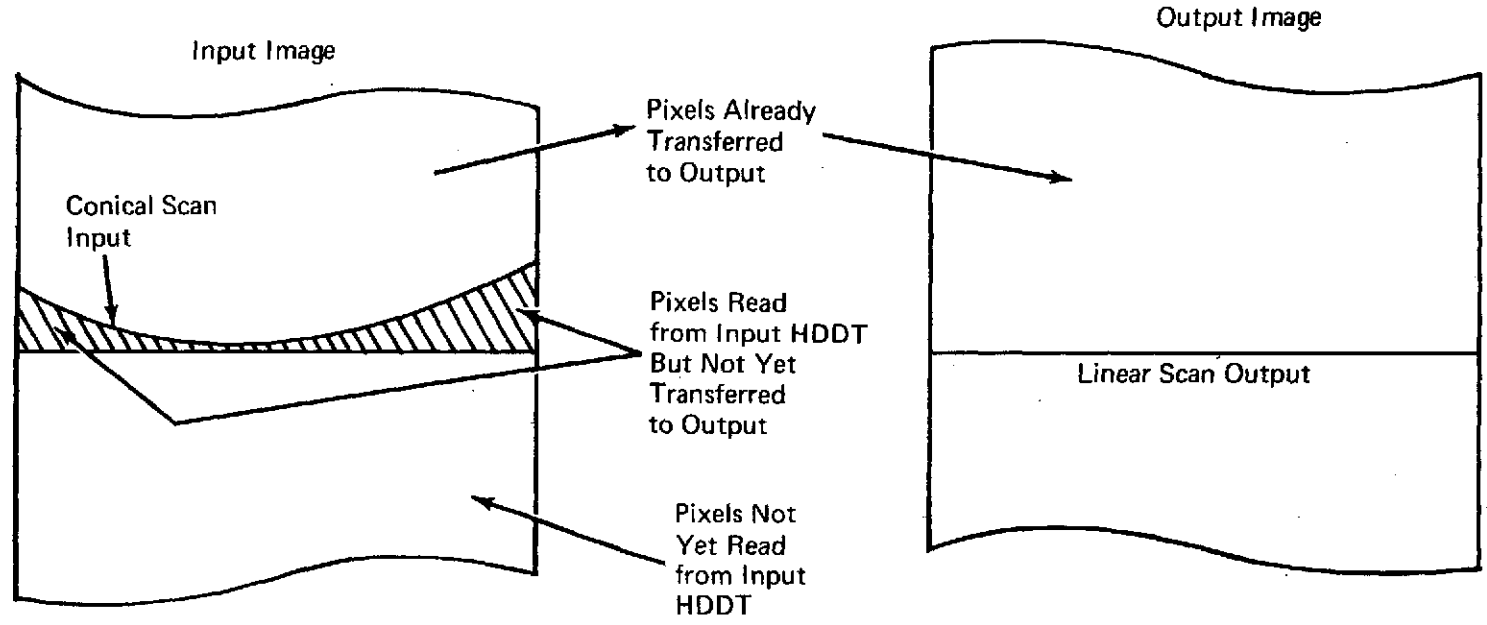

Figure 5-6 Input to Output Geometry of the Conical Scanner

The cost and throughput of the two memory approaches will now be explored. If a mass memory with rapid access time is used, the cost is merely the cost per pixel times the storage requirement of 1.8 million pixels. The throughput is merely twice the access time of the memory (one read and one write). The second approach to the storage problem is to use a medium-access, high-volume device such as a disk or drum coupled with a small volatile memory such as a semiconductor. The storage requirement is divided between the two as shown in Figure 5-7. The area stored by the volatile memory is that contained in the small triangular shaped zones and the thin rectangular zone beneath them.

Operation of this system is as follows. Assume that enough swaths have been read in to fill up the area shown in Figure 5-7. The number of output lines which may be formed is exactly the number contained in the thin rectangular area. After as many lines as possible are outputted, a corresponding number of swaths are transferred from files on the disk or drum to semiconductor memory. A new set of swaths are read from the input HDDT and placed in the disk except for the center portion which is placed directly in volatile memory. This process continues until an entire image has been formed.

One obvious question is "Into how many zones should the storage area be divided?" The answer to this question is best addressed by computing the cost and throughput for several numbers of zones. Figure 5-8 is a plot of cost/band versus throughput/band for both mass memory and disk-semiconductor memory.

Assuming 20% of the data will be digitally processed (40 scenes/day), the throughput requirement for two 8-hour shifts is 4.8 μsec/pixel-band. The optimum point of operation is to always maintain the 4.8-μsec/pixel (all bands) requirement. Using input tape rewinds, a system with rapid throughput could be made smaller and handle all bands. Thus, a system with a throughput about twice that necessary could rewind once and only have to parallel process three bands. Incorporating a 3:1 rewind to forward speed ratio into Figure 5-8 gives rise to Table 5-1, which gives the cost for each approach under consideration.

From Table 5-1 the peripheral plus volatile memory is seen to be cheaper by only a small amount. In terms of complexity the mass memory is not acceptable since two 1.8M pixel semiconductor memories cause severe addressing problems, produce unacceptable propagation delay times, and consume a large volume of space. If optical memories evolve substantially, they may offer relief in cost and complexity; however, to date, the peripheral plus volatile memory appears best.

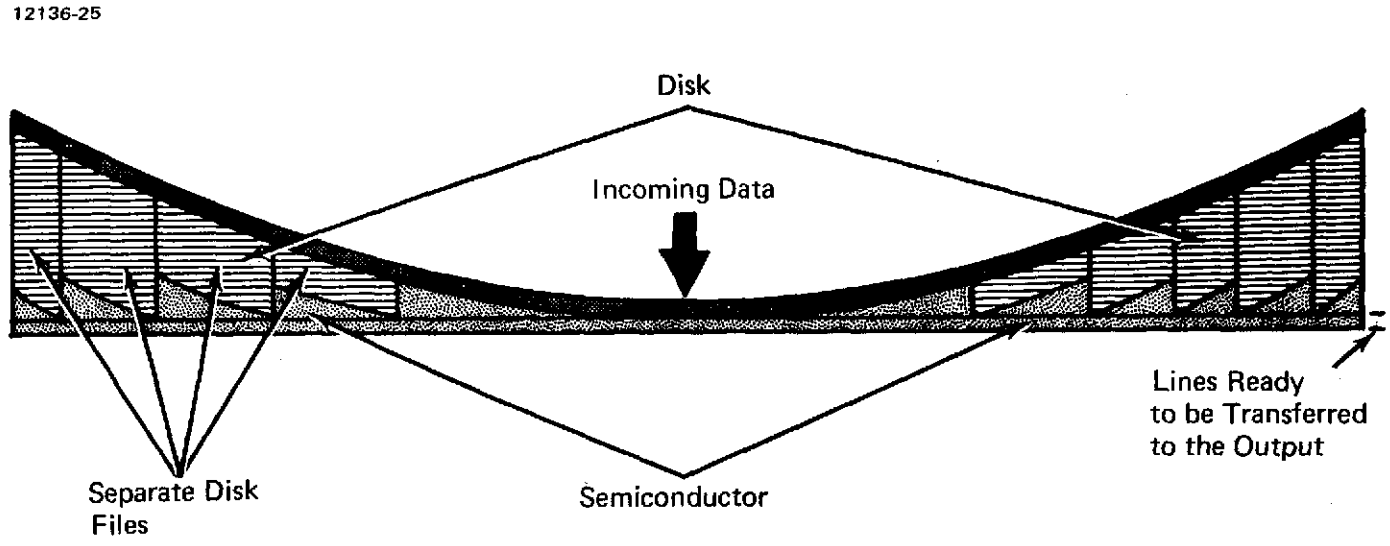

Figure 5-7 Combined Disk and Semiconductor Memory Approach

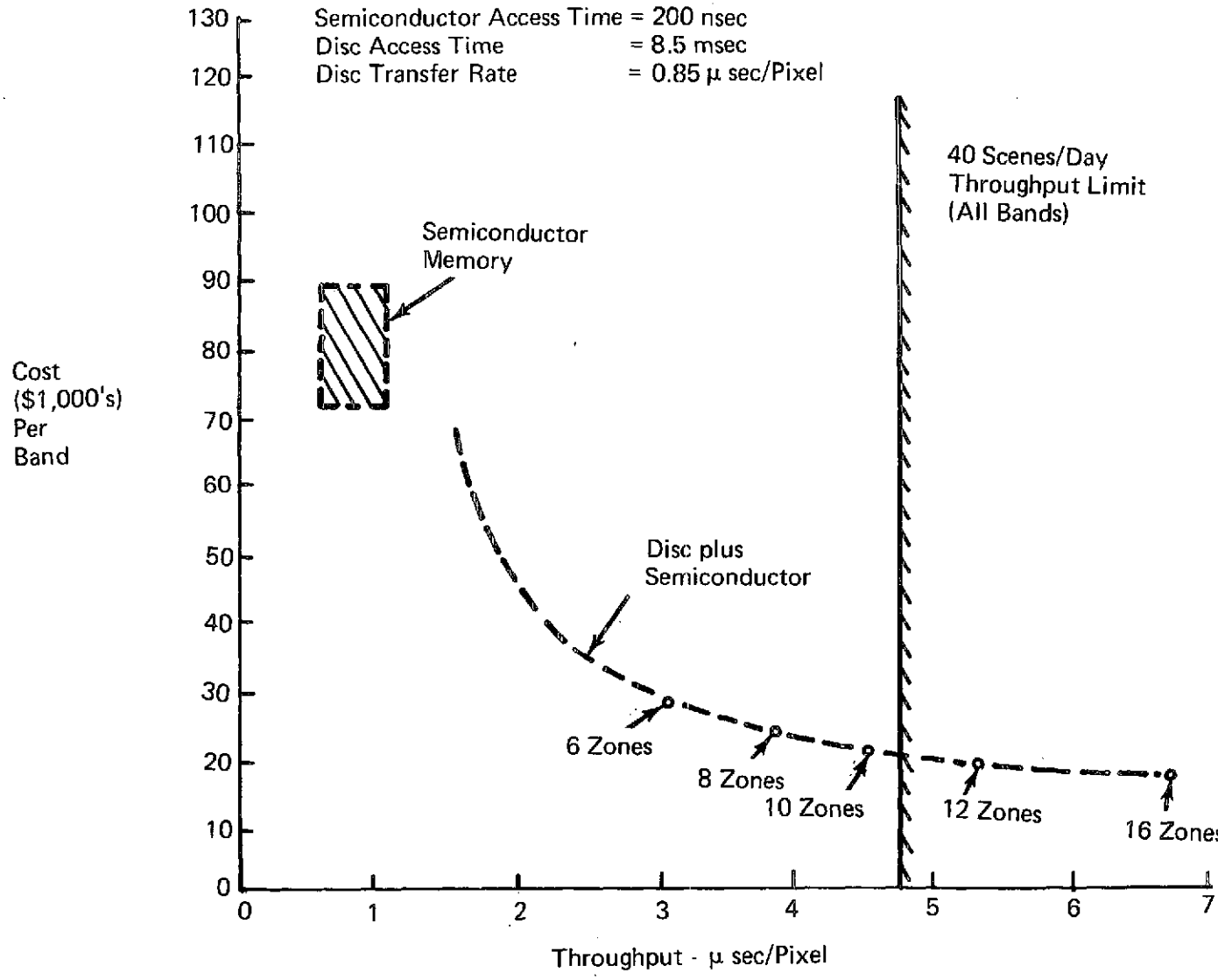

Figure 5-8 Cost vs. Throughput for Various Memory Approaches

Table 5-1

Total Memory Cost

Approach	Cost $
Mass Memory	140, 000
Peripheral plus Volatile Memory	120, 000

Ground control point (GCP) identification is performed by locating a small area on the ground in the data using some digital correlation procedure. It is used to improve the attitude and ephemeris estimates. Initially, points are selected that possess properties that make them good GCPs, e.g., high contrast, spectral and temporal contrast invariance, as well as certain geometric properties. They may be selected from ERTS imagery before EOS launch and gradually replaced with the higher resolution thematic mapper data as they become available. Their earth coordinates are recorded, and they are identified in the data set. Data obtained from subsequent passes over that same area are automatically searched using digital correlation algorithms and are identified in that data set. The difference between the true and apparent positions of the GCP provides a means of updating the attitude and ephemeris data. The volume of GCP identification will not be large; however, it is possible that only 6 to 15 selected points of each pass will be examined. In this case, they will be used to remove bias and eliminate uncertainty in the attitude and ephemeris measurement systems.

Since correlation may be performed directly on conical scan data just as easily and accurately as on linear scan data, repeatability over different passes is the key. Since the majority of radiometric drift will be external to the sensor and will have the same effect on both types of sensor data, differences in loss of correlation and hence registration accuracy will be caused by geometric distortion. The linear scanner is invariant to translation; hence, if the GCP is not sensed at the same point in the swath, it is of no consequence. For the conical scanner, two cases arise. If the orbit is maintained to a ground repeatability equivalent to ERTS (20 km), a 10% wander within the swath may occur. In one case this will cause up to a 5° rotation with respect to the GCP library and the present data. One data set must then be rotated to maintain correlation. Since the required rotation will be known, a priori, to an accuracy of about 0.05°, this is not difficult. The second case occurs when a GCP near the end of a swath is sensed by the opposite end of the swath at some later pass. The net rotation will be on the order of 48°. A rotation of this order will cause only 75% of the GCP to overlap if a square matrix is used. Even if derotation

is implemented, loss of correlation caused by lack of overlap still results. If a circularized shape is used, loss of overlap is eliminated; however, a complicated memory access procedure is needed to acquire the desired pixels. GCP identification is hampered by the fact that GCPs located at swath ends provide the highest confidence level in removing yaw effects. The problem of a 48° rotation may be solved by not using GCPs in this portion of the swath.

Although rotation of incoming GCPs will be necessary for the conical scan case, it only applies to about 2% of the cases. Since GCP identification will only be done on a small scale (6 to 15 per orbital pass), the problem of GCP rotation is not significant to the processor throughput, or accuracy.

Another area of impact is that of the computation necessary for computing the output grid corners. Because of the curved geometry of the conical scanner, about 114 lateral image points must be mapped. Fortunately, in the along-track dimension, only four per image need be mapped. Hence, a total of 456 output points must be mapped to the input for each image. The time available to perform this is 24 minutes for all bands based on 200 scenes/day and two 8-hour shifts. The available time for each mapping is thus 3.2 seconds. For ERTS, about 1 second is presently used on a Sigma 3. Consequently, enough time is available although the general-purpose controller may be taxed to a significant degree.

To determine the impact of the conical scanner, the geometric requirements of a linear scanner will be determined. These requirements will in turn be compared with those of the conical scanner above to determine the impact. With respect to geometric correction, most linear scanners require about the same software support. Because the attitude is stabilized to $\pm 0.01°$ per axis, only about one swath of data need be stored at any one time to construct one output line. Hence, the storage requirement for the linear scanner is only 70K pixels/band compared to 1.8M pixels/band for the conical scanner. The output-input computation load for the linear scanner is only 4 by 4 or 16 points. This is an almost insignificant load on the general-purpose processor. Certainly, no special-purpose hardware would be required to compute output-input mapping in this case.

In summary, the conical scan versus linear scan impact for geometric correction is in three areas. The first is data storage where use of conventional linear scanner geometry (MSS) would require about 1.7M pixels/band or 10M pixels extra for the conical scanner. Using the most cost-effective memory approach discussed involves a net cost differential of about $120,000. Incorporation of the additional support hardware and software gives a total cost differential of $160,000. Also, because a 10^8-bit memory

is necessary for the conical scanner, the system complexity is greater even with the disk carrying most of the storage load. The second area is that the general-purpose controller may be loaded in having to compute 440 more output-input mappings for the conical scan case. Additional special-purpose hardware may be needed in this case. Third, GCP identification is complicated by the possibility of rotation to ensure proper orientation during registration. The latter two areas contribute insignificantly to cost and throughput; hence, the only real impact lies in the first area. No evidence is available that indicates linear scan data can be more accurately corrected in all areas better than conical scan data.

SECTION 6

IMAGE RECORDING IMPACT

6.1 INTRODUCTION

In this section the impacts of conical scanning versus linear scanning upon an image recording system are considered. Used for the analysis are the baseline scanners outlined in Section 2 and the image processing requirements discussed in Section 4. The features examined are accuracy, complexity, film recorder performance and cost, in relation to the specified throughput requirements and a recommended standard of product. Recommendations are also made with regard to sensor configuration and operation in order to minimize the ground processing problems. Before the differences due to the two scanning modes can be discussed, it is first necessary to establish the basic characteristics of an image recorder which are common to the two modes.

In Section 5 an all-digital system was described, in which the final digital output was in fully corrected, synthetic linear form, whatever the original input, thereby allowing a relatively simple but necessarily specialized and precise form of film recorder to be used to produce high-quality output. In this section we are concerned with a system that has a sufficiently high throughput to process all the data which are worth processing, but which nevertheless gives a product of sufficient quality to satisfy the immediate needs of the bulk of users. Compromises are inevitable, the most obvious being that to achieve the necessary throughput without parallel systems and large memories, it is necessary to make all geometrical corrections, and probably at least part of the aperture correction, within the film recorder deflection and modulation circuits. This system is sometimes referred to as an "analog" system, which is a convenient means of distinction but something of a misnomer. As will be seen later, a considerable amount of digital computation is involved; the discussions of radiometric and aperture corrections in Section 5 are directly relevant, since in both systems these corrections must be applied to the raw data before the geometric corrections.

It will be realized that in the context of this section the term "linear" does not imply the vigorously orthogonal type of output which the all-digital system provides; it simply means that the sensor has a nominally linear form of scanning. The data supplied to the film recorder will be subject to all the distortions listed in Section 4, and the differences between linear and conical scanning will be a question of degree only.

Considering the basic functions that the image recording system must provide, it breaks into two distinct subsystems: (1) a digital controller/data processor and (2) a film recorder which for the purpose of this study is an Electron Beam Recorder (EBR) with a 70-mm film output. Figure 6-1 is an outline diagram of the complete image recording system.

Before proceeding to the detailed requirements for the two subsystems, it is necessary to explain briefly why the functions are distributed between the two subsystems in the way that they are, and in some detail why there is uncertainty as to where the aperture correction will be performed, if it is performed at all.

Take first the scanning waveforms in the EBR deflection circuits. These could be generated by purely analog means within the EBR, by purely digital means within the computer (followed of course by digital-to-analog converters), or by a combined digital analog piecewise linear approximation, as in the current ERTS system. It needs little study to determine that the piecewise linear approach is the only practical one. It would be difficult to maintain the required accuracy and stability in a high-order analog waveform generator while still allowing the waveform to be varied continuously throughout the scan. This argument admittedly carries less weight in the case of a linear scanner than in the case of the conical scanner, because the maximum along-track displacements are smaller, but it is nevertheless valid in both cases. The digital system would still be involved to a significant extent, since it would have to provide varying outputs to set integrator time constants, and/or diode switching levels, in the analog waveform generator.

Purely digital scanning waveform generation by direct computation on a pixel-by-pixel basis is clearly extremely wasteful of computing capacity, if not actually impossible because of speed limitations, and it is certainly not necessary on the grounds of accuracy. The process can be simplified by computing accurate deflections at only a few points and then doing a simple linear interpolation between them, but this approach is more efficiently implemented by performing the interpolation by analog means within the film recorder.

Another much simpler example is an internal system correction such as EBR exposure/scan velocity compensation. The piecewise linear slope control word from the digital subsystem is a scan velocity demand and can be used to set a binary attenuator in the EBR video circuit, thereby providing the necessary exposure adjustment.

12136-27

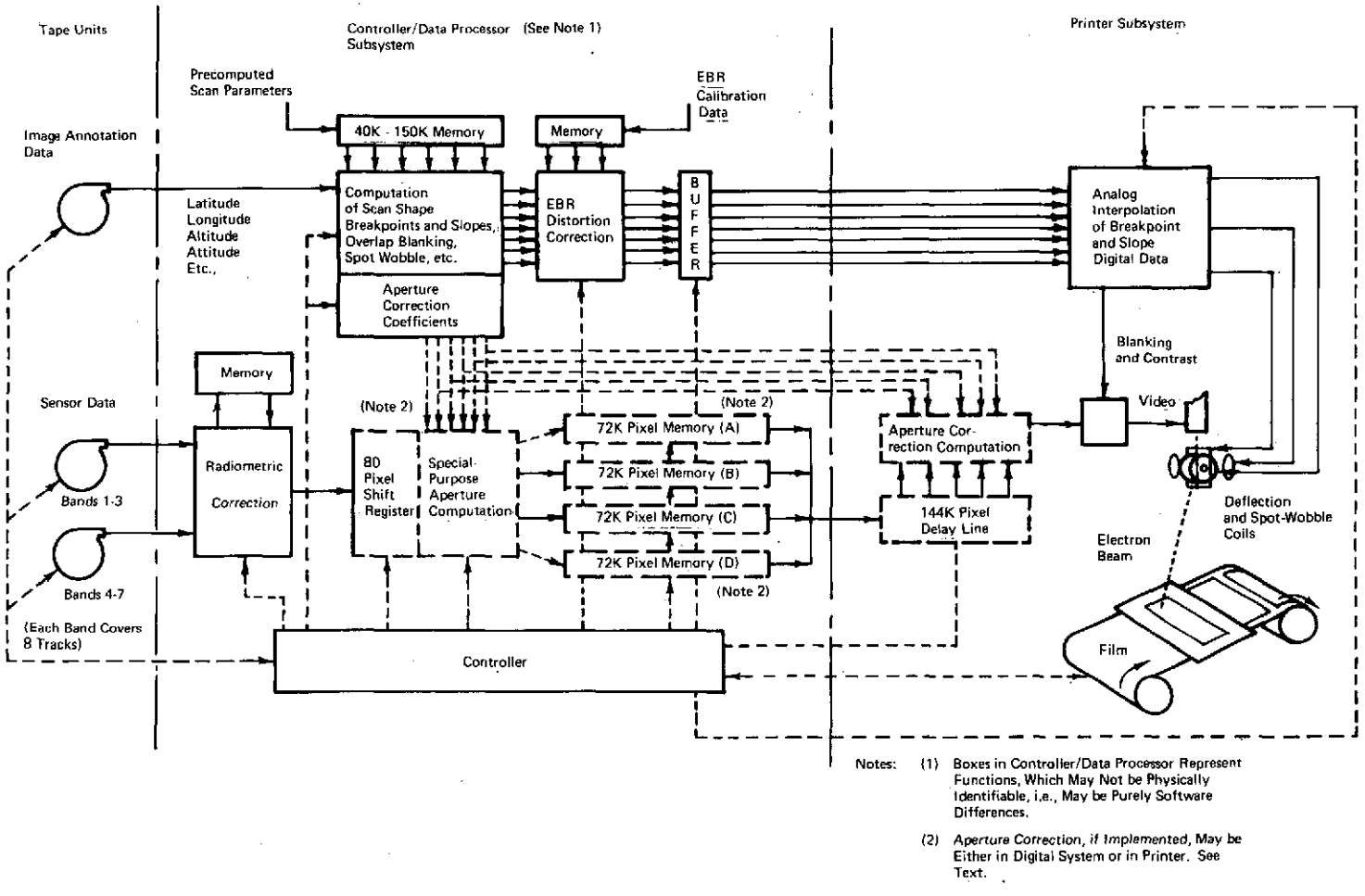

Figure 6-1 Outline Diagram of Image Recording System

In most cases the optimum functional split is for the "bookkeeping," spot-value and coefficient computation to be done digitally, with the interpolation and multiplication processes being done by analog means. This is in line with current ERTS practice, which appears to be satisfactory.

The provision of full two-dimensional aperture correction in a high-throughput system, in which we are trying to minimize cost and complexity, is extremely difficult.

The general theory of aperture correction was discussed in some depth in Section 5.4. Figure 6-2 illustrates the problem of practical implementation. To correct the radiometric value at pixel B.2.4, for example, contributions are required from all the pixels covered by the shaded diamond area. (In theory the correction process extends to infinity in all directions; in practice there are no significant contributions beyond two to five pixels in any direction.) The radiometric data from the satellite are available in the order Swath A, Swath B, Swath C, and so on. Within a particular swath the sequence in the data stream is B.1.1 to B.8.1, B.1.2 to B.8.2, B.1.3 to B.8.3, and so on. The film recorder requires the data on a line-by-line basis, i.e., B.1.1, B.1.2, B.1.3, B.1.4, ...B.1.9000; B.2.1, B.2.2, B.2.3,...B.2.9000, and so on and to implement the necessary decommutation function two 72K pixel memories are required, one being written into in a quasi-parallel manner, while the other is being read simultaneously in series.

Considering for the moment only the correction contributions to pixel B.2.4 from within Swath B, and also ignoring the very obvious speed-of-computation problem, there is a significant difference between making these corrections upon the input and the output data streams. In the input stream any B contribution to a B-pixel must appear within about $\pm$ 40 pixels of the B-pixel in question and accessing the appropriate pixel radiometric values could be very conveniently handled by a permanently tapped, 80-pixel shift register. The various multiplications and additions would still have to be performed within a pixel-period (400 nanoseconds), but at least the radiometric quantities for all contributors would be simultaneously available. The radiometric value which would be loaded into the 72K-pixel memory for decommutation would be partially corrected, no longer the observed value and not yet the best-estimate "true" value. This would affect the contribution it would make when used later to correct pixels in other swaths, but the effect is capable of analysis and in practice simply gives rise to an adjustment of the appropriate coefficient.

If the B contributions to a B-pixel are made at the output of the decommutator, the contributions from within the same line appear within about $\pm$ 5 pixels, but the contributions from other lines appear at approximately

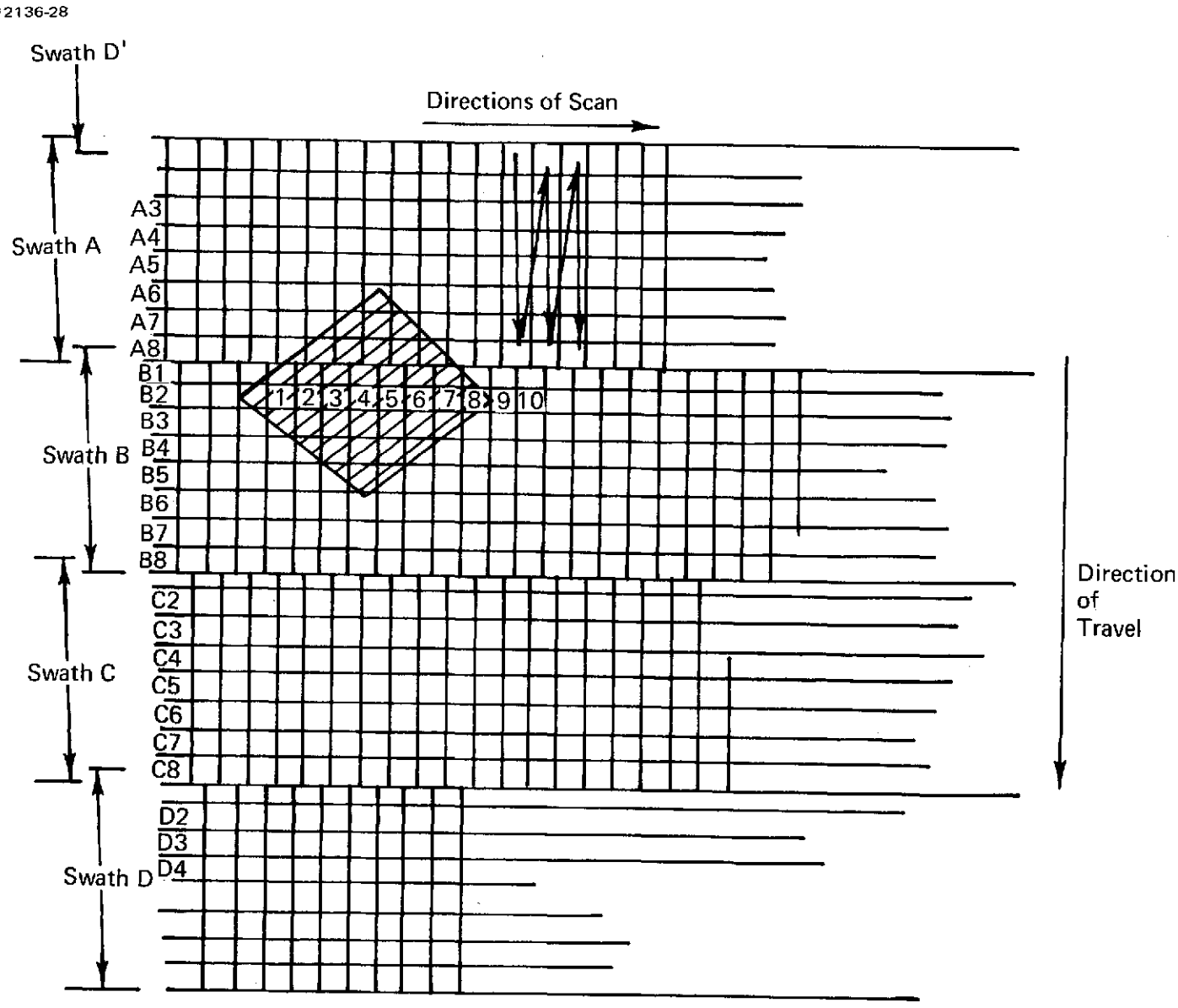

Figure 6-2 Aperture Correction Problem

$\pm$ 9,000, $\pm$ 18,000, $\pm$ 27,000, and, possibly, $\pm$ 36,000 pixels distance. There is thus, apparently, a strong argument in favor of aperture correction before insertion into the decommutator. Unfortunately, however, the contributions from other swaths cannot be ignored since, clearly, for B.1.n and B.8.n in particular they are just as important as the B-pixel contributions, and there is no way of circumventing the fact that they always appear in the data stream approximately $\pm$ 72,000 pixels from the pixel being corrected. A 144,000-pixel shift-register delay-line is a significant component capable of storing two complete swaths. Once the principle of including a special-purpose device of this size is accepted, a little further study will show that the preferred approach would simply be to expand the decommutator memory from two to four full swaths (284K-pixel) and to insert a special-purpose 80-pixel shift-register/delay line plus correction computation hardware into the input data stream, as discussed earlier. All aperture correction computations would be done at the time of data input to the decommutator. For example, as Swath D in Figure 6-2 was being read out line-by-line to the film recorder, data corresponding to Swath B would be coming in. The Swath A memory would already contain the "true" Swath A data, less the corrections from Swath B, the Swath B memory would already contain the contributions from Swath A, and the Swath C memory would be effectively blank. Corresponding single pixels in Swaths A, B, and C would be assessed simultaneously, the contributions from the stream of 80 B-pixels held in the preceding shift-register would be computed by the special-purpose hardware and added and the new values reinserted into the three memories. At the end of the Swath B input, the Swath A would be fully corrected ready for readout, the Swath B would require only the Swath C contribution, and the Swath C would contain only the Swath B contributions. D would be effectively blank. The process would then repeat, reading out A and inserting contributions into B, C, and D while Swath C data were being inputted. Each memory would be required to make one read and one write in 400 nanoseconds, and the special-purpose hardware would have to make approximately 40 multiplications and 40 additions in the same period. With some loss of accuracy the contribution coefficients could be adjusted to allow recursive techniques to be used, where fewer operations would be required.

The output video signal (digital or analog) approach is shown in Figure 6-3. With the current state of the art, it is mainly of academic interest. Analog delay lines are clearly not suitable since it is highly unlikely that synchronization to a small fraction of one pixel-period in 144,000 could be maintained, without extensive intermediate sync signals in the data stream, auxiliary pixel counters, and rate-buffers. If there are major advances in the field of charge transfer, "bucket-brigade" devices in the next 2 to 3 years, this approach might merit reconsideration.

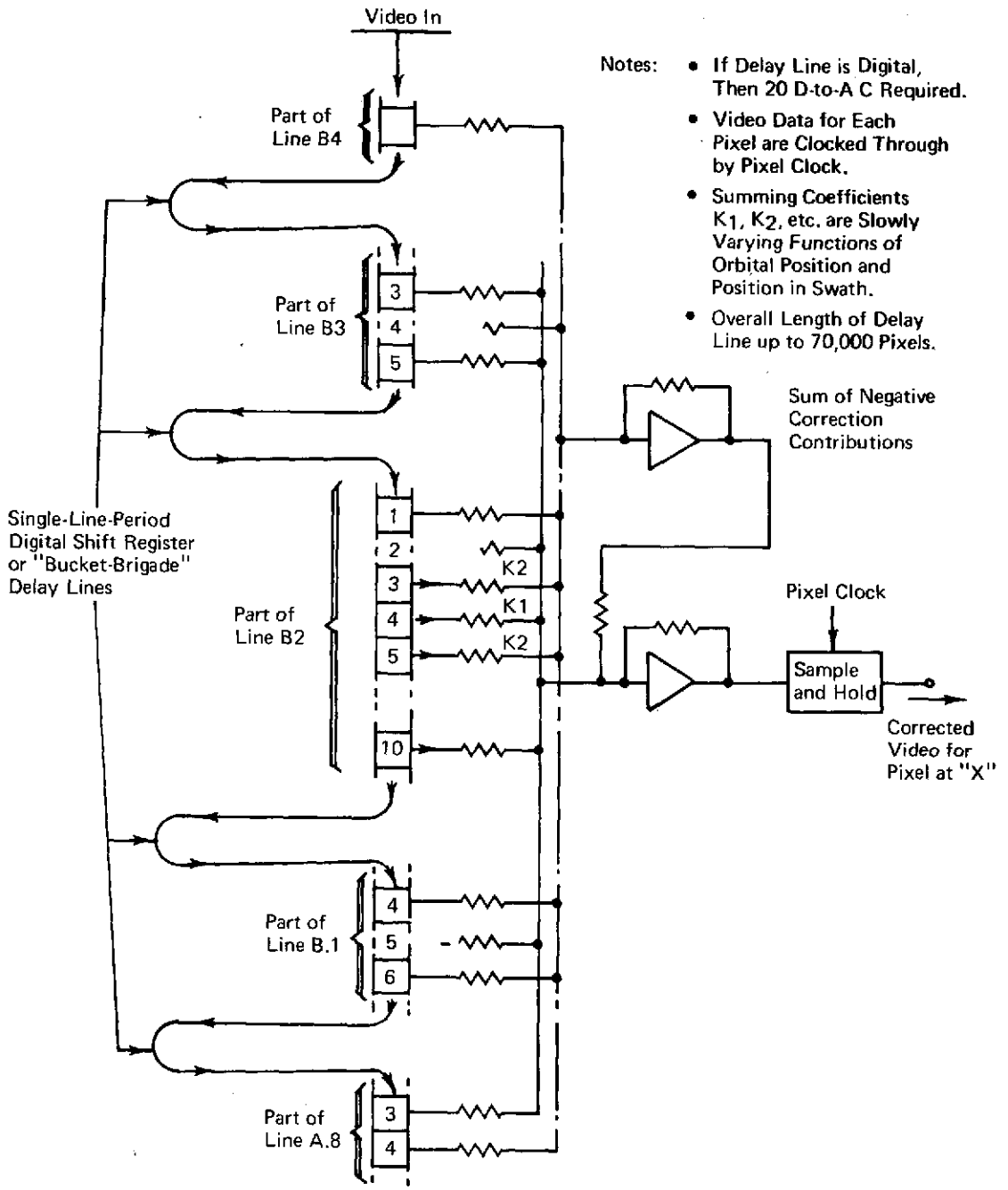

Figure 6-3 Video Delay - Line Approach to Two-Dimensional Aperture Correction

The impact of conical scanning versus linear scanning in the aperture correction process has been discussed in Section 5.4. The correction contribution of one pixel to another is a function of their relative positions, orientations, and sizes. As shown in Figures 4-9 through 4-12, variations in these quantities occur for both types of scanner, but the frequency and magnitude of adjustments are greater for conical than for linear scanning. However, the difference is not of great significance when compared to the common problems of aperture correction.

6.2 FILM RECORDER SUBSYSTEM

The film recorder is basically an analog device. Unlike the digital subsystem, one cannot obtain any desired quality of output by simply expending more hardware, money, and operating time. There are fundamental limitations plus interactions between desired characteristics. The logical approach in discussing the separate subsystems is to establish, in order, the target standard for the 70-mm film output, the consequent impact upon the film recorder subsystem, and finally the joint impact of target standard and film recorder requirements upon the digital subsystem.

The image recording system is required to process 200 scenes, each in seven spectral bands, per 16-hour working day. This corresponds to approximately 41 seconds for each of the 1,400 frames, but in practice, downtime due to contingencies, film and tape reloads and rewinds, work-breaks, etc., will reduce the effective time available per frame. The standard output frame of EOS data, as with ERTS, covers a 185.2-km (100-n.mi) square. At the nadir the time required by a linear scanner to record all points in the square is approximately 27 seconds; for a conical scanner it is approximately 30 seconds. For an offset scan without basic scan pattern twist but with the UTM mapping "droop," the times rise, respectively, to about 28.5 seconds and 32 seconds. If the scanner configuration is such that offset scan twist does occur, then the time per frame may reach 39 to 42 seconds. When throughput requirements and scan times are compared, the obvious preferred arrangement is to ensure that offset scan twist does not occur and to play the recorded data into the image recording system at the same rate at which they were received from the satellite scanner, i.e., approximately 14.4 million bits per second (Mbps) per spectral channel (0.9 Mbps for the low definition IR channel). Each frame will take approximately 30 seconds to print, and all seven spectral frames for a single scan will take at least 3.5 minutes to complete.

The output film format has a significant effect upon the film recorder subsystem. At the present time, there are two bulk film formats in use with the linear scan ERTS data – the NDPF and the INPERTS ("Brazilian ERTS").

In the NDPF system, all scans for one spectral band are grouped together (Figure 6-4); in the INPERTS system, all spectral bands for one scene are grouped together (Figure 6-5).

In the NDPF ERTS film recorder, the film moves continuously, and during the first tape pass all the successive frames for one spectral band are recorded. After the tape has been rewound, all the successive frames for the second spectral band are recorded during the second tape pass, and so on. The total number of tape passes is the same as the total number of spectral bands. The 10% overlap between successive frames is obtained by recording each line of the last 10% of each frame twice — once in the current, almost complete frame, and once in the first 10% zone of the next frame. This double writing, which must be accomplished within the time for one line of data from the tape (approximately 3.5 milliseconds in EOS), means that the writing speed for the moving film recorder must be approximately one line per 1.5 milliseconds, or faster. When the overlap printing is completed, the between-frames annotation scans are alternated with the picture scans. The picture edge tick marks and annotations are written in the dead periods at the beginning and end of each line. The ERTS EBR has a recorder gate, which allows the electron beam to move a total of 16 mm in the along-film direction; this is just sufficient to allow for all ERTS linear-scan geometric corrections, overlap, and annotation. In the case of the EOS satellite, the greater accuracy of stabilization about all axes reduces the corresponding required gate component to 0.2 mm, from the $\pm$ 2.5 mm for ERTS. The UTM mapping "droop" requires a maximum gate component of 2.3 mm, leading to a minimum gate size of 14 mm in the along-film direction, for the linear scanner. The ERTS 16-mm gate is thus more than sufficient. With an EOS conical scanner, the additional along-track deflection due to the basic curvature of the scan amounts to approximately 10 km, or 5.6 mm on the 70-mm film. The minimum along-track gate dimension for a moving film EOS conical scan recorder is thus approximately 20 mm, which is larger than the current ERTS recorder gate. However, the existing EBR can be used with gate widths up to 23 mm without penalty. In both cases it has been assumed that offset scan twist does not occur. As mentioned earlier in Section 4.9, offset scan twist can introduce a requirement for an additional 90-km (or 30-mm) movement along-track, which completely rules out any consideration of the moving-film EBR for linear or conical scan processing.

In the INPERTS system a framing film recorder is used, and the film moves only between frames. The EBR has a 76-mm gate, which covers the full picture and annotation area but does not allow overlap recording into an adjacent frame. During the first tape pass, the odd-numbered frames of the first spectral band are recorded, but the film is stepped 10 frame spaces after each frame is recorded. Before the second tape pass, the film is stepped

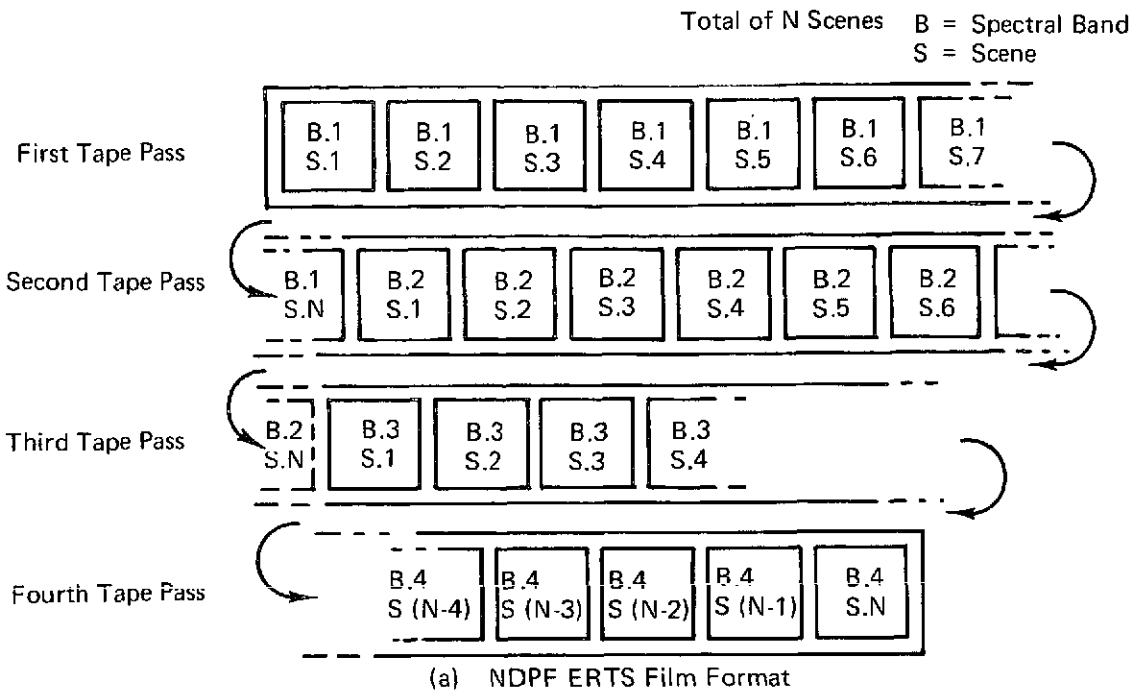

(a) NDPF ERTS Film Format

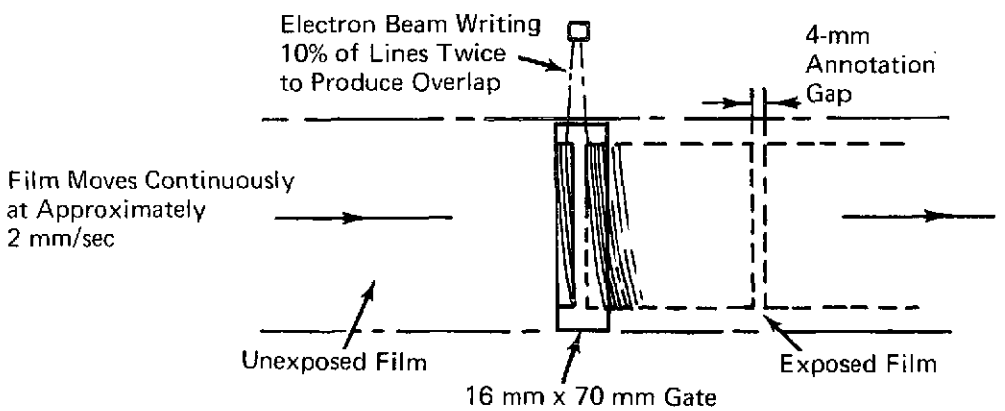

(b) Moving Film EBR Gate

12136-30

Figure 6-4 NDPF ERTS Recording

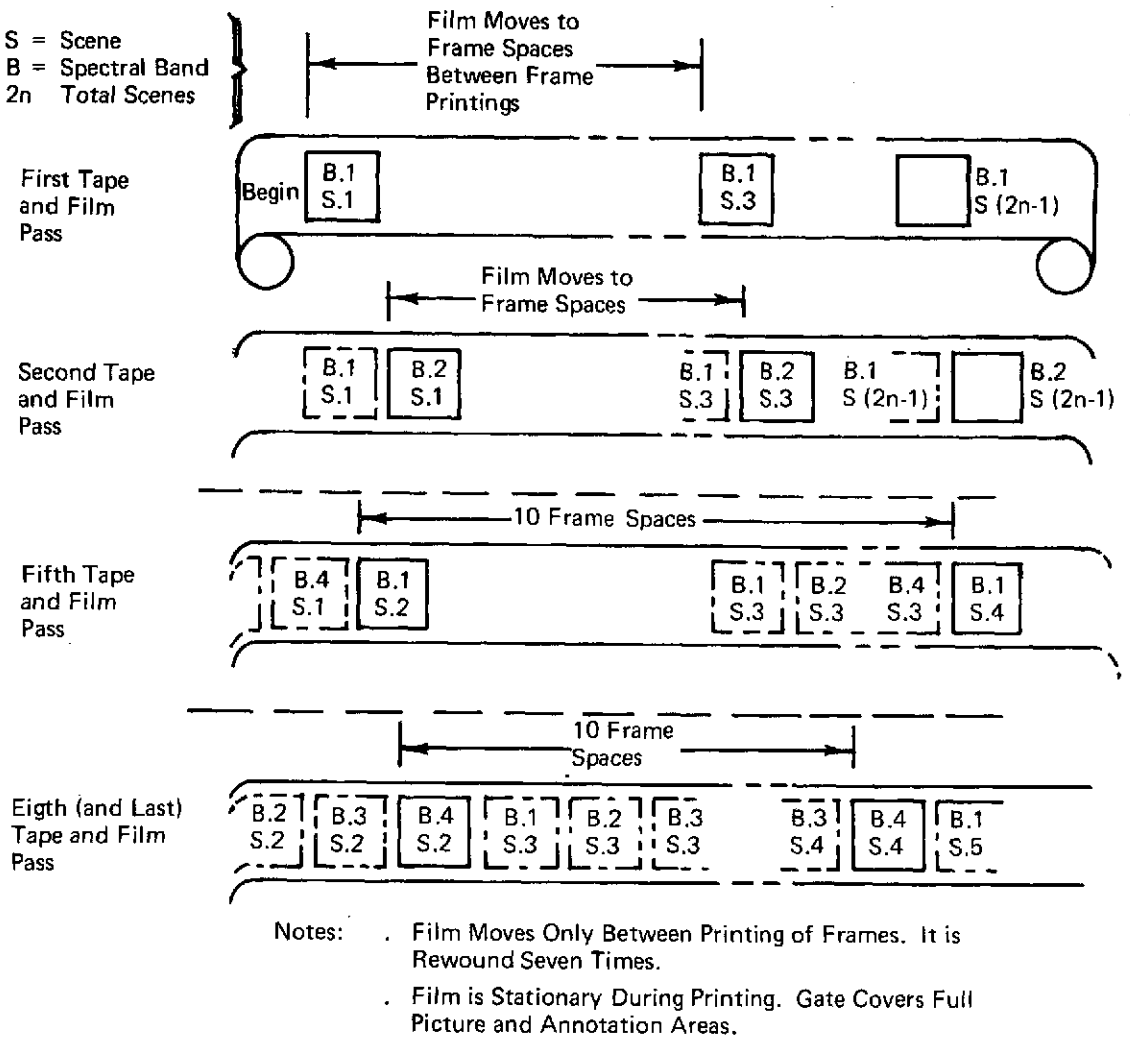

Figure 6-5 INPERTS (Brazilian ERTS) Film Format

back to the frame space immediately following the first frame recorded, and then all the odd-numbered frames of the second spectral band are recorded, again using a 10-frame space shift. This is repeated four times until all bands for all odd scenes have been recorded. The whole process is then repeated for the even-numbered frames, which fills in the gaps between the odd-numbered groups. The total number of tape passes is equal to twice the number of spectral bands. Overlap between scenes is obtained simply by reading the tape at the appropriate 90% intervals, and there is no requirement for the writing speed to exceed that required by the average video data rate, i.e., one line per 3.5 milliseconds. Since the gate covers the full picture area and the film does not move during film recording, the shape of the scan is unimportant, provided that the scanning deflection circuits have an adequate performance.

In Section 4 it was suggested that the UTM mapping standard should be the target for the output of the image recording system. This requires points to be placed on a northings-eastings grid to within 0.3 mm at whatever scale is being used. Although the primary EBR output is on 70-mm film, the normal user scale would be the 1:1,000,000 scale of enlargements onto 9-in. film. Basing the UTM mapping standard requirement on this 1:1,000,000 scale, one finds the total permissible error is 300 m, which is much greater than the satellite altitude error and ephemeris contributions. If the additional rms error from all processing sources can be kept at or below 140 m, then the image recording system output can meet UTM standards.

The two main sources of error are computational approximations and the performance of the EBR deflection systems. In a provisional error budget the computational error contribution was assumed to be 70 m rms and the deflection system contribution was assumed to be 120 m rms. The computational error will be considered in the digital subsystem section. The 120-m rms for the deflection circuits will be made up of a static (i.e., linearity) and a dynamic (i.e., frequency response) component, which are assumed to be of equal magnitude, i.e., each will be 86 m rms, or approximately three pixels — 27 microns in the 70-mm EBR. This is well within the capability of existing EBRs. Even the most severe deflection frequency response, demanded by conical scanning in a moving film recorder with the worst-case combination of scan curvature plus UTM curvature, amounts to only 3 dB down at about 80 kHz. Current ERTS EBRs have responses to well over 100 kHz. Thus, there is no significant impact from conical versus linear scanning as far as EBR gate size, deflection frequency response, and mapping standard are concerned.

The EOS sample rate corresponds to a pixel size of 20 m, or approximately 6 microns on a 70-mm film. The spot size of the current ERTS EBRs is also about 6 microns, but it is a function of scan velocity. If the framing EBR system were to be used and the writing speed held to the lowest possible level, then the spot size could be reduced to about 3 microns. The necessarily faster writing speed of the moving film type of recorder would give a spot size of about 4 to 5 microns. Because the spot sizes and the pixel size are comparable, there will be significant one-dimensional aperture effects to be corrected. However, compared to the two-dimensional satellite scanner aperture correction, the impact upon either the EBR video circuit or the digital computer is trivial. It is not affected significantly by the type of scanner which is used.

In Section 4 it was shown that at one point on the scan, whether conical or linear, at one latitude and altitude it is possible under ideal, error-free conditions to arrange that all pixel samples are contiguous and lie on a rectangular grid aligned along and across track. At all other points, deviations from this ideal will occur. In general, pixel size and shape will alter, leading to gaps or overlaps, the pattern will twist, swaths will partially overlap, and adjacent lines in successive swaths will be shifted relative to each other in a variable manner along the length of the swath. The worst-case conditions will occur at the ends of an offset conical scan. To produce a picture that is both radiometrically as accurate as possible and cosmetically acceptable, most of these deviations from the ideal will have to be corrected.

Although any of the corrections can be predetermined once the scanner parameters, orbital parameters, latitude, and position in the scan are known, a considerable "bookkeeping" job is involved. Fortunately, the rate of change of the constants in the associated correction algorithm will be relatively slow and can be accommodated by look-up tables or piecewise linear approximations, as appropriate. An example of the type of operation which is involved is as follows (see also Figure 6-6). Consider the case where two lines in adjacent swaths converge slowly and overlap. In the EBR, if two lines are actually written one over the other, the effect will be additive and an unacceptable bright band will appear. If the minimum spot size is a significant fraction of the line width and one line is simply suppressed as the lines overlap, then a black band will appear. The optimum approach is to reduce the spot wobble on each line as they converge, applying minor deflection corrections to ensure that each line just remains in touch with its outside neighbor as well as its converging partner. When the spot wobble amplitude in each has reached zero, one spot is suppressed and the remaining one is deflected and spot wobbled so as to just fill the total gap. Since current EBR spot sizes are in the region of 3 to 6 microns, line width (pixel width) is about 9 microns and the convergence may cover several hundreds of pixels; this is a very practical problem.

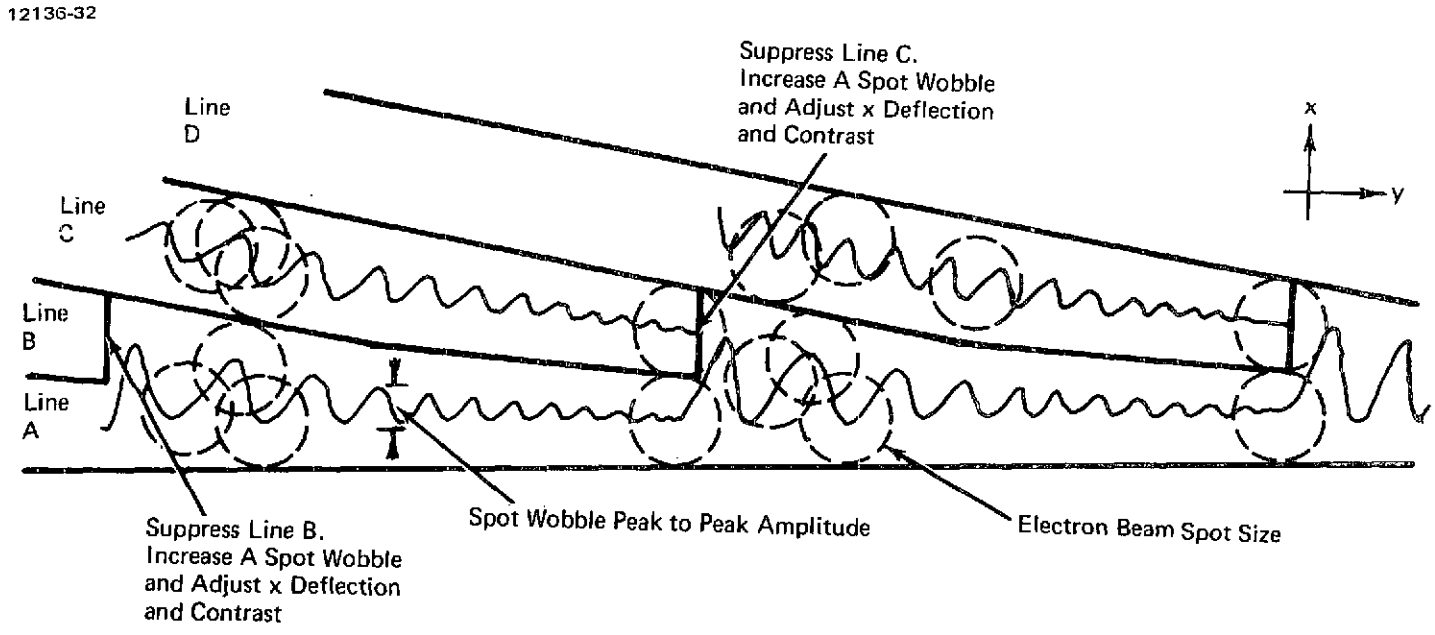

Figure 6-6 Line Deflection and Spot Wobble at Overlap

6.3 DIGITAL SUBSYSTEM

The digital subsystem comprises two separately identifiable functional blocks, a controller and geometry computer/radiometric data processor. In practice, these may be simply different software blocks within one computer. The tasks of the digital subsystem, as outlined in Figure 6-1, are:

1. Supervise data flow, including input from the sensor and correction data tape recorders, parallel-to-serial decommutation, and output to the EBR video and deflection circuits.

2. Control tape and film movements.

3. Perform radiometric corrections, using detector calibration data.

4. (Possibly) perform scanning aperture corrections.

5. Compute break-points and slopes for along-track deflection, cross-track deflections, spot wobble amplitude, and video gain.

6. Compute contribution coefficients for the aperture correction process.

In general, only Tasks 5 and 6 will be affected by the choice of a conical or a linear scanner.

As described in Section 5, the first operation to be performed on the data is radiometric correction. The comments in Sections 5.1 and 5.3 apply here without modification.

If it is incorporated, the next operation is two-dimensional aperture correction. This subject was discussed in considerable detail in Sections 5.4 and 6.2. It only remains to note here that the computer must modify the coefficients in the correction contribution function, depending upon the positions in the orbit and in the swath, the latter producing the greater variation, particularly for conical scan. As pointed out in Section 5.4, the main impact from conical versus linear scanning is in the one-time computation of the coefficient arrays beforehand, ready for storage. If the change points for conical and linear scanning are made the same, then the relative impact during actual processing operations will be negligible.

After the aperture correction process, the radiometric data will be transmitted to the film recorder.

The scan shape generation and correction will be the major task for the computer in the nonradiometric area. It is also in this area that the major impact of conical versus linear scanning will be found. In Section 6.2 it was shown that the preferred approach is the existing ERTS printer technique — the piecewise linear approximations. The number of break-points required for a given accuracy of approximation is a function of the degree of curvature of the scan, namely:

$$n = \frac{\ell}{4\sqrt{\delta R}} + 1$$

where

n = number of break-points

ℓ = total length of scan

δ = maximum permitted error

R = radius of curvature of scan line.

Reference to Section 4 will show that, for a conical scan, R is approximately 288 km whereas for worst-case linear scan distortion, R is not less than about 17,000 km, due primarily to the UTM mapping "droop." If the error from the piecewise linear approximation is not to exceed, say, 40 m, or just over one pixel, then at least 15 break-points are required for a conical scan, but only about four for a linear scan. (The current ERTS system provides nine.) The slope variation which must be provided is $\pm 27^{\circ}$ for a conical scanner and $\pm 3^{\circ}$ for a linear scanner. (The current ERTS system provides about $\pm 12^{\circ}$.)

The shapes of the scans vary slowly with the position in the orbit, but the overall twists and displacements for offset scans, due to the UTM mapping, vary significantly. Without offset, a conical scan basic shape would need to be adjusted about once per frame to keep the error down to about 10 m. With offset and UTM mapping, the scan shape for both linear and conical scanning would need to be modified approximately 15 times per frame to maintain an error not exceeding 10 m.

Over one frame, the systematic shape variations can be dealt with quite satisfactorily by linear interpolation along track. The current ERTS system, which provides for nine along-track break-points with two-way linear interpolation, would be more than adequate.

The correction functions for contrast, spot wobble, scan blanking, etc., are directly related to the geometrical variations and, for a first approximation, may be assumed to require adjustment at about the same intervals. Assuming that the minimum necessary break-point and slope constants are precomputed off-line and stored, ready to be selected as a function of offset, orbital position, and swath position, and allowing for the symmetries which exist, then the systematic scan constants require about 150K words of memory for a conical scan system and about 40K words of memory for a linear scan system. After the set of constants appropriate to the next frame have been selected, along-track interpolations will be performed to generate the larger number of break-points required for the EBR correction matrix. In the worst case, seven values have to be interpolated between each of about 180 pairs of points, i.e., about 1,300 output points. Since approximately 30 seconds is available, the computing load is not heavy and, as will be shown later, even this can be eliminated by the use of a backup tape or disc store.

The systematic scan break-point and slope data will be combined with the nonsystematic scanner state vector corrections and the EBR calibration corrections to generate the final correction matrix for transmission to the EBR.

The state-vector corrections and the EBR calibration corrections are not affected by the type of scanner.

Since the correction functions vary slowly and only about 2K words (conical) or about 500 words (linear) are actually needed for each frame, the main storage could be on tape or disc. If the tape or disc system is capable of holding up to 3 million words (24 million bits), then the individual break-point inputs can be stored, eliminating subsequent on-line interpolation and allowing a slight, probably insignificant increase in accuracy. A slow access, 3-million-word tape or disc store is readily available and, provided that there are no objections to the increase in peripheral equipment, this is undoubtedly the preferred approach.

The differences which conical versus linear scanning would produce in the associated bookkeeping and coefficient selection logic would be negligible.

6.4 GENERAL COMMENTS AND RECOMMENDATIONS

In the previous sections, the digital subsystem and the film recorder subsystem were discussed separately without considering in detail the interactions between them. No comments were made with regard to the tape recorder input. In this section the complete image recording system is examined with the intention of defining in outline the overall optimum approach.

Consider first the tape recorder input and the necessary downlink demultiplexing equipment.

In the satellite detector circuits, and in the framing type of ground processor, the analog video signal for any spectral band should not contain frequencies in excess of approximately 1.2 MHz, with only 75 kHz required for the low definition IR band. A frequency of 1.2 MHz with 6-bit resolution is equivalent to 14.4 Mbps, and 75 kHz is equivalent to 0.9 Mbps. The Ampex FR 1928 recorder, which is used in the ERTS system, can provide 22,000 bits/in. at 120 in./second, i.e., 2.4 Mbps, on each of 28 tracks for a total period of 15 minutes per tape reel. Although the EOS bit rates could be matched by allocating six tracks to each high-definition spectral band and one track to the single low-definition band, i.e., 37 tracks in all, it is more convenient to allocate eight tracks to each spectral band, whether high definition or low definition, and to record one line of the eight-line swath in one spectral band on each track. This requires 56 tracks, which can be provided by two recorders. The low-definition data will simply be repeated as often as necessary to generate a synthetic high-definition swath. All subsequent operations, e.g., tape reading, computer line demultiplexing, print, etc., will treat all data as high-definition data.

The latest developments in tape recorders, which should certainly be available as state of the art by 1978, could provide 20,000 bits/in. at up to 900 in./second, i.e., 18 Mbps, on up to 40 tracks. This exceeds the total EOS requirements by a considerable margin. However, even if the tape speed and number of tracks were optimized for EOS purposes, it is doubtful whether a single recorder of this type would have any significant cost or other advantages over two well-proved FR 1928 recorders. There may, in fact, be a definite advantage in using multiple recorders so that one may be playing back while the other rewinds or is being reloaded.

Since raw linear scan data are indistinguishable from raw conical scan data, there is no direct conical versus linear scan impact upon the tape input system.

In Section 6.2 the two types of film recorders were mentioned, the continuous moving film type and the stationary film, framing type. The moving film transport mechanism increases the cost of the EBR by approximately 30% (or roughly $100,000), and the 10% overlap scanning raises the required scanning and video circuit responses, plus the transfer of information from the computer, by a factor of at least 2.5. On this basis the framing printer would appear to have a strong advantage. However, it should be noted that: (1) the faster operation of the moving film EBR is well within

existing system capabilities and (2) a framing EBR requires twice as many tape passes for a given total output. This last factor is most important as the moving film EBR system only just achieves the throughput requirement. The framing of data into 185-km sections along-track is quite artificial — on the tape the data are continuous; however quickly the recorder could be stopped and started it is inevitable that effective gaps would be generated. With a framing EBR the data input must be temporarily suppressed while the film is being moved; without frame length (i.e., 2.6 billion bit) buffers and a higher writing speed, there is no way in which data can be extracted continuously from a single tape and used, without loss, for picture production in a framing EBR. After study of this problem, it has been concluded that a framing EBR system will be able to match approximately the throughput of a moving film EBR system only if twice as many input tape recorders are provided, with special variable delay synchronization between pairs of recorders, so that immediately after the film has been moved the data for the next frame will be available from the alternate recorder. In addition, special synchronization generators and tape tracks and a more complicated form of down-link demultiplexer would be required. The two additional FR 1928 tape recorders would cost a total of at least $160,000, which more than offsets the apparent saving in cost of a framing EBR by at least $60,000. This applies whether the scanner is conical or linear. It is therefore recommended that the image recording system use a moving film EBR.

In Section 6.3 it was noted that linear scanning processing would require a 40K-word memory for correction coefficient storage, with a 9 x 4 break-point array, small skew angle, capability in the EBR. Conical scanning processing would require a 150K-word memory with a 9 x 15 break-point array, large skew angle capability in the EBR. The memory difference would cost about $20,000. The existing types of EBR could meet the linear scan requirements, but special development would be required to meet the conical scan requirement at a provisionally estimated cost of $50,000. The impact of conical versus linear scanning in this area therefore amounts to a cost difference of approximately $70,000, and it will be found that this is the only significant impact in the complete image recording system.

SECTION 7

DATA PROCESSING OF OTHER LINEAR SCANNERS

A qualitative analysis was performed on three additional scanners potentially applicable to the EOS mission. The first is a high-resolution pointable imager (HRPI), which is a four-band solid-state "pushbroom" imagery system. The second is a six-band opto-mechanical linear scanner with a high duty cycle achieved by active scanning during mirror reversal. The third is a seven-band opto-mechanical linear scanner with a high duty cycle achieved by a rotating circumferential set of 24 roof mirrors.

The orbital parameters used for evaluating the conical scan impact will be invoked during this analysis as well.

7.1 HIGH-RESOLUTION POINTABLE IMAGER (HRPI)

The HRPI is a four-band solid-state "pushbroom" type imaging system whose operation is shown in Figure 7-1. It contains 4,800 detectors per band oriented transverse to the ground track. At 735-km altitude, it has a swath width of 38.4 km with each detector having an 8-m square instantaneous field of view (IFOV) on the ground. The integration time per detector is about 1 msec.

One major problem with this sensor is radiometric correction processing. There are a total of 19,200 individual detectors, each of which must be calibrated and corrected. If this activity is performed on the ground by a table look-up procedure, about 1.2M pixels of memory will be required. Radiometric corrections of this magnitude are ideally suited for performance onboard the spacecraft. In addition, the spacecraft telemetry bandwidth would increase significantly because of the calibration data. Also, with 19,200 detectors the probability of a faulty or failed element is considerable. The operational reliability of solid-state imagery devices should be carefully examined.

Aperture correction is straightforward and virtually identical to that of a conventional opto-mechanical line scanner. Nonetheless, the telescope and detector integration times are critical in the derivation of the deconvolving function.

Geometric processing should be very similar to an opto-mechanical linear scanner. The error modeling will be simpler because random or irregular scan motion does not exist for the HRPI. This results in improved

geometric mapping accuracy. Finally, two facts must be remembered for "pushbroom" scanners: (1) overlapping IFOV through increased sampling rates in the across-track direction is not possible because the 4,800-detector array physically forces IFOV adjacency and (2) spatial frequencies in the across-track direction will be aliased if they are sufficiently high.

7.2 COMPENSATED SINE WAVE SCANNER

The high duty cycle sine wave scanner shown in Figure 7-2 is a six-band opto-mechanical imaging system. It has a swath width of 185 km and an IFOV on the ground of 30 m. There are 132 detectors in an array for each of the five visible and near-infrared bands and 33 in the single far-infrared band. The detector integration time is 45 μsec and 180 μsec for the two sets of detector arrays. Unlike conventional linear scanners, the data are recorded in a back-and-forth fashion. A compensating mirror is used to place each swath adjacent to the next.

With respect to radiometric correction, if a table look-up approach is used, 44K words of memory would be required for all six bands. Since the total number of detectors is 693, the probability of a faulty one may not be significant.

Aperture correction is similar to the conventional linear scanner except that each swath is scanned in the opposite direction. Reversal on a small scale would have to be done during the deconvolution process.

Geometric correction is complicated by the scan reversal on alternating swaths. This will require two sets of correction algorithms and twice the memory for computation support data.

If a simple electromechanical scan film recorder such as a laser beam recorder is used, then swath reversal must be incorporated. Similarly, output on computer-compatible tape should be in a standard format with single direction swath scan. Swath reversal in support of these outputs requires a memory of about 12M words. Implementation of this large a memory can most economically be in the form of disc and a small volatile memory which is possible because of the well-defined operation involved in reversal.

Data obtained with this scanner are sensitive to the attitude elements of the spacecraft. If the attitude stability is the same as that assumed in the baseline system, no problems are expected. However, if the ERTS value of 0.015°/sec per axis is used, an overlap or gap of 3 x 5,800 pixels may result. Consequently, care should be taken to ensure excellent attitude stability.

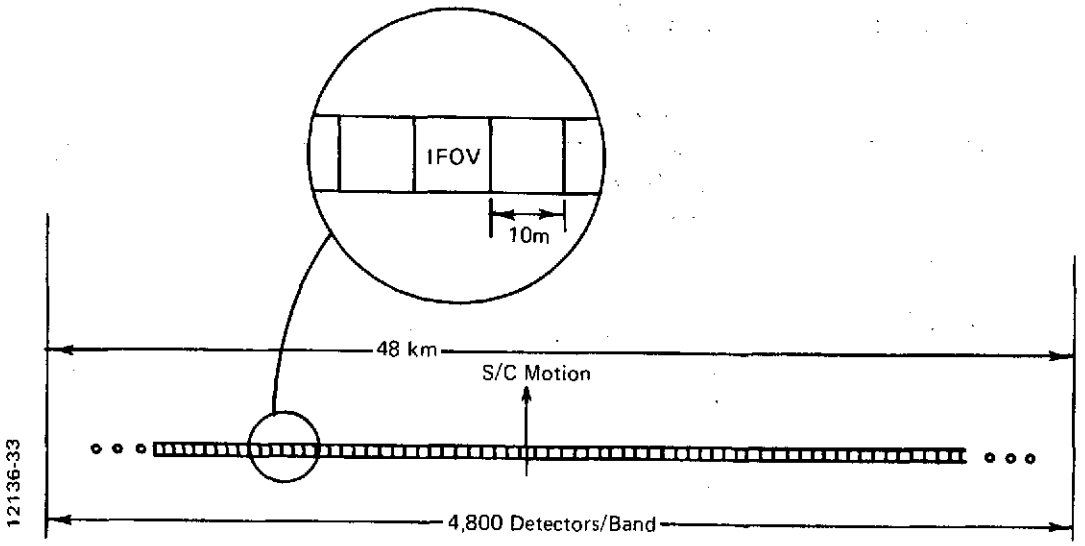

Figure 7-1 High-Resolution Pointable Imager

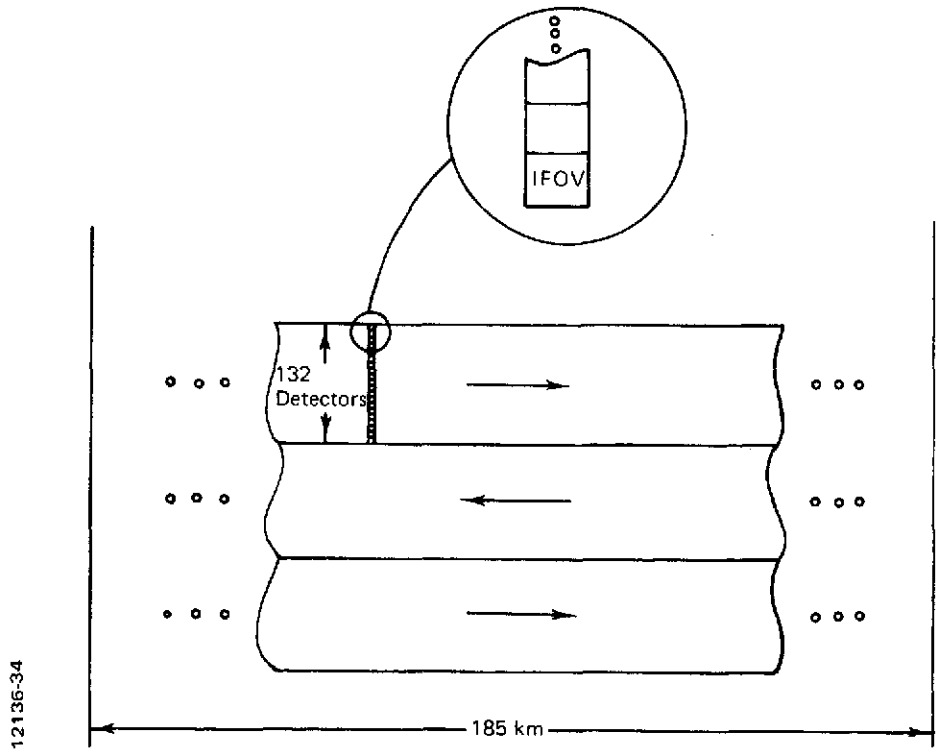

Figure 7-2 Compensated Sine Wave Scanner

7.3 ROOF MIRROR LINEAR SCANNER

The roof mirror linear scanner is a high duty cycle six-band opto-mechanical imaging system. It has a swath width of 185 km and an IFOV on the ground of 30 m for the visible and near-IR bands and 120 m for the IR. There are nine detectors in each band with a detector integration time of 6 μsec and 24 μsec for the two sets of bands.

No significant difference in ground processing requirements are expected for the data compared to the ERTS MSS. Because the spacecraft stability is so great, the magnitudes of many errors will be considerably reduced.

SECTION 8

CONCLUSIONS AND RECOMMENDATIONS

The conclusions and recommendations resulting from this study are as follows:

1. If, as in this study, a rectilinear format digital data output on magnetic tape is required, then the all-digital precision processor must contain memory to store sufficient conical scan lines to synthesize linear scan lines by interpolation or nearest-neighbor assignment techniques. The most economical memory for this function is a combination of mass memory such as a disc and high-speed semiconductor memory. It is estimated that the additional memory and support hardware and software will incur a total cost differential of about $160,000.

2. If there is no specific need to output the data in rectilinear form, then there are no large impacts on the ground data processing operations resulting from conical scan geometry. In this case, all required operations of correction and image recording can be performed in the curved scan line space for the conical scanner as readily as in the linear scan line space of the linear scanner. The conical scan image recorder system will cost approximately $70,000 more than the linear scan system, primarily for additional break-point storage and recorder scan circuits.

3. There is no evidence to indicate that the data quality of conically scanned data will differ from the data quality of linear scan data.

4. For both conical and linear scan data, an image recorder system using a continuous motion film recorder will have twice the throughput of a system using a framing recorder unless additional data tape recorders or two framing recorders are used.

5. In the image recording system, although more break-points in the linear interpolation would be required for the conical scan data correction, the computational load on the digital controller computer would not be excessive.

6. Because of the need for storage of data over several scan lines usually embracing two detector-array swaths or sweeps, an analog implementation of aperture correction is not currently feasible. Including the required digital memory and computational capability in an image recording system transforms such a system into the functional equivalent of the all-digital precision processor.

7. The principal impact of the conical scanner versus the linear scanner relative to aperture correction is in the computation of the deconvolving array. Although the conical scan computation is more complex, it is a one-time computation estimated to require approximately one-half man-month more than the equivalent linear scan computation.

8. Offset pointing of either the linear or conical scanner produces, at a 20° offset, approximately a 20% change in image scale and resolution and less for lesser offsets.

9. Lateral offset pointing of either the linear or conical scanner requires significantly more memory in the digital processor and prevents the use of the higher throughput continuous motion image recorder if the pointing is implemented such that the scan line rotates appreciably relative to the normal scan line when offset pointed. It is highly recommended that offset pointing be implemented so that scan line rotation does not take place. Offset pointing with rotation will also produce gaps in the data under certain conditions which can only be cosmetically compensated.

10. As a result of the precise attitude measurement and control system planned for EOS, ground control point (GCP) identification will be done on a small scale (6 to 15 GCPs per orbital pass) so that the problem of GCP rotation with the conical scanner is not significant to the processor throughput or accuracy.

11. An all-digital precision processor for data from a scanner (linear or conical) with the resolution, number of spectral bands, and throughput requirements as presently projected for EOS must be configured as a special-purpose digital processor. A general-purpose computer configuration is presently not available to meet the need, and it is unlikely that one will be economically available in the EOS time frame.

12. The High Resolution Pointable Imager (HRPI) presents a major problem to the ground data processor in the need to calibrate 19,200 individual detectors. If this is performed by a table look-up procedure, about 1.2 million words of memory will be required. Other techniques for HRPI calibration should be investigated, including onboard calibration. Also, the present HRPI detector sampling sequence requires that the full scan line for all four spectral bands be stored and assembled into a linear sequential scan for further processing. This will require an additional 38.4K words of memory over that required if the detectors were sampled in a linear sequence. Furthermore, with 19,200 detectors and associated electronics, it is likely that some will become inoperative or faulty. A strategy must be developed for correction, compensation, or cosmetic alteration of the data in this event.

13. The compensated sine wave scanner with 132 detectors in each band will require an additional 44K words of memory in the ground data processor if radiometric calibration is achieved by table look-up. Geometric correction is considerably more complex for this scanner because of the scan reversal on alternating swaths. Memory is required for somewhat more than two swaths or about 12M words of storage.

14. With respect to ground data processing, the linear scanner containing 24 roof mirrors mounted on a wheel rotating at a constant angular velocity and nine detectors per band appears to produce data most readily processed of all the scanners studied. This evaluation, however, considers only error factors external to the scanner itself. A more detailed evaluation of internal scanner geometric errors should be undertaken if this scanner is to be used in EOS.

15. It is recommended that a conical scanner be configured so that the conical scan line is concave in the direction of spacecraft motion. This configuration will result in a requirement of over 50% less memory in the ground data processor for scan line linearization than that required for the scan concave in the direction opposite to spacecraft motion.

16. It is recommended that a conical scanner be configured so that the normal nonoffset scan line passes through the spacecraft nadir. This configuration will produce data with minimum geometric error resulting from terrain effects.

APPENDIX A

SCANNER GEOMETRY RELATIONSHIP TO IFOV ROTATION

A.1 MODEL TO DETERMINE THE ORIENTATION OF THE FIELD OF VIEW

The question whether an FOV rotates when moving along the scan line can be answered without any detailed knowledge of the scan mechanism, even without knowing if it is an object space or an image space scanner. The model to determine the orientation of the FOV, presented below, is applicable to any scan mechanism having a single rotating system regardless of the number of elements. In the case of more than one rotational system, each system has to be treated separately and can subsequently be superimposed.

A.2 DESCRIPTION OF THE MODEL (SEE FIGURE A-1)

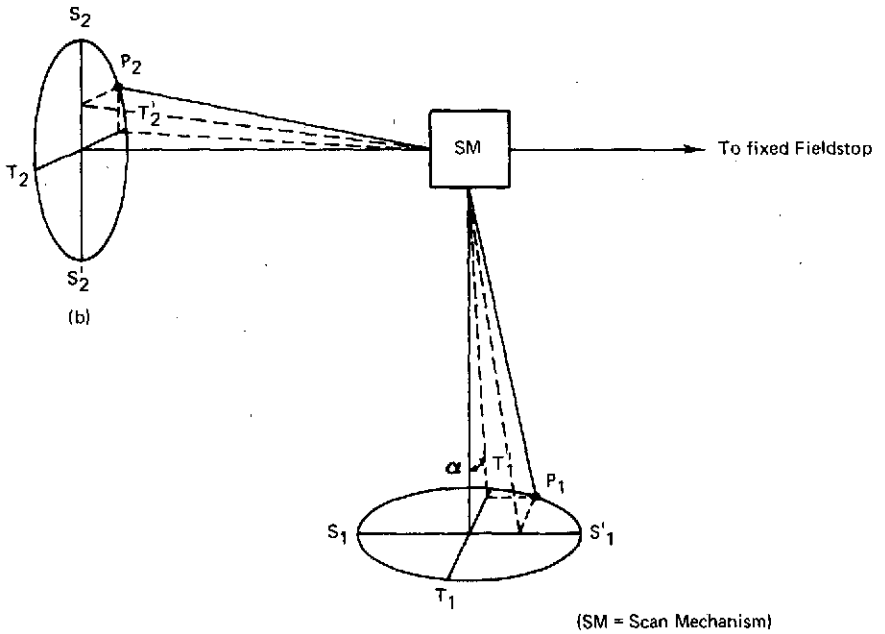

Figure A-1 Scan Pattern Produced by Different Scan Mechanisms

The key terms are defined as follows:

Field Stop Direction: Direction of the radiation bundle (chief ray) from the scan mechanism to the field stop.

Scanning beam: Chief ray of the radiation bundle leaving the scan mechanism.

Scan circle: A circle cut out on a unit sphere centered at the scan mechanism after a complete revolution.

Target plane: The plane on which the scan circle is projected as seen from the place of the scan mechanism.

The orientation of the FOV is determined by the geometric relationship between the scan circle, the target plane, and the field stop direction. If the field stop distance to the top of the cone is zero, the direction is given by the normal to the field stop plane.

A description of the four basic configurations is given below. Any different configuration can be reduced to one or more of these basic types by dividing into an appropriate set of components.

- Type I - The scan circle is perpendicular to the target plane and parallel to the field stop direction (circle through S_1 S'_1 or S_2 S'_2 or T_2 T'_2 in Figure A-1):

  Straight scan line; no rotation of the FOV

  Examples: oscillating mirror, rotating mirror prism (Figure A-2).

- Type II - The scan circle is perpendicular to the target plane and perpendicular to the field stop direction (circle through $T_1T'_1$ in Figure A-1):

  Straight scan line; FOV rotates about d, which is the angle of rotation of the scan mechanism.

  Example: axe head scanner.

- Type III - The scan circle is parallel to the target plane and parallel to the field stop direction (circle described by P_1 in Figure A-1):

  Circular scan line; the motion of P_1 can be divided into two components corresponding to Types I and II. A rotation of the FOV is caused by the Type II component.

  Example: conical object space scanner.

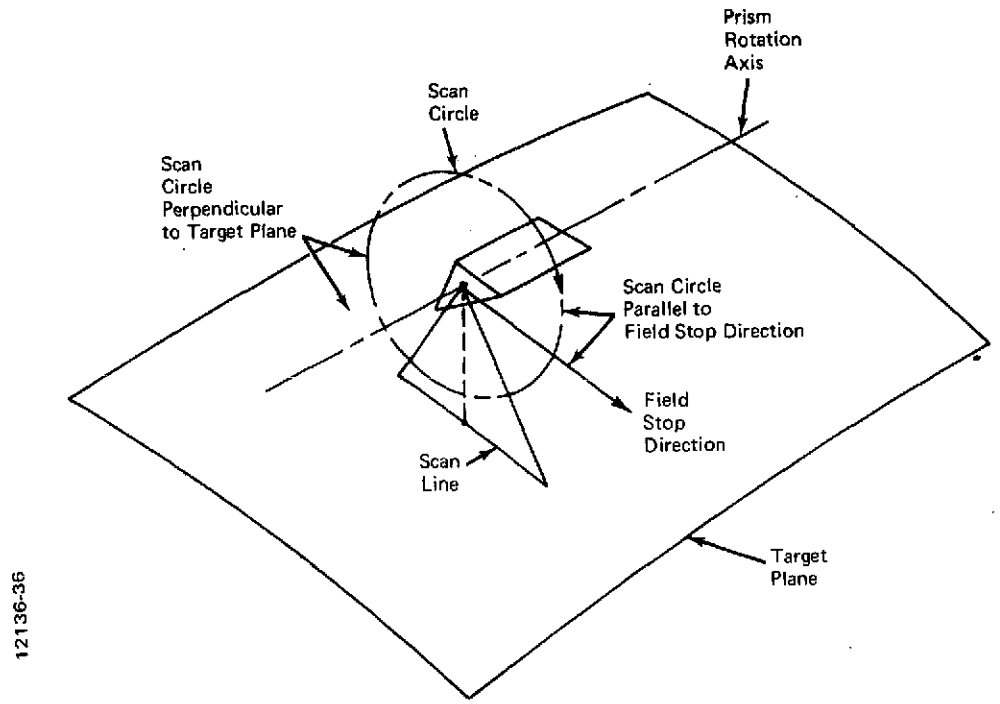

Figure A-2 Geometry of Type I Scanner

- Type IV - The scan circle is parallel to the target plane and perpendicular to the field stop (circle described by P_2 in Figure A-1):

  Circular scan line; the motion of P_2 can be divided into two components both of which correspond to Type I. No rotation of the FOV.

  Example: conical image space scanner.